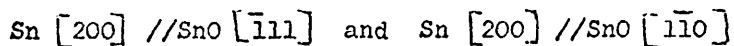


SUMMARY

Using the Siemen's Elmiskop I, the morphology of α -SnO grown under reduced pressure on thin polycrystalline tin films was studied. The effects of varying the exposure time, oxygen pressure and reaction temperature were investigated.

Epitaxial (200) oriented tin films were grown by the condensation of tin onto a cooled rocksalt substrate. The films were oxidised under reduced pressure and the orientation of α -SnO with respect to the tin substrate was determined. Two orientation relationships were found:



Oxidation of the epitaxial films inside the electron microscope at a temperature below the melting point of β -Sn resulted in the formation of SnO₂.

The effect of water vapour on the structure and morphology of the oxide was also studied

ProQuest Number: 11011935

All rights reserved

INFORMATION TO ALL USERS

The quality of this reproduction is dependent upon the quality of the copy submitted.

In the unlikely event that the author did not send a complete manuscript and there are missing pages, these will be noted. Also, if material had to be removed, a note will indicate the deletion.



ProQuest 11011935

Published by ProQuest LLC (2018). Copyright of the Dissertation is held by the Author.

All rights reserved.

This work is protected against unauthorized copying under Title 17, United States Code
Microform Edition © ProQuest LLC.

ProQuest LLC.
789 East Eisenhower Parkway
P.O. Box 1346
Ann Arbor, MI 48106 – 1346

INDEX

SUMMARY

1. Introduction

- i) Tin and tin oxidation
 - a) Historical development
 - b) Mechanism of tin oxidation
 - c) Purpose of work.
- ii) Epitaxial films of tin
 - a) Definition of terms
 - b) Theories of epitaxy
 - c) Growth of epitaxial films by metal vapour deposition
 - d) Growth of epitaxial tin films.
- iii) Electron microscopy
 - a) The electron microscope
 - b) Electron diffraction
 - c) The interpretation of electron diffraction patterns
 - d) Image contrast

2. Experimental Work

- i) Bulk single crystals
- ii). The preparation of thin evaporated films
 - a) Epitaxial films
 - b) Decoration techniques
 - c) Polycrystalline films
- iii) Oxidation
 - a) Oxidation in coating unit
 - b) Effect of water vapour on reaction

Index (contd.)

- c) Oxidation at atmospheric pressure
- d) Oxidation inside the electron microscope
- iv) Viewing of specimens in electron microscope
 - a) Techniques used
 - b) Measurement of micrographs of diffraction patterns

3. Results

- i) Orientation of thin films
 - a) Decoration of rocksalt substrates
 - b) Effect of substrate, substrate temperature and substrate preparation on orientation of thin evaporated films.
 - c) Effect of electron beam bombardment
 - d) Polycrystalline films.
- ii) Morphology of thin films
 - a) Textured films
 - b) Single crystal films
 - c) Polycrystalline films
- iii) Oxidation of thin films
 - a) Composition of oxide
 - b) Orientation of oxide
 - c) Morphology of oxide

4. Discussion

- i) Unsuitability of mechanically thinned specimens
- ii) Orientation and crystal growth of tin films
- iii) Oxidation of tin films

Index (contd.)

Acknowledgements

References

Diagrams

Plates.

1. INTRODUCTION

i) Tin and Tin Oxidation

a) Historical development

Electron microscopy and electron diffraction have proved useful techniques for the study of the oxidation behaviour of β -Sn.

Oxidation products have been identified by electron and X-ray diffraction and the upper and lower limits for the formation of crystalline α -SnO and of the higher oxide SnO₂ have been established (1932-1961).

Extraction replica techniques have been used to remove the oxide α -SnO from the tin substrate. Using this technique, the oxide morphology and its dependence on pressure and temperature have been extensively studied in the electron microscope (1956-1963).

The reaction kinetics of tin oxidation have also been investigated (1952-1961). By correlating reaction rates with oxide morphology possible mechanisms for the oxidation of tin have been derived (1961).

It is now well established that oxide growth is influenced by the orientation of the metal substrate and many metal-oxide systems have been investigated. There are few references to this aspect of tin oxidation behaviour. However, some studies have been made of the rate of oxidation at selected faces of tin single crystals and there is evidence that the oxidation rate is influenced by the orientation of the tin substrate (1956-1958).

Tin exists in two modifications⁽¹⁾. Below 13.2°C, the stable form is white or cubic tin (α -Sn) with $a = 6.4912 \text{ \AA}$ ⁽²⁾. Above 13.2°C, the stable modification is grey tin (β -Sn). The unit cell is body-centred tetragonal with lattice parameters $a = 5.8197 \text{ \AA}$ and $c = 3.17488 \text{ \AA}$ ⁽²⁾. Atomic positions are 000; $0\frac{1}{2}\frac{1}{2}$; $\frac{1}{2}0\frac{1}{2}$; $\frac{1}{2}\frac{1}{2}\frac{1}{2}$. The unit cell of β -Sn is shown in Fig. 1.

Early electron diffraction studies by Bragg and Derbyshire⁽³⁾ revealed that when tin foil was heated in a gas flame to a temperature just above its melting point, a body-centred tetragonal oxide, α -SnO, was formed. The unit cell of α -SnO has lattice parameters $a = 3.796 \text{ \AA}$, $c = 4.816 \text{ \AA}$. There has been some doubt as to the crystal structure of the oxide but Pauling and Moore⁽⁴⁾ report the atomic positions in the unit cell as 2O at 000; $\frac{1}{2}\frac{1}{2}0$; 2Sn at $\frac{1}{2}0\frac{1}{2}$; $0\frac{1}{2}\bar{Z}$ where $Z = 0.2356$.

Steineil⁽⁵⁾ and Jenkins⁽⁶⁾ heated tin foil in air and observed the presence of a higher oxide, SnO₂, which was formed at elevated temperatures. This oxide was tetragonal also.

Later work by Hart⁽⁷⁾ - again by heating tin foil in a gas flame in air and studying the oxidation products by electron diffraction - established that the lower limit for the formation of crystalline SnO was 130°C. Below this temperature the oxide was believed to exist as an amorphous protecting film. At elevated temperatures SnO and SnO₂ were identified, the concentration of SnO₂ increasing with increase in temperature.

Britton and Bright⁽⁸⁾ studied the oxidation of tin foil in air by electron microscopy and electron diffraction. The oxide films were detached from the tin substrate by extraction replica techniques. They observed that the oxide was amorphous below 170°C and that between 200°C and 270°C α -SnO was formed. Shimaoka and Yamai⁽⁹⁾ also report that α -SnO is the only oxide formed between 200°C and 270°C and that between 280°C and 390°C the oxidation products are α -SnO and SnO₂, and above 390°C only SnO₂ is formed.

Trillat, Tertian and Plattard⁽¹⁰⁾ oxidised thin tin films (300-500 Å) inside the electron diffraction camera, by heating on a hot stage. At 5×10^{-3} torr air pressure, α -SnO was not observed until the temperature of the tin exceeded 400°C and SnO₂ was observed only when the temperature exceeded 600°C. At high temperatures, the concentration of SnO₂ increased while the concentration of α -SnO decreased. At 2×10^{-4} torr air pressure, oxidation proceeded extremely slowly and SnO₂ was not observed.

In a recent study of the oxidation of tin foil, Boggs, Trozzo and Pellisier⁽¹¹⁾ reported that crystalline α -SnO is formed on tin foil at temperatures as low as 75°C provided that the time of exposure to oxygen is sufficiently long. They concluded that previous determinations of the temperature limit for the formation of crystalline α -SnO were erroneously high because the period of oxidation was too short to allow a detectable concentration of crystalline α -SnO to form.

They also studied the morphology of α -SnO grown on annealed tin foil. The oxide film was removed from the substrate by amalgamating the tin substrate with mercury and then examined in the electron microscope, a technique devised by Britton and Bright⁽⁸⁾.

The oxide morphology was found to be markedly dependent on oxygen pressure. Above 1 torr oxygen pressure, the oxide grew in the form of platelets which developed laterally until they touched. As oxidation proceeded cavities developed at the oxide-metal interface and extended nearly through the oxide film. At oxygen pressures below 1 torr, the oxide grew as fine dendrites. Direction of growth appeared to be related to the orientation of the underlying tin grain. The relationship between the direction of oxide growth and the orientation of the underlying tin grain became less obvious as oxygen pressure increased and the most highly oriented growths were observed at 10^{-3} torr oxygen pressure.

Certain characteristic structures, identified as growth centres were observed in the early stages of oxidation. At oxygen pressures greater than 1 torr, the growth centres were wheel-shaped and of limiting diameter 1-1.5 μ . Segments of the rims of some of these developed outwards as platelets. Below 1 torr oxygen pressure, the growth centres were rosette-like and their size varied greatly. The oxide dendrites developed from them. Since the number of growth centres observed was of the same order as the number of dislocation etch pits in the tin foil, it was deduced that growth was initiated at the dislocations.

By correlating these studies of tin oxide morphology with observations of oxidation rates⁽¹²⁾, Boggs postulated possible reaction mechanisms for the oxidation of β -Sn⁽¹³⁾. The suggested mechanisms are described in detail in section ib, entitled 'Mechanism of tin oxidation'.

Spinedi and Verdini⁽¹⁴⁾ studied the oxidation of a simpler system, namely single and bi-crystals of tin. Oxidations were carried out at atmospheric pressure in oxygen of 3% humidity and the effects of temperature and time of oxidation were investigated. Above 190°C, regularly shaped oxide platelets were formed. Needle-like nuclei were also observed. The size of the needles increased with increase in temperature whilst prolonging the time of exposure to oxygen led to an increase in the number of nuclei per unit area.

It has been shown that the rate of oxidation is a function of the orientation of the tin substrate. Nikulin et al⁽¹⁵⁾⁽¹⁶⁾, used plates or single crystals of tin as electrodes in a phosphate buffer solution and determined the rate of reduction of oxygen at the electrodes polarographically. The rate of reduction was high when plates electro-coated with tin crystals of a (211) texture and less rapid when crystals of a (101) texture were used. The reduction rate was intermediate when cast tin was used⁽¹⁵⁾. Using specially grown tin crystals, it was found that reduction of oxygen was faster at the (001) face than at the (110) face⁽¹⁵⁾.

b) Mechanism of tin oxidation

A knowledge of reaction rates and kinetics, the temperature and oxygen pressure dependence of the reaction and the composition, structure and growth mechanism of the oxidation products is necessary for the detailed understanding of the oxidation behaviour of a metal.

Although rate equations alone are insufficient for interpretations of oxidation mechanisms, they may be used to classify the oxidation behaviour of the metal and as such limit the interpretation to a class of alternative mechanisms. The correct mechanism may then be elucidated by correlation with other studies.

Three types of rate equation, logarithmic, parabolic and linear, have been used to describe the oxidation behaviour of tin:-

When the oxidation rate is initially rapid and then falls off to a very low or imperceptible rate, then this behaviour can often be described by logarithmic rate equations. Such behaviour has been rationalised by a number of theories, based on various rate determining mechanisms. These mechanisms include the rate determining transport of electrons or ions due to electric fields in the oxide film, rate determining chemisorption and the formation of cavities in the film⁽¹⁷⁻²⁰⁾.

When the oxidation reaction may be described by a parabolic rate equation, this usually signifies that a thermal diffusion process is the rate determining step. Such a process may be the uniform diffusion of one or both reactants through the growing compact scale or the uniform diffusion of oxygen into the metal.

The third type of oxidation behaviour, described by linear rate equations, is a reaction whose rate is constant with respect to time. In this case, a surface or phase boundary process is rate determining. This may involve a steady state reaction limited by the supply of oxygen at the surface or a steady state formation of oxide at the metal/oxide interface.

The results reported in the literature describing the oxidation behaviour of tin in terms of the various rate equations tend to be somewhat conflicting:

Britton and Bright⁽⁸⁾ reported that at 30°C, the reaction rate was logarithmic and that at 180°-450°C, it was parabolic. However, the data obtained by Luner⁽²¹⁾ for tin foil oxidised at low pressure were best fitted by a logarithmic equation at about 200°C for oxide film thicknesses up to 700 Å. Bilbrey, Wilson and Spendlove⁽²²⁾ and Gruhl and Gruhl⁽²³⁾ reported that above 475°C the rate of oxidation was irregular. Spinedi⁽²⁴⁾ observed that above 475°C, the rate equation was linear rather than parabolic.

It has also been observed that the oxidation rate of tin foil in air with 80% humidity is twice as fast as the oxidation rate in dry air⁽⁸⁾.

A thorough investigation of the reaction kinetics of tin oxidation has been made by Boggs, Kachik and Pellisier⁽¹²⁾. Above 1 torr oxygen pressure, the rate of oxidation was initially low, increasing to a maximum after which the rate decreased as it

entered a period of logarithmic behaviour. After long periods the oxidation rate became erratic. Below 1 torr oxygen pressure, it was observed that the oxidation rate increased linearly with time and that dissociation of oxygen was the rate controlling step.

The morphology of the growing oxide film was studied by electron microscopy⁽¹¹⁾ and by correlating the reaction kinetics with the direct observations of the growing film, Boggs⁽¹³⁾ postulated the following mechanisms for the oxidation reaction:

At all pressures, characteristic structures, identified as oxide growth centres, were observed. Since the number of growth centres was of the same order as the number of dislocation etch pits in the tin foil, it was thought that the oxide nucleated at dislocations.

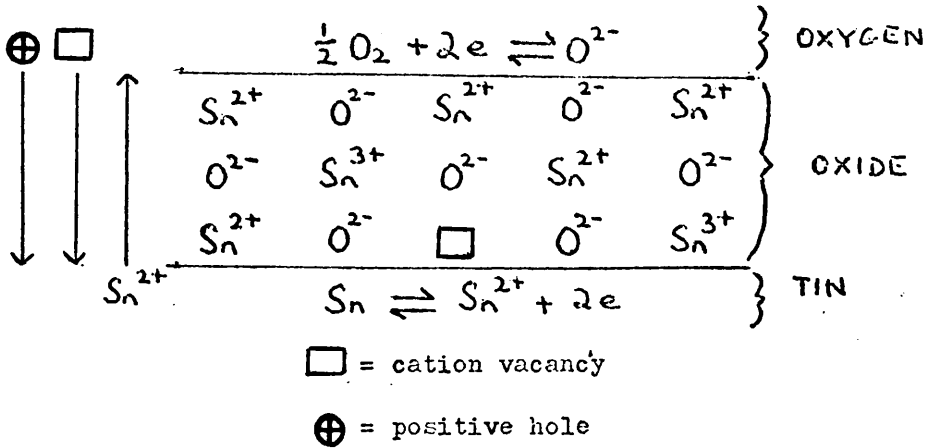
At oxygen pressures above 1 torr, the initial region of increasing growth rate was shown to be associated with the nucleation and lateral growth of the oxide crystals.

Above 1 torr oxygen pressure, the growth centres developed laterally and vertically until they reached a critical size. Laterally spreading platelets grew from some of the growth centres until they impinged mutually.

During the period of logarithmic growth, cavities appeared at the oxide-metal interface. There are several explanations for the formation of such cavities but the mechanism proposed by Evans⁽²⁵⁾ provided the most satisfactory explanation of cavity formation in

α -SnO. This mechanism involves the movement of cationic vacancies towards the oxide-metal interface where they may coalesce as vacancies.

If α -SnO is a p-type semi-conductor with cationic vacancies, then the oxidation reaction may be represented as follows:-



Oxygen reacts with tin at the oxygen interface, removing two electrons from the tin ions thus forming two positive holes and a cation vacancy.

A tin ion can jump from a lower atom layer into the vacancy, leaving a vacancy in the lower layer. As this process continues the vacancy eventually reaches the oxide-metal interface. Electrons change places with positive holes in a similar manner. Now a tin atom at the oxide-metal interface can fill a cation vacancy in the oxide lattice and the electrons produced can change two positive holes to normal cations. This produces a stoichiometric crystal and leaves a vacancy at the oxide-metal interface. Since it is generally held that ions are not free to move by thermal diffusion

at temperatures below the Tamman temperature, then the ions in α -SnO must move under the influence of the electrical field set up by the disociation of oxygen at the oxide-metal interface. Vacancies remaining at the interface may collect to form cavities. Others may pass into the metal and be annihilated at a dislocation or pass right through the metal (if in sheet form) to join a cavity on the other side.

As the cavities grew and coalesced they acted as a progressively greater barrier to the diffusion of tin ions through the oxide film. The decreased speed of tin ions moving through the film and the decrease in oxide area in contact with the metal caused the observed logarithmic rate.

The period of erratic growth was attributed to the fracture of cavity walls, thereby allowing oxygen to come into direct contact with the metal and producing a sharp increase in oxidation rate.

At oxygen pressures below 1 torr, the break-down of oxygen into oxide ions was the rate controlling step and the oxide grew in the form of dendrites. These two observations indicated that the oxygen on the metal surface was depleted by reaction faster than it was replenished from the gas phase.

The mechanism postulated by Boggs for the dendritic growth involved the assumption of an initial incomplete layer of adsorbed oxygen or a non-stoichiometric mobile film of tin ions and oxygen

ions on the metal surface. Growth was thought to be initiated at active sites such as dislocation and grain boundaries and as the oxide grew outward from the growth centre, the metal between adjacent oxide filaments became depleted oxygen. Therefore the oxide crystals grew outward in the form of dendrites to areas which were rich in oxygen. As the oxygen pressure was increased, the tin surface became saturated with oxygen so that platelets rather than dendrites were formed.

c) Purpose of present work

The aim of the present work was to study the oxide morphology further and also to determine the crystallographic relationship between the lattice of β -Sn and α -SnO.

It was decided to oxidise thin evaporated tin films and to study the oxide morphology directly, thus avoiding the necessity for elaborate replication techniques.

To determine the orientation of the oxide grown on tin crystals of a particular orientation, epitaxial tin films were grown. In this way the crystallographic relationship between the lattices of β -Sn and α -SnO could be determined directly by electron diffraction.

ii) Epitaxial films of tin

a) Definition of terms used

Epitaxy describes two crystals of different species growing together in such a way that there is a definite and unique orientation relationship between their crystal axes.

A polycrystalline film is composed of crystals which are randomly oriented with respect to each other.

A single crystal film is one in which each crystal has its three crystallographic axes parallel to the corresponding axes in all other crystals in the film. For instance, an $(h00)$ single crystal film is one in which each crystal has its $[h00]$ axis perpendicular to the plane of the film. The $(0k0)$ axis of each crystal is parallel to the $[0k0]$ axis of every other crystal. Similarly the $[00l]$ axes are parallel.

A textured film is one in which each crystal has one particular axis perpendicular to the plane of the film, while the other axes in each crystal are randomly oriented with respect to the corresponding axes in the other crystals of the film. Thus, an $(h00)$ textured film is one in which the $[h00]$ axis of each crystal in the film is perpendicular to the plane of the film, while all other axes of each crystal are randomly oriented.

b) Theories of epitaxy

The phenomenon known as epitaxy has been investigated by many workers over the last forty years. Numerous examples of epitaxial growth have been recorded. Epitaxial growths have been produced by a number of techniques including the vapour deposition of metals onto crystalline substrates, electrochemical deposition and the direct chemical attack of the substrate from the gas phase.

Although many theories have been proposed to explain the occurrence of epitaxy none has proved entirely satisfactory.

The term 'epitaxy' was first used by Royer in 1928 to describe the oriented growth of one crystal on another⁽²⁶⁾.

Early investigations such as those of Royer dealt mainly with the geometric fit between the substrate and overgrowth lattices and with the derivation of empirical rules governing epitaxial growth:

Investigations into the growth of alkali halides upon themselves and upon a mica cleavage surface indicated that the misfit between the two lattices expressed as $100 \frac{(b - a)}{a}$,

where a = substrate network spacing

b = overgrowth network spacing.

did not exceed 15%. On the basis of these observations, Royer postulated three rules for the formation of an oriented overgrowth:-

- (1) Lattice planes with networks, elementary or multiple, which are identical in form and of nearly the same dimensions in the two structures, implying that the two networks are parallel.
- (2) Where ionic crystals are involved, the ions of the overgrowth should take up positions which corresponding ions of the substrate of the same polarity would have occupied, had the substrate continued to grow.
- (3) The same type of bonding in substrate and overgrowth.

It soon became apparent that the first rule, demanding near perfect fit between the two lattices, was not always obeyed. The most striking example was that of metals condensed on heated rocksalt surfaces, for which misfits from -39% to +90% were observed⁽²⁷⁾

Several theories have been expounded since 1928, but all involve the necessity of a small misfit.

In 1933, Finch and Quarrell⁽²⁸⁾ introduced the concept of basal plane pseudomorphism, according to which, the deposit crystals are constrained so that the atomic planes parallel to the substrate surface have the same spacing as parallel planes in the substrate. Thus the initial oriented film has an abnormal crystal structure.

A detailed theory of epitaxy was developed from this concept by Frank and Van der Merwe⁽²⁹⁾ in 1949:- It was deduced that the lowest energy state for the system, for misfits of less than 9%,

was a pseudomorphic arrangement in which the spacing of the overgrowth monolayer was changed to match that of the substrate. For very high misfits, the monolayer contained "dislocations" but on average, the original spacing was preserved. These predictions were linked to experiment by assuming that the latter arrangement did not lead to an epitaxial growth.

However, it has been shown that these initial constrained monolayers would not necessarily be thermodynamically stable. Furthermore, the concept of basal plane pseudomorphism has not been verified by further experiment and it has been shown that, in many cases, constrained monolayers of abnormal structure are definitely not formed.

Some attempts to explain the occurrence of large misfits have been based on the idea that an oriented layer, corresponding to a low misfit, occurs during the initial stages of growth, and that subsequent growth gives rise to different orientations. Menzer⁽³⁰⁾, in 1938, postulated that the initial orientation of the film was arrived at by twinning of the original layer. However it has since been demonstrated that twinning occurs at a later stage of growth.

An extensive study of metal vapours condensed on heated salt substrates was made by Bruck⁽³¹⁾ in 1936. He recorded the minimum substrate temperature (known as the epitaxial temperature) required

for the formation of an epitaxial deposit and the lattice misfit between deposit and substrate. In 1952 Engel⁽³²⁾ attempted to rationalise these observed lattice fits and the dependence of epitaxy on substrate temperature. Engel postulated that the occurrence of orientation depended on the possibility of suitable ionisation processes and upon the fit between the intermediate salt formed by ionisation with both the substrate and the deposit. Thus the first stage of epitaxial growth was the ionisation of the first layer of the metal so that a two dimensional chemical reaction occurred resulting in a monolayer of deposit-metal salt at the substrate-deposit interface. In fact, it was found that a linear relationship existed between Bruck's epitaxial temperatures and the ionisation potentials of the most commonly observed ionisation states of the metals. Engel's theory, however, does not stand up to rigorous scrutiny of the lattice fits of the substrate, metal and postulated metal salt.

During the last fifteen years, much work has been devoted to the early stages of metal vapour deposition. It has been established by reflection electron microscopy and radio-tracer techniques that isolated three dimensional nuclei form when the average film thickness is less than one monolayer⁽³³⁾. The nuclei were randomly oriented with no preferred sites for nucleation. This was to be expected since the supersaturation of metal vapour was very high. However, one surface feature, namely the surface step, has been established as a preferential site for nucleation⁽³⁴⁾.

No satisfactory theory of epitaxy has as yet been derived. The conclusions to be drawn from the observations of epitaxial growth are:

1. Although a small misfit is significant in certain cases, it is not an essential condition for the occurrence of epitaxy.
2. The orientation which occurs is not always that corresponding to the best geometric fit.
3. Many cases of observed large misfits are not satisfactorily explained by the assumption of an intermediate orientation of smaller misfit and the occurrence of large misfits must be taken into account in any theoretical treatment.
4. The initial oriented deposit has its normal bulk structure and spacing and grows initially in the form of isolated nuclei.

c) Growth of epitaxial films by metal vapour deposition

The phenomenon of epitaxy is dependent on several variables:

- (1) the temperature of the substrate during deposition of the metal vapour.
- (2) the preparation of the substrate surface.
- (3) the rate of deposition of the metal.
- (4) the thickness of the deposit.

The effects of these variables on epitaxial growth have not yet been studied systematically.

In 1936, Bruck⁽³¹⁾ established that a critical substrate temperature was required, below which face centred cubic metals would not be deposited epitaxially on rocksalt. However, there has since been considerable disagreement about the values of the 'epitaxial temperatures'. It is thought that increase in substrate temperature favours the formation of an epitaxial overgrowth by

- (1) providing some of the activation energy required by the deposit atoms to take up the positions of potential minima associated with epitaxy,
- (2) increasing surface and volume diffusion thereby facilitating the accommodation of misfits as neighbouring nuclei grow together,
- (3) cleaning of the substrate surface.

The substrate may be pre-heated in vacua to anneal out surface defects, but is thought more likely that increased surface perfection is brought about by the sublimation of the upper layers of the substrate, leaving a perfectly clean surface⁽³⁵⁾. However, it has been reported that prolonged annealing may result in undesirable thermal etching of the surface⁽³⁶⁾.

The state of perfection of an alkali halide substrate is very much influenced by its method of preparation. The technique known as decoration⁽³⁴⁾ gives an indication of the degree of surface perfection. Decoration involves the vacuum deposition of gold or silver atoms onto the substrate surface. The metal atoms nucleate

preferentially at surface steps. For example, when the substrate crystal has been cleaved in vacuo, the metal particles are aligned in straight lines, and when air-cleaved, the the particles are aligned in a less ordered fashion, namely in swirls⁽³⁶⁾⁽³⁷⁾.

Recent U.H.V. experiments have shown that surface contamination of the substrate has a marked effect on epitaxial growth. For example, the epitaxial temperature for Au, Cu and Ag deposited on rocksalt which has been cleaved in U.H.V. is considerably lower than when air-cleared rocksalt is used⁽³⁸⁾. By contrast, however, it is reported that at 80°K, there is no appreciable difference between silver films deposited on vacuum cleaved or air contaminated rocksalt⁽³⁹⁾.

There is little systematic evidence on the effect of deposition rates. Genrally, the slower the rate of deposition of metal atoms, the more likely is epitaxy to occur. However, metal films which have been deposited slowly are more likely to be contaminated. A high rate of deposition will increase the substrate temperature, favourably or otherwise. It has also been suggested that a high rate of deposition is favourable to epitaxial growth because of its effect on the coalescence of metal nuclei⁽⁴⁰⁾.

It is reported that the orientation of a thin deposited film can change appreciably with film thickness⁽⁴¹⁾. In the case of

/...

gold deposited on mica at 330°C , orientation was found to improve with further deposition. It was suggested that re-orientation of the initial deposit occurred thereby improving the orientation of the entire film⁽⁴¹⁾. Generally, however, a good orientation is maintained up to a certain thickness of deposit.

d) Growth of epitaxial tin films

Several workers have studied methods of producing epitaxial tin films by the vacuum deposition technique. The effects of substrate, substrate temperature, deposition rate and film thickness on the structure of evaporated tin films have been studied.

Vook⁽⁴²⁾ obtained (002) oriented single crystal films (i.e. films comprising single crystals all oriented with their c-axes normal to the deposit plane) and (200) oriented textures (i.e. films comprising polycrystalline aggregates with their a-axes normal to the deposit plane and with b- and c-axes randomly oriented) by the rapid, discontinuous evaporation of tin onto a single crystal of rocksalt which was cooled to -196°C .

Curzon⁽⁴³⁾ studied the deposition of tin onto various heated substrates. He reported that galena proved a satisfactory substrate whereas rocksalt, potassium bromide, mica and zinc blende were not satisfactory. Increase in substrate temperature up to 160°C resulted in improved orientation of the tin films but above 160°C the films were poorly oriented. The maximum film thickness at which the crystals were well oriented was 200 \AA . The films were studied by reflection microscopy.

Collodion and quartz substrates were used by Gandais⁽⁴⁴⁾ in a study of the effect of film thickness, substrate temperature and evaporation rate on the orientation of the tin film. Two orientations were found to occur: In thin films, the predominant orientation was that in which the a-axis of the crystal was normal to the deposit plane. As the film thickness increased, a less well defined orientation, in which the c-axis of the crystal was normal to the deposit plane, became predominant. It was thought that the first orientation corresponded to the formation of small, well oriented islands; as these islands grew in size, recrystallisation, favoured by a decrease in grain boundary energy, occurred and the second orientation appeared.

Preece and Wilman⁽⁴⁵⁾ studied the effects of pressure, deposition rate and film thickness on the orientation of tin films deposited on glass substrates. The films were studied by reflection electron microscopy.

At film thicknesses of 500 Å, the tin was strongly oriented with (100) crystal planes parallel to the substrate surface at pressures 10^{-8} - 10^{-7} torr. At pressures 10^{-6} - 10^{-5} torr, the strong (100) orientation was mixed with a weaker (001) orientation for deposition rates up to 70 Å per second. At pressures 10^{-5} - 2×10^{-5} and for deposition rates up to 70 Å per second the film was (001) oriented. At pressures 2×10^{-5} - 10^{-3} torr the films were weakly oriented with (110) crystal planes parallel to the substrate surface for deposition rates up to 70 Å per second

and for deposition rates 70 - 150 Å per second the films were polycrystalline.

At constant pressure, the orientation of the tin films changed with thickness. For example, at 2×10^{-6} torr pressure and for deposition rate of 70 Å per second, the orientation of the film was initially a mixture of (100) and (001) but changed to the (001) orientation as the film thickness increased above 1000 Å. At deposition rate 70 - 150 Å per second, the initially polycrystalline film developed a (001) orientation followed by a (301) orientation or mixture of (301) and (001) orientations as the film thickness increased to 2000 Å.

Ehrhart and Maraud⁽⁴⁶⁾ have studied the structure of thin films of Pd, Ag, In and Sn as a function of substrate temperature. Their results were expressed in terms of the ratio T_t/T_f , where T_f = melting point of the metal at atmospheric pressure and T_t = substrate temperature.

For values of $T_t/T_f = 0.2 - 0.4$, they obtained films of uniform thickness with little disorientation. For $T_t/T_f = 0.7$, the metal crystals were very well oriented. For $T_t/T_f > 0.8$, the metal films were polycrystalline. The substrates used were glass and polished quartz.

iii) Electron Microscopy

a) The electron microscope

Basically, the electron microscope consists of an electron gun, and an assembly of electron lenses.

The gun comprises a directly heated tungsten filament, the emitted electrons being accelerated toward the anode plate by a negative bias.

The lenses employed are magnetic, the soft iron pole-piece of the lens producing an axially symmetric magnetic field for the focusing of electrons. The rest of the lens is a magnetic yoke containing the windings for energising the lens with d.c. current which can be varied thus altering the focal length of the lens.

Fig. 3 depicts the ray paths in a microscope employing three stages of magnification (objective, intermediate and projector) and a single condenser lens system for illuminating the specimen. (In high resolution work, requiring optimum specimen illumination, a double condenser lens system is usually employed). The specimen to be examined by transmission of electrons is placed near the entrance to the bore of the objective lens pole-piece. The objective lens produces a magnified image known as the first intermediate image which serves as an object for the intermediate lens which produces a second intermediate image. This is further magnified by the projector lens to produce a final image on the fluorescent viewing screen. The magnification of the objective lens is fixed and the

final magnification varied by regulation of the energising current in the intermediate or projector (as in Siemen's Elmiskop 1) lens. In some instruments, e.g. Siemen's Elmiskop 1, the projector pole-piece may be changed during operation so that low magnification, distortion-free images may be obtained by using a pole-piece of wide bore, while pole-pieces of narrower bore enable total magnifications of up to x 160,000 to be obtained.

The electron beam is collimated by a series of apertures situated in the bores of the various lens pole-pieces. With a double condenser lens system, condenser 1 usually contains a fixed aperture of about $750\ \mu$ diameter. Condenser 2 may be equipped with a range of interchangeable apertures, about 100 - $400\ \mu$ diameter. The objective lens also has interchangeable apertures of about 30 - $100\ \mu$ diameter.

Since electrons are strongly absorbed by air, the system is kept under vacuum. Vacuum conditions are achieved by use of an oil diffusion pump, which, in the Siemen's Elmiskop 1, is backed by a mercury diffusion pump, backed in turn by a mechanical rotary pump. The pressure in the column during operation of the microscope should not exceed 2×10^{-4} torr.

Under the vacuum conditions in the column of the electron microscope, there are sufficient hydrocarbon molecules present to cause specimen contamination. This contamination has a serious

effect on image resolution. The sources of these molecules include the oil diffusion pump, rubber gaskets and any oil or grease which may be present on the metal surfaces. It is believed⁽⁴⁷⁾ that the electron beam causes local cracking of the hydrocarbon molecules adsorbed on the surface of the specimen and a carbonaceous deposit is built up around the object being examined. At normal beam intensities, the rate of contamination build-up is 1 A per second. Contamination of the specimen is reduced either by the insertion into the column of a metal finger which is externally cooled by liquid nitrogen, so that hydrocarbon molecules are preferentially adsorbed⁽⁴⁸⁾, or by passing a stream of oxygen over the specimen and oxidising the products of electron beam cracking or by heating the specimen, either by the electron beam or by a heating stage, so that the concentration of condensed molecules is lowered.

The heating effect of the electron beam is well known and is frequently used deliberately as a substitute for a heating stage. The extent of heating is a function of the operating conditions in the electron gun, the collimation of the electron beam and the effectiveness of the specimen as a thermal sink. The last of these is the greatest variable and also the least controllable, since it depends on the thickness and thermal conductivity of the specimen and on the thermal contact with the grid and cooling ring leading to the object cartridge which acts as a thermal sink.

Temperature rises can be high, under extreme conditions. The most important parameter appears to be the thermal conductivity of the specimen. Under normal operating conditions (100 kV accelerating voltage, 10 μ A beam current with 4 μ diameter beam), temperature rises of 70°C for Fe, 30°C for Al and 20°C for Au have been recorded⁽⁴⁹⁾.

b) Electron diffraction

When a parallel, monochromatic beam of electrons of wavelength λ , impinges at angle θ on a set of parallel atomic planes of interplanar spacing d , the electrons are diffracted if the condition $n\lambda = 2 d \sin \theta$, where n is integral, is satisfied. This condition is known as Bragg's Law. The only planes which diffract are those parallel to the electron beam and the angles of diffraction are very small, not more than 1° or 2°.

The Bragg diffracted beams, travelling at small angles to the incident beam, are focused by the objective lens to form a transmission diffraction pattern in the back focal plane. Under transmission microscopy conditions, the objective lens aperture does not allow the Bragg reflections to pass through to the final image. Normally, the intermediate and projector lens systems are focused on the first intermediate image of the objective lens to produce a magnified image on the final screen. If, however, the objective and condenser apertures are withdrawn, and if the strength of the intermediate lens is reduced so that the back focal plane is focused on the final screen, a transmitted diffraction pattern of the

illuminated area of the specimen is observed. The area of the specimen illuminated by the beam and contributing to the diffraction pattern is controlled by the insertion of a diffraction aperture.

Since θ is always small for electron diffraction, it can be shown from Fig. 4 that $L.2\theta = R$, where L = focal length of the objective lens and R = distance from the diffraction spot to the centre of the screen. Now, the Bragg equation may be written:

$$\lambda L = 2 d\theta.$$

$$\text{Hence } \lambda L = Rd \text{ and } d = \frac{\lambda L}{R}.$$

Thus the interplanar spacing d may be determined by measuring distance R from the spot to the centre of the screen if λL is known.

λL is termed the diffraction or calibration constant.

Determination of calibration constant

Variations in H.T. supply and focussing errors of the intermediate and objective lenses may give rise to error in evaluating d but the most likely source of error is variation in specimen position with respect to the final screen. Since the constant λL is directly proportional to the focal length of the objective lens (for focussed specimens), there is normally a change of about 30%/mm specimen shift. For the Siemen's Elmiskop 1, the calibration constant decreases by 4%/mm rise in specimen provided no lens currents are changed.

For accurate work, the calibration constant must be determined for each diffraction pattern recorded. The simplest method of

determining the calibration constant is to use an evaporated film of thalloys chloride. This substance is stable in the electron beam and exhibits sharp diffraction rings with no anomalous reflections. It is easier to measure the diameter D of the ring rather than R , the distance from the ring to centre of the screen. The diameters of the three most intense diffraction rings are measured, and the interplanar spacings corresponding to these reflections found from the A.S.T.M. file. Hence a mean value of $\lambda L = \frac{d \times D}{2}$ is determined.

Selected area diffraction

This technique enables one to take diffraction patterns from very small areas of the specimen and to correlate the features observed in the micrographs and the crystallographic structure of the specimen.

By the insertion of an aperture of diameter D in the plane of the intermediate image, only those electrons passing through an area of diameter D/M on the specimen will reach the final screen, where M is the magnification of the objective lens (usually about $\times 25$). If D is 25μ , the diameter of the selected area is about 1μ . A bright field micrograph of the area selected by the diffraction aperture and the diffraction pattern from that area may be recorded on the same photographic plate.

c) The interpretation of electron diffraction patterns.

The concept of the reciprocal lattice and the sphere of reflection

The easiest way of interpreting electron diffraction patterns is by means of the reciprocal lattice concept:

The reciprocal lattice of a crystal lattice is a three dimensional network of points, the origin of the reciprocal lattice coinciding with the origin of the real lattice. Each point in the reciprocal lattice represents a family of planes in the real lattice. The distance from each point in the reciprocal lattice to the origin is inversely proportional to the interplanar spacing of the set of planes it represents. The direction from the origin to the reciprocal lattice point is the same as the direction of the normal to the planes. The higher order diffractions corresponding to $n = 2, 3, \dots$, are considered equivalent to 1st order diffractions having phase difference λ and arising from imaginary planes having interplanar spacing of $d/2, d/3$, and having indices $(2h \ 2k \ 2l), (3h \ 3k \ 3l)$ etc. Each of the higher order diffracted beams, or imaginary higher order diffracting planes, is represented by a reciprocal lattice point. Since Miller indices are reciprocal quantities, the indices of the reciprocal lattice points are the same as the Miller indices of the corresponding planes in the real lattice.

A concept to be considered in conjunction with that of the reciprocal lattice is the Ewald sphere of reflection:
Let a set of atomic planes be drawn at point C, and an incident beam impinge upon them at angle θ . As shown in Fig. 5, consider the vector length $1/\lambda$ from C to O, this vector being parallel with the incident beam. Let O be the origin of the three dimensional reciprocal lattice

corresponding to the real lattice of the crystal, but for this purpose displaced by $1/\lambda$ from the centre of the crystal. A sphere of reflection of radius $1/\lambda$ is drawn about C. Consider the reciprocal lattice point R, drawn at a distance ρ from O and lying on the sphere of reflection as shown.

Vector CR must represent a diffracted beam since

$$\rho = \frac{2 \sin \theta}{\lambda}$$

and, by definition $\rho = \frac{1}{d}$

hence $2 d \sin \theta = \lambda$ - Bragg equation.

Thus diffraction occurs only when the corresponding reciprocal lattice point lies on the sphere of reflection corresponding to the wavelength of the incident radiation. In the electron microscope, the wavelength of the electron beam is about 0.05 Å whereas d , the interplanar spacing is usually 1 - 2 Å and so the radius of the sphere of reflection is large compared to the distance between reciprocal lattice points. Hence, for practical purposes, the surface of the sphere of reflection may be considered planar.

Thus, the complete diffraction pattern to be expected from a crystalline specimen for any given orientation with respect to the electron beam can be predicted merely by plotting that reciprocal lattice plane of the crystal which lies normal to the electron beam and passes through the origin of the reciprocal lattice.

Structure factor

The resultant wave scattered by all the atoms of a unit cell is called the structure factor F , and $|F|$ is the ratio of the amplitude of the wave scattered by all the atoms in the unit cell to the amplitude of the wave scattered by one electron. In terms of reciprocal lattice co-ordinates the structure factor may be written

$$F_{hkl} = \sum_i f_i(\theta) e^{-2\pi i (hu_i + kv_i + lw_i)}$$

where u_i , v_i and w_i are fractional co-ordinates of the atom i and $f_i(\theta)$ is the atomic scattering amplitude for atom i . For a unit cell with a centre of symmetry the sine terms in the above expression cancel out and the expression becomes

$$F_{hkl} = \sum_i f_i(\theta) \cos 2\pi (hu_i + kv_i + lw_i).$$

From this expression it is obvious that not all reciprocal lattice points will give rise to Bragg reflections. Depending on symmetry and on the values of h , k and l the structure factor will be zero and reflections from the hkl reciprocal lattice point will not be observed.

In the case of a body-centred tetragonal lattice, reflection from the reciprocal lattice point hkl will arise only if $h + k + l = 2n$ where n is an integer. Thus for β -Sn, the allowed reflections are: 200, 101, 301, 002, 400, 202, 501, 103, 600, 303

Forbidden reflections, however, are sometimes observed as a result of double diffraction. That is, they arise from the vectorial addition, in reciprocal space, of two allowed reflections which are simultaneously activated.

Diffraction patterns

Polycrystalline specimen

For randomly oriented aggregates of polycrystals, the reciprocal lattice becomes a series of spheres concentric with the origin of the reciprocal lattice. The diffraction pattern may be regarded as the superposition of all possible reciprocal lattice planes, corresponding to all possible orientations of the crystals with respect to the electron beam. The radii of the rings are given by $1/d_{hkl}$.

Single Crystals

As demonstrated previously by the construction of the sphere of reflection, the diffraction pattern from a single crystal will be the reciprocal lattice plane of the crystal which lies normal to the incident beam and which passes through the origin of the reciprocal lattice.

The condition for the reciprocal lattice point (hkl) to lie on the (uvw) reciprocal lattice plane containing the origin is $hu + kv + lw = 0$. This geometrical relationship is used to determine the orientation of the crystal with respect to the electron beam i.e. in assigning values to (uvw) , the reciprocal lattice plane of those

planes of the crystal which lie normal to the beam.

If the diffraction pattern is known, then (hkl) indices can be assigned to the spots, once d_{hkl} has been evaluated. It is usual to assign indices to three spots which, together with the origin, make up a parallelogram. By trial and error, a consistent set of indices is chosen such that

$$[h_1 k_1 l_1] = [h_2 k_2 l_2] + [h_3 k_3 l_3]$$

All other points in the diffraction pattern may now be indexed by simple vector addition. Since these points all lie in the

(uvw) reciprocal lattice plane, $h_1 u + k_1 v + l_1 w = 0$,

$$h_2 u + k_2 v + l_2 w = 0,$$

$$h_3 u + k_3 v + l_3 w = 0.$$

Hence, $(uvw) = (k_1 l_2 - l_1 k_2, l_1 h_2 - h_1 l_2, h_1 k_2 - k_1 h_2)$. This immediately gives the crystal axis $[uvw]$ which is parallel to the electron beam.

A spot pattern will also be obtained from a specimen consisting of an aggregate of single crystals, where the three crystallographic axes of each crystal are all parallel to the corresponding crystallographic axes of every other crystal.

Textured polycrystals

Consider an aggregate in which each crystal has the same crystallographic axis $[uvw]$ aligned in a certain direction, while the other two axes are randomly oriented with respect to the corresponding axes of the other crystals. The reciprocal lattice for such an aggregate is obtained by rotation about the axis of

preferred orientation $[uvw]$, so that each reciprocal lattice spot is extended to a continuous ring. The hkl indices of the rings which lie in the successive planes is given by $hu + kv + lw = N$ where $N = 0, 1, 2 \dots$

If the axis of preferred orientation $[uvw]$ is parallel to the electron beam, only those rings in the diffraction pattern which satisfy the condition $hu + kv + lw = 0$ will be present. That is, the indices of the rings in a diffraction pattern from a polycrystalline aggregate with axis of preferred orientation $[uvw]$ parallel to the electron beam will be the same as the indices of the spots in a diffraction pattern of a single crystal whose crystallographic axis $[uvw]$ is parallel to the beam.

Thus for an textured aggregate of β -Sn where $[uvw] = 020$, the rings present in the diffraction pattern will have indices 200, 101, 301, 401, 501, 600, 303 and 701, i.e. only rings with indices $h0l$, where $h = 0 \dots n$, $l = 0 \dots n$, except those rings where $h + l = 2n$ (which are forbidden by the structure factor for a body centred tetragonal lattice) will be observed.

If the specimen is tilted about an axis perpendicular to $[uvw]$, the ring pattern is broken into a series of arcs. Along the diameter parallel to the axis of tilt, the arcs coincide with the original ring pattern, but become shorter as the tilt angle is increased. Along the perpendicular diameter, the original rings disappear and new ones appear as tilting causes the sphere of reflection to cut the

plane of the reciprocal lattice circles $ku + kv + lw = 1, 2, 3$ etc. Each new arc first appears as a single arc along the diameter perpendicular to the tilt axis, but further tilting causes it to split into two and these two arcs travel in opposite directions around the normal diffraction ring, towards the diameter parallel to the tilt axis.

d) Image contrast

Image contrast arises from the Bragg scattering of the electron beam by the crystalline specimen. Of the electrons emerging from the crystal, some have been diffracted by lattice planes and the rest are transmitted. Diffraction contrast is obtained by placing an aperture in the system which lets through either the transmitted beam (bright-field image) or a diffracted beam (dark-field image).

In the bright-field image, if the incident electron beam intensity is taken as unity and that of the diffracted beam as I_D , then the intensity of the transmitted beam is $1 - I_D$. If the incident beam passes through a defect in the crystalline lattice, it will encounter a localised change in diffraction conditions and so the transmitted intensities are correspondingly modified. Since Bragg angles are small, only those planes approximately parallel to the electron beam are capable of diffracting electrons out of the objective aperture and giving rise to image contrast.

In order to explain the contrast observed at lattice defects

it is necessary to calculate the intensity from a perfect crystal and see how this intensity is modified by the presence of defects.

If an electron wave, represented by the function $\exp [2\pi i k_0 r]$ where k_0 is the wave vector of magnitude $1/\lambda$ is incident on an atom at position r , there will be an elastically scattered wave $\exp [2\pi i k_1 r]$, with a phase difference of $2\pi (k_1 - k_0)$ when k_1 is the wave vector of the diffracted wave. If the crystal is not oriented exactly at the Bragg angle, then the reciprocal lattice point will lie either inside or outside the sphere of reflection as shown in Fig. 5. The phase difference is then $2\pi r (\rho + s)$ where ρ is the reciprocal lattice vector of the lattice plane giving rise to the reflection and s is the vector indicating the deviation of the reciprocal lattice point from the reflection sphere. To obtain the total scattered amplitude from a crystal it is necessary to sum all the scattered amplitudes from all the atoms in the crystal, i.e. to take account of all the different path lengths for rays scattered by different atoms. Since most of the intensity is concentrated near the reciprocal lattice point it is sufficient to calculate the amplitude diffracted by a column of crystal in the direction of the diffracted beam. Thus, if t is the crystal thickness, the amplitude scattered is proportional to

$$\int_{-t/2}^{+t/2} \exp. [2\pi i (\rho + s) \cdot r] dr$$

Since $p \cdot r$ is an integer, this reduces to

$$\int_{-t/2}^{+t/2} \exp. [2\pi i s r] dr \simeq \sin \pi t s / \pi s.$$

Thus the diffracted intensity from such a column is

$$I \propto \sin^2 \pi t s / (\pi s)^2.$$

From this equation, it is evident that the diffracted intensity oscillates with the depth of the crystal with periodicity $1/s$. This sinusoidal variation in intensity gives rise to the dark and light fringes observed in wedge-shaped crystals. Another type of contrast observed in perfect crystals is the bend or extinction contour, observed in crystals which are slightly bent or buckled, so that the orientation of the crystal varies from place to place. Part of the buckled area will be oriented at the Bragg angle, so that strong diffraction occurs and that area appears dark.

When the crystal is imperfect, certain atoms are displaced from their true lattice positions. Thus, if an atom at r_n is displaced by a vector R , the amplitude of the wave diffracted by this atom is multiplied by an additional phase factor $\exp [2\pi i (k_1 - k_0)R]$.

Since $(k_1 - k_0) = p + s$, the amplitude scattered by the imperfect crystal is proportional to

$$\int_{-t/2}^{+t/2} \exp. [2\pi i (p+s)(t+R)] dr$$

which reduces to

$$\int_{-t/2}^{+t/2} \exp [2\pi i (s \cdot r + p \cdot R)] dr.$$

since $\rho \cdot r$ is an integer and $s \cdot R$ is small and may be neglected in comparison with $\rho \cdot R$. Thus the amplitude and hence the intensity may differ from that scattered by a perfect crystal depending on whether the phase factor $2 \rho \cdot R$ is finite or not. Image contrast is obtained when $\rho \cdot R = 0$, where R is the atomic displacement. This is mechanism for contrast at dislocations and stacking faults.

If the objective aperture is displaced from its normal axial position so as to receive an elastically scattered diffracted beam, a dark field image is obtained. Only these parts of the crystal contributing to the selected reflection will be in bright contrast. A dark-field image obtained in this way tends to be distorted since it is formed by rays travelling at an angle to the instrument axis and therefore suffers from spherical aberration and astigmatism. Alternatively, a perfect dark field image is obtained if the electron gun is tilted so that the selected reflection travels down the axis.

The dark-field image is the complement of the bright field image. The technique provides a means of relating morphology to crystallographic structure.

/...

2. EXPERIMENTAL

1) Bulk Single Crystals

The material originally received for this work was in the form of single crystals of tin which had been grown by zone refinement. It was intended that the orientation of the crystal be determined by back-reflection Laue X-ray photography. A particular face of the crystal would be prepared and tin oxide grown on this face. The oxide film would be removed by a suitable extraction replica technique and the orientation of the oxide film determined by electron diffraction. Thus the relative orientation of the lattice of β -Sn to that of α -SnO might be determined.

However, the recrystallisation of tin takes place very readily and the material must be prepared in such a way that no mechanical deformation is introduced into the crystal. Ideally, the material should be cut with a chemical saw or electric spark cutter and polished or thinned in an electrolytic bath.

The crystals were cut to suitable size with a jewellers saw and hand polished on SiC papers followed by γ -alumina in paraffin. Even after very light and careful hand polishing, grain structure was observed when the etched material was observed in the light microscope, showing that recrystallisation had occurred.

Attempts to produce good extraction replicas from a polished face of a tin crystal were not successful. Among the methods employed was Bright's technique⁽⁸⁾ of coating the tin surface with carbon, or with carbon and then formvar for mechanical support, and then removing the replica by amalgamating the substrate with mercury. Another extraction technique involved the removal of the replica in an I_2/KOH bath. Other methods included the coating of the tin surface with carbon, formvar, collodion, formvar/carbon and bedacryl and removal of the replica either by stripping in water or stripping manually with sellotape.

ii) The preparation of thin evaporated films

a) Epitaxial films

In order to obtain epitaxial films, several techniques were employed whereby tin was evaporated in vacuo onto various substrates at different temperatures.

Apparatus

All evaporations were carried out in the Edwards 12E coating unit. One of the electrodes in the coating unit was modified in order that the substrate might be cooled externally by liquid nitrogen.

For this purpose, a brass plate was brazed onto a narrow copper tube which encased a similar tube of narrower bore. The two concentric tubes were carefully bent and passed through the modified electrode in the coating unit. The metal base of a modified electrode was screwed onto threads on the copper tube and a vacuum seal ensured by a rubber O-ring between glass tube and metal base. The tubes outside the coating unit were bent upwards and lagged with asbestos and tin foil for thermal insulation. A glass funnel was sealed onto the innermost copper tube. Liquid nitrogen was poured into the funnel which was then covered with a rubber bung to force the liquid nitrogen up the inner tube to the brass plate and to escape via the outer tube. In this way, it was possible to lower the temperature of the brass plate, inside the bell-jar, to -160°C . The apparatus is shown in Fig. 6.

Method of evaporation

It proved extremely difficult to evaporate tin from a metal filament and obtain consistent film thickness. Tungsten and molybdenum filaments in the form of loops and helices were used without success. Due to the large difference between the M.Pt. of tin (232°C) and the B.Pt. (1189°C at 10⁻² torr), the tin would frequently drop off the filament wire before evaporation was complete. Satisfactory results were obtained when tin was evaporated downwards onto the substrate through small holes drilled in the bottom of a molybdenum boat.

A molybdenum boat was cleaned by flashing in vacuo and three holes, 1 mm in diameter, were drilled in the bottom of the boat. Sufficient tin to form a continuous evaporated film, 100 Å in thickness, was placed in the boat. The thickness of the evaporated film was calculated from the formula

$$t = \frac{4}{3} \times \frac{m}{4\pi r^2 p}$$

where t = thickness of evaporated film

r = distance between substrate and evaporating source

p = density of tin

m = mass of tin evaporated.

A metal shield with a hole 1 cm in diameter was placed between the filament and substrate to minimise damage done to the growing film by radiant heat. The pressure inside the bell-jar was reduced

to 10^{-5} torr and tin was continuously evaporated from the molybdenum boat at the high rate of 50 - 100 A per second. The high evaporation rate ensured that the minimum number of residual gas atoms were incorporated into the growing film. For several experiments the distance from the evaporator to the substrate was varied.

Preparation of substrates

Sodium chloride substrates of suitable size, $0.5 \times 1 \times 2 \text{ cm}^3$, were cleaved from a large single crystal along a (100) plane. The crystals were not polished as there is evidence that polishing may result in surface recrystallisation, rendering the substrates unsuitable for the formation of an epitaxial overgrowth⁽⁵⁰⁾.

In some cases the crystals were heated in vacuo at 480°C for 3 hours, prior to evaporation.

Mica substrates were also used. A sheet of mica was cleaved just prior to evaporation.

Evaporation of tin onto cooled substrates

The prepared substrate was placed on the brass plate and the pressure inside the bell-jar reduced to 10^{-5} torr. The inner copper tube was filled with liquid nitrogen and the plate cooled to -160°C for one hour. After this time the substrate reached a minimum temperature of -130°C .

After the evaporation, the substrate and condensed metal film were allowed to warm up in vacuo to room temperature.

Evaporation of tin onto a heated substrate

A prepared rocksalt crystal was clamped in a clean molybdenum boat. A Pt/Ir thermocouple was fixed into a small hole carefully drilled in the side of the crystal. The bell-jar was evacuated and the crystal heated electrically to 150°C. Tin was evaporated upwards from a clean molybdenum boat onto the surface of the rocksalt. A metal screen was again placed between substrate and evaporating source to minimise damage to the metal film. After evaporation, the substrate was allowed to cool in vacuo to room temperature.

Evaporation of tin onto a glass substrate

A glass substrate was cleaned and placed inside the bell-jar. Tin was evaporated onto the surface through the holes drilled in the bottom of a molybdenum boat.

Mounting of films for electron microscopy

A film of carbon, 100 Å thick, was evaporated onto the surface of the evaporated metal films to give mechanical support.

The combined films were removed from their substrates by partial immersion in a tank of distilled water. The combined carbon/tin film floated away from the substrate and was washed several times to remove traces of sodium chloride. The films were picked up on 200 - mesh copper grids and dried in an oven at 60°C for several hours, prior to examination in the electron microscope.

It was feared that the carbon backing film might inhibit the oxidation of the tin films or that the carbon film itself might be preferentially oxidised.

Attempts were made to back the epitaxial tin films with silica which is inert to oxidation:

A tin film was condensed onto a rocksalt substrate in the usual way and sufficient silica to form a film 100 Å thick was evaporated onto the surface of the film. The heat radiating from the evaporator was minimised by placing a metal screen over the rock-salt crystal. It was found, however, that the silica backing film was too brittle and inflexible to permit the combined film to be removed from the rocksalt without disintegrating.

Another approach involved covering the tin film with a 2% solution of formvar. The formvar was allowed to dry and the combined film removed from the substrate by wet stripping. The film was picked up on silica covered Pt/Ir mounts and allowed to dry. The mounts were washed in a bath of ethylene dichloride to dissolve away the formvar. However, difficulties arose at this stage. It was found impossible to dissolve away the formvar completely without the tin film curling up.

Since no alternative to carbon could be found, epitaxial films supported on carbon backing films were used for the oxidation experiments.

b) Decoration of rocksalt substrates

The state of perfection of the surface of a rocksalt crystal is very much influenced by the method of preparation of the surface⁽³⁴⁾. In order to examine the surface, decoration replicas were prepared:

A freshly cleaved piece of rocksalt was supported on a clean molybdenum boat clamped between two electrodes. The pressure in the bell-jar was reduced to 2×10^{-5} torr and the crystal annealed at 480°C for 3 hours. The temperature of the crystal was then lowered to 300°C and a small amount of gold was evaporated onto its surface.

After allowing the crystal to cool to room temperature in vacuo, a carbon film, about 100 Å thick, was evaporated onto the surface. The carbon film, with the gold nuclei adhering to it, was removed from the substrate by flotation in distilled water. The film was picked up on 200-mesh copper grids and dried before examination in the electron microscope.

c) Polycrystalline films

Several Pt/Ir mounts were covered with a thin film of formvar. The mounts were clamped in the bell-jar above a clean molybdenum boat. Sufficient 'silica' (an SiO/SiO₂ mixture was used) to form a film 100 Å thick was evaporated onto the mounts. The formvar film was removed from the mounts by firing them for a few seconds over a hot Bunsen.

Sufficient tin to form a 100 Å thick film was then evaporated onto the silica covered mounts. During the evaporation, the mounts were kept at room temperature.

The films were examined in the electron microscope and then heated in a vacuum of 10^{-5} torr for 1 - 2 hours at 200°C. The films were re-examined to check that no significant change had occurred in the size of the tin grains or in the degree of coverage of the silica film.

iii) Oxidation

a) Oxidations carried out in coating unit

The specimens were supported, tin film facing uppermost, on a molybdenum tray clamped between two electrodes. The bell-jar was evacuated and oxygen flushed through the bell-jar and roughing line. The pressure of oxygen in the bell-jar was then adjusted to $1 - 2 \times 10^{-2}$ torr. The temperature of the specimens, monitored by a Pt/Ir thermocouple attached to the molybdenum tray, was increased to $180 - 220^{\circ}\text{C}$. The specimens were oxidised under these conditions for times varying from 30 min to 7 hours.

After oxidation, the specimens were allowed to cool to room temperature before removal from the bell jar.

b) Effect of water vapour on reaction

In order to determine the effect of water vapour on the oxidation of epitaxial tin films, oxygen was passed through a bubbler of distilled water prior to admission to the bell-jar.

Specimens were heated as before to 200°C in this atmosphere for 90 min. The oxygen pressure in the bell jar was 2×10^{-2} torr.

c) Oxidations at atmospheric pressure

Polycrystalline tin films, mounted on silica covered Pt/Ir mounts, were introduced into a small open furnace. After flushing oxygen through the system, the rate of oxygen flow was regulated to 10 cc per minute. The specimens were heated to 180 - 200°C and oxidised for 60 - 90 min.

d) Oxidations carried out inside the electron microscope

A 5 litre bulb was attached to a vacuum line and evacuated. The bulb and line were then filled with oxygen to a pressure of 30 torr. The apparatus is shown in Fig. 7.

The fixed 300 μ aperture was removed from the electron microscope and the objective aperture drive replaced by a gas probe. The probe, shown in Fig. 8, consisted of a modified aperture drive, the driver of which was replaced by a hollow tube fitted with needle valve and coupling connections to the vacuum line. Fig. 9 shows the position of the gas probe in the microscope column.

A well oriented epitaxial tin film was inserted in the specimen holder, with the tin film facing downwards, and brought to sit in the normal position, about 4 mm above the gas inlet. The vacuum line was connected to the gas probe and the connecting line evacuated to 10^{-5} torr by the diffusion pumps of the electron microscope.

The electron beam current was increased to 24 μ A and oxygen bled into the electron microscope until the pressure recorded on the Penning gauge was $1 - 5 \times 10^{-4}$ torr. The local oxygen pressure

around the specimen would be considerably higher than this, since the Penning gauge is situated outside the microscope column, next to the diffusion pumps. The oxygen pressure was not allowed to exceed 5×10^{-3} torr, since the electron beam safety cut-out operates above this pressure.

Part of the tin film was selected by the 20μ diffraction aperture and was heated by the electron beam in this atmosphere for periods of time up to 90 min. The progress of oxidation was observed at 5min intervals by electron diffraction.

The usual build-up of contamination around the specimen at the rate of 1 A per minute would be counteracted by the continuous flow of oxygen around the specimen.

Oxidations were also carried out in a atmosphere of 1×10^{-4} - 5×10^{-4} torr of air.

iv) Viewing of specimens in electron microscope

All specimens were examined in the Siemen's Elmiskop I, operating at 80 kV.

Dark field microscopy and selected area diffraction techniques were frequently employed to enable correlation to be made between morphological features and crystallographic structure.

Measurement of micrographs of diffraction patterns

The accuracy of the determination of lattice spacings depends to a large extent on the evaluation of the camera constant λL .

A diffraction pattern of an evaporated film of thallos chloride was taken to calibrate every diffraction recorded. By measuring the diameter of the three most intense rings, which correspond to known interatomic spacings, λL the camera constant was evaluated from the

equation

$$\lambda L = \frac{d_{hkl} \times D}{2} .$$

/...

3. RESULTS

1) Orientation of thin films

a) Decoration of rocksalt substrates

Examination of the decoration replicas revealed that the gold nuclei were not aligned in straight lines characteristic of perfect vacuum-cleaved rocksalt, but in the swirls characteristic of air-cleaved rocksalt. A typical decoration replica is shown in Plate 1.

b) Effect of substrate, substrate temperature and substrate preparation on the orientation of thin evaporated films

Evaporation of tin on unannealed rocksalt cooled to -130°C

Most of the films examined consisted of textures oriented so that the $[200]$ axis of each crystal was parallel to the electron beam.

Plate 2 is a typical diffraction pattern from such an aggregate.

The experimentally determined interatomic spacings, the interatomic spacings recorded in the A.S.T.M. file and the hkl indices of the reflecting planes are listed overleaf:

Camera constant, determined from TlCl rings, = 40.0.

<u>D (mm)</u>	<u>d (Å)</u>	<u>d_{lit.} (Å)</u>	<u>hkl</u>
13.6	2.93	2.915	200
14.3	2.79	2.793	101
24.1	1.66	1.693	301
25.1	1.60	-	002
27.6	1.45	1.458	400
28.8	1.39	-	202
36.5	1.10	1.095	501
37.2	1.07	-	-
38.5	1.04	1.040	103
41.5	0.97	0.9718	600
44.0	0.91	0.9219	303

By inspection, only those rings are present which satisfy the condition $hu + kv + lw = 0$, where $[uvw]$, the axis of preferred orientation, is $[020]$. Reflections (002) and (202), normally forbidden by the structure factor for β -Sn were observed, and their present is attributed to simultaneous diffraction events⁽⁵¹⁾.

Quite frequently, it was observed that parts of the films were single crystals. Diffraction patterns from such areas showed that the single crystal films were oriented so that the $[200]$ or more rarely, the $[002]$ axis was parallel to the electron beam. A diffraction pattern from a (002) single crystal film is shown in Plate 3. (The reciprocal lattices of (200) and (002) oriented single crystals of β -Sn are shown in Figs. 10 and 11 respectively.)

Occasionally, diffraction patterns from (200) textured films, such as that shown in Plate 4, were observed. Here the rings have been split up into arcs. The crystals are tilted about an axis perpendicular to the $[020]$ axis. Along the diameter parallel to the tilt axis the arcs coincide with the original ring pattern of Plate 2 but become shorter as the tilt angle increases. Along the perpendicular diameter, the original rings have disappeared and new rings, or rather arcs, whose hkl indices satisfy the condition $0h + 2k + 0l = 2$ appear.

The spacings and indices for Plate 4 are listed below:

Camera constant = 39.4

Arcs corresponding to condition $0h + 2k + 0l = 0$ (i.e. along diameter parallel to tilt axis)			Arcs corresponding to condition $0h + 2k + 0l = 2$ (i.e. along diameter perpendicular to tilt axis)		
<u>D (mm)</u>	<u>d (Å)</u>	<u>hkl</u>	<u>D (mm)</u>	<u>d (Å)</u>	<u>hkl</u>
13.5	2.92	200	19.5	2.00	211
14.0	2.81	101	26.8	1.48	112
23.7	1.66	301	30.5	1.29	411
27.0	1.46	401	32.9	1.20	312
36.0	1.09	501			
38.0	1.04	103			
40.8	0.97	600			

In Plate 5, the arcs along the diameter perpendicular to the tilt axis have been split in two by further tilting.

On these diffraction patterns, corresponding to a (200) oriented film tilted about its $[002]$ axis, it was observed that segments of

arc which were diametrically opposed were not in the same straight line. The angular deviation from 180° was $+5^\circ$.

All films examined were stable in the electron beam.

Evaporation onto vacuum annealed rocksalt cooled to -130°C

Tin films deposited on rocksalt which had been vacuum annealed at 480°C for 3 hours exhibited better orientation than those deposited on unannealed rocksalt.

Electron diffraction showed that these films approximated to single crystal films of (200) orientation. The azimuthal deviation in crystallite orientation was about 10° , as seen in Plate 6. The spacings and hkl indices of the reflections in this pattern are shown below:

Camera constant = 38.0

<u>D (mm)</u>	<u>d (Å)</u>	<u>hkl</u>
13.0	2.92	200
13.6	2.79	101
22.9	1.66	301
24.0	1.58	002
26.1	1.45	400
27.6	1.38	202
35.0	1.09	501
35.6	1.08	

All films examined were stable in the electron beam.

Evaporation onto rocksalt at room temperature

Electron diffraction revealed that the tin films were polycrystalline. Some degree of preferred orientation was indicated by the arcing on the 200, 101, 301 and 400 rings and, perpendicular to these arcs, arcing on the 411, 420 and 312 rings. The intensity of the 220 reflection was unusually low. This indicated that there was some tendency toward a (200) orientation.

b) Effect of electron beam bombardment on tin films deposited at increased distance from the evaporator

Tin was deposited onto cooled rocksalt as before but the distance between evaporating source and substrate was greatly increased. The structure and properties of the (200) textured films differed from those prepared earlier.

At the relatively low beam current of $12\mu\text{A}$, the (200) textures were observed to recrystallise within a few seconds to perfect (200) single crystal films. An example of a perfect (200) single crystal film is shown in Plate 7.

During recrystallisation, the distribution of electron scattering planes in the crystals altered, as indicated by changes in image contrast, but the shape and size of the crystals remained the same. * The (200) single crystal orientation was quite stable and persisted while the specimen was heated in the electron beam up to the point when the heat dissipated by the beam current ($40\mu\text{A}$)

* i.e. no significant crystal growth took place.

was sufficient to melt the tin. At this point, two diffuse halos, characteristic of molten tin, were observed.

Occasionally, the (200) textured film recrystallised to form a (002) single crystal film.

c) Evaporation techniques producing polycrystalline films

When tin was evaporated onto rocksalt heated to 150°C or onto mica cooled to -130°C or onto silica films at room temperature, polycrystalline films were obtained.

The diffraction pattern of a polycrystalline tin film is shown in Plate. 8.

ii) Morphology of thin films

a) Textured films

Regardless of film thickness, tin was deposited in the form of inter-connected islands of mean diameter 1400 Å. The island diameters varied from 500 - 3300 Å. They were separated by channels of mean width 90 Å. Channel width varied from 25 - 150 Å.

The typical morphology of the textured films is shown in Plate 9.

b) Single crystal films

These were very similar in appearance to the textured films.

c) Polycrystalline films

The substrate was covered by a continuous tin film. The crystallites were faceted, unlike those observed in the oriented films. No channels were observed between the crystals. The films were very contrasty and dislocations and extinction bands were observed in the crystals. Average grain size was 2,500 Å.

A typical polycrystalline tin film (silica substrate) is shown in Plate 10.

iii) Oxidation of thin tin films

a) Composition of oxide

1) Oxidation of epitaxial tin films in coating unit

Epitaxial tin films of orientation (200) and of thickness 200 Å were heated in the coating unit to 120°C in an atmosphere of 10^{-2} torr oxygen for periods of 10 min and 20 min. Electron diffraction revealed that no crystalline oxide had formed.

Similar specimens were heated to 200°C for 30 min. Selected area diffraction, using a 30μ aperture, revealed reflections belonging to α -SnO. Such diffraction patterns were weak and the reflections attributed to α -SnO were observed not as spots but as spikes which increased in length as d_{hkl} increased, characteristic of a very thin film. A typical diffraction pattern is shown in Plate 11.*

The same specimens were replaced in the bell-jar and oxidised for a further 40 min at 200°C, bringing the total exposure time to 70 min. Selected area diffraction revealed that all the tin had been oxidised to α -SnO. A selected area diffraction of the α -SnO film is shown in Plate 12.

Repetition of the oxidation of the tin films for one hour at 200°C in 10^{-2} torr oxygen showed that α -SnO was the only oxidation product formed under these conditions.

The presence of the carbon backing film did not appear to have any significant effect on the progress of oxidation.

* Plate 11 shows spots arising from sectioning by the Ewald sphere of spikes originating in a upper lower plane of the reciprocal lattice - characteristic of a very thin film. /...

2) Effect of water vapour on reaction

Prior to admission into the bell jar, oxygen was passed slowly through a bubbler of distilled water. Epitaxial (200) tin films, 100 Å in thickness were heated to 200°C for 95 min in an atmosphere of 10^{-2} torr moist oxygen. Examination of the specimens by electron diffraction revealed that only α -SnO was formed.

3) Oxidation in electron microscope

An area of a perfect single crystal tin film, oriented so that the [200] crystal axis was parallel to the electron beam was selected by the diffraction aperture. The electron beam current was adjusted to 12 μ A and the selected area was heated by the beam in an atmosphere of 2×10^{-4} torr of air for 30 min. After this time, electron diffraction revealed the presence of a thin film of α -SnO.

Another area of the specimen was selected and the beam current adjusted to 24 μ A. The specimen was oxidised at 2×10^{-4} torr air pressure for 60 min. Electron diffraction revealed strong reflections attributed to α -SnO, and in addition, diffuse rings which could not be assigned to α -SnO or to β -Sn. The rings were not sufficiently sharp to be measured accurately.

The experiment was repeated using beam current of $22\mu\text{A}$, and in atmosphere 2×10^{-4} torr oxygen. After 30 min, strong reflections from α -SnO were observed along with weak diffuse rings. After 60 min exposure, the diffuse rings became sharp and more intense. The three strongest rings corresponded to the three most intense reflections from SnO_2 . As the period of oxygen exposure increased, it was observed that the α -SnO reflections decreased in intensity while the reflections attributed to SnO_2 increased in intensity.

Plate 13 is an electron diffraction pattern taken after 60 min exposure to an atmosphere of 2×10^{-4} torr oxygen with beam current of $22\mu\text{A}$.

Camera constant = 40.8

<u>D (mm)</u>	<u>d (Å)</u>	<u>Sn (spots)</u>	<u>hkl</u>	
			<u>SnO (arcs)</u>	<u>SnO₂ (rings)</u>
8.5	4.80		001	
12.2	3.34			110
13.9	2.915	200		
14.4	2.82	101		
14.6	2.79	101		
15.6	2.62			101
16.9	2.42		002	
23.3	1.75			211
24.6	1.66	301		
25.5	1.60		211	
27.5	1.49		{ 103	
			{ 202	
38.2	1.07	501		

4) Oxidation of polycrystalline films in coating unit

A 100 Å film of polycrystalline tin, on a silica substrate, was oxidised for 20 min at 190°C under an oxygen pressure of 10^{-1} torr. Electron diffraction patterns exhibited

reflections belonging to β -Sn and to α -SnO, indicating that oxidation was not complete.

The films were oxidised under the same conditions for a further two hours. After this time, the tin film had been completely oxidised to α -SnO, as shown by electron diffraction. See plate 14. The spacings and hkl indices of the reflections shown in Plate 14 are listed below:

Camera constant = 40.85

<u>D (mm)</u>	<u>d (A)</u>	<u>d (A)</u> _{lit.}	<u>hkl</u>
0.86	4.85	4.85	001
1.38	2.96	2.989	101
1.45	2.70	2.688	110
1.73	2.40	2.418	002
2.00	2.04	2.039	102
2.15	1.90	1.901	200
2.28	1.79	1.797	112
2.54	1.59	1.604	211
2.75	1.49	1.484	103
3.50	1.16	1.152	104
4.00	1.02	1.020	204
4.90	0.83	-	-

SnO₂ was not detected.

The experiment was repeated but the time of oxygen exposure was increased to 7 hours. Again, α -SnO was the only product of oxidation.

Tin films, 100 A in thickness, were heated at 240°C for 30 min in an atmosphere of 10⁻¹ torr of oxygen. Examination in the electron microscope revealed that the tin, which melts at 232°C had coalesced into dense globules. Highly crystalline flakes of α -SnO were identified.

5) Oxidation of polycrystalline films at atmospheric pressure

^o
Tin films, 500 Å in thickness, were oxidised in a stream of oxygen at 200 °C for 1 hour. Examination of the films showed that α -SnO was the only product of oxidation.

/...

b) Orientation of oxide

1) Oxidation of epitaxial films in coating unit

When textured tin films of orientation (200) were oxidised for 30 min at 200°C in an atmosphere of 10^{-1} torr oxygen, spikes attributed to α -SnO were observed in the diffraction patterns. The reflections were very weak and it was difficult to assign an orientation to the thin oxide layer. A typical diffraction pattern is shown in Plate 11. The spacings corresponding to the reflections observed on this pattern are listed below:

Camera constant = 39.3

<u>D (mm)</u>	<u>d (Å)</u>	<u>d_{lit} (Å) SnO</u>	<u>hkl</u>
7.1	5.45		
8.5	4.83	4.85	001
13.9	2.83		
16.2	2.42	2.418	002
21.5	1.83	1.79	112

On the basis of the reflections which could be indexed, it would appear that there is some degree of preferred orientation, and the orientation of the oxide tends to be (110).

Generally, some reflections were absent from the diffraction patterns observed, indicating a tendency for the oxide to grow in an oriented manner. For example:

Camera constant = 40.0

<u>D (mm)</u>	<u>d (Å)</u>	<u>hkl</u>
6.6	6.07	-
8.4	4.85	001
12.8	3.11	-
16.6	2.41	002
19.2	2.06	102
20.8	1.92	200
25.0	1.60	211
33.2	1.20	004

In the diffraction pattern on which the above spacings were measured reflections from planes 101, 110, 112, 103, 104 were absent. However the orientation of the oxide cannot be specified from the reflections observed.

When the same film was oxidised, under the same conditions for further 40 min., selected area diffraction revealed that the oxide was strongly oriented with the $(\bar{1}11)$ plane perpendicular to the electron beam. A selected area diffraction pattern of the oriented oxide is shown in Plate 12. The spacings are recorded below:-

Camera constant = 40.0

<u>D (mm)</u>	<u>d (Å)</u>	<u>hkl</u>
13.45	2.98	101
14.90	2.68	110
22.20	1.88	112 (see over)
25.00	1.00	211
26.90	1.49	202
29.70	1.35	220

The above indices (hkl) satisfy the relation $hu + kv + lw = 0$ where $[uvw]$, the axis of preferred orientation, is $[\bar{1}11]$.

/...

Although the $(\bar{1}11)$ orientation was predominant, other weaker diffraction patterns were observed occasionally. * These weak reflections corresponded to a $(\bar{1}\bar{1}0)$ orientation as shown in Plate 15. The degree of orientation of the crystals was poor, as judged from arcing of the spots. Spacings and reflections from the pattern shown in Plate 15 are given below:

Camera constant = 40.0

<u>D (mm)</u>	^o <u>d(A)</u>	<u>hkl</u>
8.4	4.85	001
13.5	2.96	101
15.0	2.66	110
16.5	2.42	002
22.0	1.82	112
24.5	1.60	211
30.0	1.34	220

All reflections except those with indices 101 and 211 arise from the $(\bar{1}\bar{1}0)$ orientation of a single crystal film.

Over large areas, i.e. those selected by the 150μ diffraction aperture, the structure of the oxide was not that of an oriented single crystal film. All reflections were present in the electron diffraction patterns. However, those reflections which would be absent from the diffraction pattern of a $(\bar{1}11)$ oriented film, namely 002 and 200, were significantly very weak.

The experiment was repeated under the same conditions but for exposure time of 60 min. Electron diffraction confirmed that the structure of the oxide film consisted of areas of strongly oriented $(\bar{1}11)$ single crystals with a few areas corresponding to a less well defined $(\bar{1}\bar{1}0)$ orientation. Reflections corresponding

* The 112 reflection is an example of this.

/...

to the $(\bar{1}11)$ oriented oxide were much more intense than those from the $(\bar{1}10)$ oriented oxide.

2) Effect of water vapour on reaction

When (200) oriented tin films were oxidised at 200°C in the presence of 10^{-1} torr moist oxygen for 95 min., the structure of the oxide film was markedly different. The oxide film did not comprise an aggregate of crystals, predominantly oriented with their $[\bar{1}11]$ axes parallel to the electron beam, but of very large perfect single crystals, each single crystal flake being randomly oriented with respect to the neighbouring crystals.

3) Oxidation of epitaxial tin in electron microscope

At oxygen pressures of $1-2 \times 10^{-4}$ torr, the reaction proceeded extremely slowly. The reaction was much slower when carried out at $1 \times 10^{-4} - 2 \times 10^{-4}$ torr of air. Consequently the oxide diffraction patterns were weak and usually orientation was poor. It was found that the orientation of the oxide layer improved with increased exposure to oxygen.

A perfect single crystal tin film, with its 200 axis parallel to the electron beam, heated by an electron beam current of 12 A, was oxidised in 2×10^{-4} torr air pressure for 30 min. After this period of time, the electron diffraction pattern was characteristic of a thin, poorly oriented oxide film. Spacings and indices from a typical diffraction pattern are shown below:

/...

Camera constant = 40.05

<u>D (mm)</u>	<u>d (Å)</u>	<u>Intensity</u>	<u>hkl</u>	
8.4	4.82	S	001	SnO
13.6	2.98	W	101	SnO
13.8	2.93		200	Sn
14.25	2.79		101	Sn
16.7	2.42	S	002	SnO
19.6	2.06		102	SnO
22.5	1.80		112	SnO
24.9	1.62	S	003	SnO
27.1	1.49		202	SnO
			103	SnO
28.9				
33.6	1.21	S	004	SnO

Characteristic of all diffraction patterns of α -SnO grown under these conditions, there was an obvious preferential orientation along the $[010]$ crystal axis.

Another area, of the film comprising a (200) oriented single crystal, was selected. The electron beam current was adjusted to $24 \mu\text{A}$ and the selected area of tin heated in 2×10^{-4} torr of air for 60 min. After this time, the single crystal diffraction pattern corresponding to an oxide film oriented with its $[\bar{1}10]$ axis parallel to the electron beam was observed. Spacings and hkl indices are shown below:

Camera constant = 40.0

<u>D (mm)</u>	<u>d (Å)</u>	<u>hkl (SnO)</u>
8.3	4.82	001
16.5	2.42	002
22.0	1.82	112
24.8	1.62	003
28.7	1.39	113
33.5	1.21	004

Diffuse rings which could not be attributed to β -Sn or α -SnO were also observed. These could not be measured accurately. No reflections from β -Sn were observed in the diffraction pattern.

The experiment was repeated. An area of (200) single crystal tin film was selected by the diffraction aperture and heated by a beam current of 22μ A in an atmosphere of 2×10^{-4} torr oxygen. After 30 min exposure to oxygen, arcs attributed to α -SnO were observed and also the diffuse rings observed previously. With increased exposure to oxygen the reflections from α -SnO grew less intense while the rings grew more intense and were identified as SnO₂. The diffraction pattern taken after 60 min exposure is shown in Plate 13. This micrograph shows a thin film of SnO₂ (diffuse rings) which exhibits no tendency to preferred orientation and a film of α -SnO (arced rings) exhibiting some degree of preferred orientation have grown on a (200) oriented single crystal of β -Sn (spot pattern).

The experiment was repeated in an atmosphere of 2×10^{-4} torr of air using an electron beam current of 24μ A.

After about 30 min, faint arcs corresponding to the 001 and 002 reflections of α -SnO were observed. As the oxidation reaction proceeded spots were observed on the arcs. With prolonged exposure to oxygen, higher orders of reflection were

observed. These could be assigned to a $(\bar{1}\bar{1}0)$ oriented oxide layer. Gradually the intensity of the arcs decreased while the spot pattern increased in intensity indicating that the oxide layer was becoming more perfectly oriented as the period of exposure to oxygen increased.

After 90 min exposure to oxygen, a diffraction photograph was recorded which shows unequivocally the lattice fit of a $(\bar{1}\bar{1}0)$ oriented oxide layer growing on a (200) oriented single crystal tin film. - Plate 16. The spacings and hkl indices are shown below:

Camera constant = 41.2

<u>D (mm)</u>	<u>d (Å)</u>	<u>hkl (SnO)</u>	<u>hkl (Sn)</u>
8.5	4.85	001	
14.0	2.94		200
14.6	2.81		101
14.7	2.80		101
16.9	2.44	002	
23.0	1.79	112	
25.4	1.62	003	
25.8	1.60		002
30.2	1.36	113	
33.9	1.22	004	
37.1	1.11	114	
45.2	0.91	115	

The $[020]$ or $[200]$ axis of β -Sn and the $[\bar{1}\bar{1}0]$ axis of α -SnO are seen to be perpendicular to the plane of the film i.e. parallel to the electron beam. The $[200]$ or $[020]$ axis of β -Sn is parallel to the $[\bar{1}\bar{1}0]$ axis of α -SnO and the $[002]$ axis of β -Sn is parallel to the $[002]$ axis of α -SnO. Thus the $(\bar{1}\bar{1}0)$ plane of α -SnO lies parallel to the (020), or (200),

plane of β -Sn.

Examination of large number of diffraction patterns recorded after similar oxidation experiments, showed that the oxide layer, although not always a single crystal layer, was strongly oriented. All oxide diffraction patterns were characterised by strong arcs of index (001). The predominant oxide orientation was ($\bar{1}10$).

4) Oxidation of polycrystalline films

The oxide flakes were highly crystalline and were mainly large perfect single crystals oriented randomly with respect to each other and to the electron beam.

Double diffraction effects were frequently encountered. For instance, Plate 17 is a selected area diffraction photograph of a single crystal aggregate oriented with its [$\bar{1}11$] axis parallel to the electron beam. Plate 18 is also the diffraction pattern from a single crystal oriented with its [$\bar{1}11$] axis parallel to the electron beam, but features reflections normally forbidden by the structure factor for α -SnO.

5) Oxidation at atmospheric pressure

Electron diffraction revealed that the oxide film comprised large single crystals which were oriented randomly with respect to each other and to the electron beam. Many of the crystals

were very thick, and gave rise to anomalous diffraction effects.

c) Morphology of oxide

1) Oxidation of epitaxial films in coating unit

Light field micrographs showed that the oxide film grows in the form of interconnected islands whose diameter varies from 400 - 3000 Å. The average diameter of the islands was 1200 Å. The islands are separated by channels of mean diameter 120 Å as shown in Plate 19.

This form of growth was typical of all oxide films produced by the oxidation of epitaxial films under reduced pressure.

2) Effect of water vapour on the reaction

As shown in Plate 20, the morphology of the oxide films produced in moist oxygen is markedly different from those grown in dry oxygen.

Large highly crystalline sheets of oxide were observed. A common feature of the sheets was the large number of extinction contours visible, indicating that the oxide sheets were highly strained and buckled. The oxide flakes exhibited a number of cracks which appeared to radiate from the holes visible in each flake. Some of the cracks along the edges of the oxide flakes were saw-toothed. Generally, very narrow cracks appeared to broaden out into cracks with saw-toothed edges. The saw teeth were perfectly aligned across the crack.

Ridges, indicative of the buckling of the oxide flakes, were observed. These were enhanced when the specimen was shadowed with platinum/carbon at 15° , as shown in Plate 21. It was hoped that growth steps might be revealed by the platinum/carbon shadow on these large single crystals. (It has been postulated that α -SnO grows by a spiral growth mechanism⁽¹¹⁾). However growth steps were not observed.

An interesting feature of Plate 21 is the annular growth of α -SnO (Area A). These oxide rings were fairly common and always the oxide was highly strained and buckled as indicated by the extinction contours.

3) Oxidation in the electron microscope

The appearance of the oxide film was essentially the same as that of oxide films grown under reduced pressure in the coating unit. (See section (i) and also Plate 19).

4) Oxidation of polycrystalline films

Polycrystalline tin films, 100 Å in thickness, were oxidised for $2\frac{1}{2}$ hours at 200°C in a partial vacuum of 10^{-1} torr oxygen. Electron diffraction showed that the tin film had been completely oxidised to α -SnO.

From an examination of the samples in the electron microscope it was obvious that much surface diffusion had

taken place during or after oxidation. The silica film which had, before oxidation, been completely covered with a continuous tin film was now void of material in many areas.

Much of the oxide comprised crystalline aggregates of interlinked islands, very similar in appearance to the oxide formed when epitaxial films were oxidised under reduced pressure. Growing from these islands were oxide platelets which appeared to have grown laterally until they touched. Plate 22 shows an aggregate of interlinked islands from which several platelets have developed.

An interesting feature of the micrographs was the presence of loops of material visible on the silica background and at certain edges of the crystals, particular at angular edges. Although insufficient material was present to give rise to diffraction patterns which could be identified with certainty, it is reasonable to assume that these loops are composed of α -SnO. The effect is illustrated in Plate 23 (Areas A, B, C).

The experiment was repeated but this time the period of exposure to oxidation was 7 hours:

After exposure to oxygen for 7 hours, the appearance of the oxide crystals was generally similar to that observed in the previous experiment. However, surface diffusion, was enhanced, as was the size of the crystals and the perfection of

crystallinity. A feature which was not observed in the previous experiment was the formation of whisker-like growths of α -SnO. These are shown in Plate 24 (Areas A and B).

The specimens were shadowed with nickel/palladium from an angle of 15° . The oxide crystals were shown to be completely flat and thin enough for the coarser structure of the silica substrate to be highlighted through them, as seen in plate 25.

It is noteworthy that all regularly shaped, rectangular oxide platelets were found to have the same orientation (120) with respect to the electron beam. A selected area diffraction pattern of such a platelet is shown in Plate 26.

The effects of decreased exposure to oxygen were studied. Tin films were partially oxidised by heating at 190°C in an atmosphere of 10^{-1} torr oxygen for 20 min. Dark field microscopy proved a useful technique for the study of these specimens. Reflections from β -Sn and α -SnO were observed in the diffraction patterns. By placing the objective aperture over the tin reflections (101) and (200), those planes in the tin matrix film were highlighted leaving the large tin oxide crystals in dark contrast. This effect is shown in Plate 27. Conversely, when the (110) reflection of tin oxide was selected, the (110) planes in the tin oxide crystals were in bright contrast as shown in Plate 28.

The oxide was again highly crystalline and frequently of single crystal nature. Several elongated platelets were found oriented with their $[3\bar{3}1]$ crystal axes parallel to the electron beam.

Several tin films, 100 Å thick, were heated in an oxygen atmosphere of 10^{-1} torr for 30 min at 240°C .

The tin, which melts at 232°C , had coalesced into dense globules. The regions of silica devoid of tin were very contaminated. Thin flakes of α -SnO could be seen at the edges of the dense tin globules. Although the oxide flakes were highly crystalline their morphology was poorly defined, as shown in Plate 29. The well defined growth forms, such as platelets and whiskers, observed on specimens oxidised at lower temperatures were not observed.

The tin crystals were too thick to allow electron diffraction and so it was impossible to ascertain how thick an oxide layer had formed on the top surface of the tin globules. Plate 30 is a selected area diffraction photograph of an oxide flake growing at the edge of a tin globule. The oxide flake is a perfect single crystal oriented with its $[002]$ axis parallel to the electron beam.

5) Oxidation at atmospheric pressure

500 Å thick films of tin were heated at 200°C in an open furnace in a stream of oxygen for one hour.

The tin was completely oxidised after this time. The appearance of the specimens very different from that of the oxide films produced when 100 Å tin films had been oxidised under reduced pressure. Distinct needles and platelets and aggregates of small interlinked islands were not observed. Individual forms of crystal growth were not well defined and the surface of the mounts were almost completely covered by α -SnO. A typical micrograph is shown in Plate 31. Large oxide crystals were separated by narrow cracks of grain boundaries. Pin holes were frequently observed along these boundaries. From the large number of extinction contours, it was evident that the oxide film had undergone considerable stress. Evidently the strain arising from the 20% increase in specific volume during oxidation had been aggravated by a high oxidation rate.

Electron diffraction showed that the oxide film comprised large single crystals of varying orientation with respect to the electron beam.

4. DISCUSSION

i) Advantages of evaporation techniques of over replication

For the study of the lattice fit between β -Sn and α -SnO, bulk specimens consisting of single crystals of tin were found to be manifestly unsuitable.

The tin crystals could not be reduced to a manageable size and polished by mechanical means without the occurrence of recrystallisation.

Further difficulties arose in the production of good replicas. Several extraction replica techniques were employed in order to study the surface of a polished (and recrystallised) tin face. Some success was achieved using the mercury amalgam extraction technique devised by Britton and Bright⁽⁸⁾. However, the amalgamation of the tin substrate by mercury was a lengthy process and great difficulty was encountered in producing clean replicas uncontaminated by traces of tin or mercury. The "washing" of a carbon replica in a pool of mercury was rather unsatisfactory.

The study of tin oxidation using thin evaporated tin films proved much more satisfactory. The method was direct, involved no complicated stripping techniques and provided clean specimens.

The technique proved most useful for morphology studies and it was thought that more information about crystal growth would be obtained than by indirect replica methods. Using any replication technique there is a possibility that all particles or all types of particles are not extracted from the substrate. Also the fragments removed from the substrate are not necessarily present in the same relation to each other on the replica as they were on the substrate.

Once the technique for growing oriented tin films had been perfected, the orientation relationship between β -Sn and α -SnO could be derived in a relatively simple way, particularly when a selected area of tin film, whose crystal orientation was known, was oxidised inside the electron microscope and the reaction monitored directly by electron diffraction.

ii) The orientation, morphology and crystal growth of thin tin films

Epitaxial tin films were produced by the condensation of tin vapour onto freshly cleaved annealed rocksalt in a manner similar to that described by Vook⁽⁴²⁾.

Mechanism

Generally, metal films deposited onto low temperature substrates are highly disordered and contain a high concentration of defects. The condensation of a metal vapour corresponds to a very rapid quenching because the metal atoms impinging on the surface lose their energy very quickly. Consequently, many defects are frozen into the film. Indeed, ordered epitaxial films are usually produced by evaporation of the metal onto a heated substrate.

In order to explain this anomaly, Vook⁽⁴²⁾ suggested that at liquid nitrogen temperatures the evaporated tin film is polycrystalline and as the substrate temperature increases, the defects tend to anneal out. Also, the film is strained during warm-up by the greater thermal expansion of the rocksalt substrate. The strain prior to and during warm-up is relieved by the tin atoms orienting themselves in their minimum energy positions with respect to the rocksalt surface atoms and with respect to each other. That is, in order to relieve strain, the polycrystalline tin film recrystallises to an ordered, or epitaxial, film of lower energy.

Phase change

Above 13.2°C , tin exists as the body-centred tetragonal phase (β -Sn) but at 13.2°C undergoes a phase change to the low temperature modification (cubic α -Sn). Thus in the temperature range -160°C to 13.2°C , the cubic form is the most stable configuration, describing the minimum energy positions of the tin atoms with respect to each other.

Vook has apparently assumed, in his strain-anneal mechanism, that the tin is deposited as β -Sn. It is not unusual, when a crystal is being built up from its atoms, to find a modification which is unstable at the prevailing temperature and Ostwald's rule states that, in such circumstances, it is most likely to be the high temperature modification.

If the tin were initially deposited as polycrystalline α -Sn, then it is difficult to explain the formation of an epitaxial β -Sn film by the strain-anneal mechanism.

A polycrystalline deposit of α -Sn might recrystallise to an epitaxial deposit to relieve the strain of the greater thermal expansion of the substrate. However, at 13.2°C , α -Sn would recrystallise to β -Sn, the high temperature modification. Now, between 13.2°C and room temperature, there will be no appreciable thermal expansion of the substrate and therefore no driving force for the formation of an epitaxial growth. Therefore, one might expect the film at room temperature to comprise randomly oriented crystals of β -Sn.

Vacuum conditions

The admission of the equivalent of a few monolayers of reactive gas into the vacuum chamber markedly inhibits grain growth in a vacuum annealed metal film⁽⁵²⁾. The reactive gas probably prohibits surface diffusion in the metal film.

In this series of experiments, films were deposited onto the substrate and allowed to warm up to room temperature under a vacuum of 10^{-5} torr. Although the tin films were oriented with the a-axes of the crystals perpendicular to the plane of the film, they were generally not single crystal films but textures. It is felt that the presence of 10^{-5} torr air pressure inhibited the recrystallisation of oriented textures to form single crystal films.

Lattice fit between tin and the rocksalt substrate

The lattice fit of a- and c-axis oriented β -Sn crystals and a-axis oriented α -Sn crystals with the (100) of the rocksalt substrate will be considered.

When the a-axes of the β -Sn crystals are perpendicular to the (100) plane of the rocksalt substrate, then the parallel axes are Sn $[100]$ // NaCl $[\bar{1}00]$ with parallel faces Sn (100)//NaCl (100). A possible relationship between lattice planes is shown in Fig. 12, where parallel axes in the plane of the film are Sn $[010]$ //NaCl $[\bar{0}10]$ and Sn $[001]$ //NaCl $[001]$.

$$\% \text{ misfit along Sn } [010] \text{ axis} = \frac{100 \times (5.82-5.63)}{5.63}$$

$$= 3.38\%$$

$$\% \text{ misfit along Sn } [001] \text{ axis (taken over two Sn (001) spacings)} = 100 \times \frac{(2 \times 3.2)-5.63}{5.63}$$

$$= 12.8\%$$

When the c-axes of the β -Sn crystals are perpendicular to the (100) rocksalt plane, parallel axes are Sn $[001] // \text{NaCl } [100]$ with parallel faces Sn (001)//NaCl (001).

A possible lattice relationship is shown in Fig. 13, where parallel axes in the plane of the film are Sn $[100] // \text{NaCl } [100]$ and Sn $[010] // \text{NaCl } [010]$.

$$\% \text{ misfit along Sn } [100] \text{ axis} = 3.38\%$$

$$\% \text{ misfit along Sn } [010] \text{ axis} = 3.38\%$$

Let us consider now the possibility that the tin is condensed onto the rocksalt in the cubic form, α -Sn ($a = b = c = 6.49 \text{ \AA}$).

When the a-axes of the α -Sn crystals are perpendicular to the (100) rocksalt plane, as shown in Fig. 14, parallel axes in the plane of the film are Sn $[010] // \text{NaCl } [010]$ and Sn $[001] // \text{NaCl } [001]$.

$$\% \text{ misfit along } \alpha \text{-Sn axes } [010] \text{ and } [001] = \frac{6.49-5.63}{5.63} \times 100$$

$$= 15.3\%$$

The percentage misfit between a-axis oriented α -Sn and the (100) rocksalt plane is much higher than the misfit between a- or c-axis oriented β -Sn and the (100) rocksalt plane. The smallest misfit, 3.38% along two crystal axes, occurs for c-axis oriented

β -Sn crystals.

It must be remembered, however, that the best lattice fit is not the only criterion determining the most stable orientation for an epitaxial overgrowth.

Recrystallisation

In the present series of experiments, thin a-axis oriented textures were observed to recrystallise in the electron beam to form perfect a-axis oriented single crystal films and occasionally c-axis oriented single crystals. The latter observation was also made by Vook⁽⁴²⁾. The transformation from a- to c-axis orientation might be expected to occur quite readily since there is considerable similarity between the two structures. Fig. 15 shows two superimposed projections of the unit cell of β -Sn, one with the a-axis perpendicular to the plane of the paper and the other with the c-axis perpendicular to the plane of the paper. The ratio c:a is 0.5457.

Recrystallisation of the tin films occurred after 2 - 3 secs. in an electron beam current of $10\mu\text{A}$ and in a vacuum of 10^{-5} torr. Moreover recrystallisation was not impeded by the admission of oxygen in the electron microscope column. The oxygen pressure measured by the Penning gauge was 2×10^{-4} torr but the localised pressure around the specimen would be considerably higher than this. However a-axis

oriented textures, annealed at 200°C for 1 - 3 hours in the coating unit under similar vacuum conditions did not recrystallise to single crystal films.

Morphology

The films comprised a large number of interlinked islands separated by narrow channels.

It would appear that the tin nuclei were initiated all over the surface of the rocksalt. (There may have been some initial preferred nucleation at the rocksalt surface steps and dislocations but no evidence to support this was obtained.) The tin crystals appear to have extended laterally from the initial nuclei to form interlinked islands. Extinction contours were not observed implying that the films were essentially strain-free.

iii) The oxidation of thin films of tin

There are several differences between growing epitaxial films by deposition from the vapour phase and growing them by chemical attack from the vapour phase. The manner in which adsorption takes place on a surface is not clearly understood. The adsorbing atoms may dissolve in the substrate to some extent so that the chemical compound, in this case α -SnO, may form initially below the tin surface. The major difference between the two methods of epitaxial film growth is, of course, that in the case of chemical attack, the substrate contributes material to the deposit.

1. Oxidation of a-axis oriented textures in coating unit

The orientation of the oxide layer was predominantly $(\bar{1}11)$. Occasionally diffraction patterns corresponding to a thin layer of (110) oriented oxide were observed. The crystals in the $(\bar{1}10)$ orientation were not perfectly oriented.

All oxygen positions in the α -SnO structure may be described by a series of (111) planes as shown in Fig. 16.

Fig. 17 is a stereographic projection of the tin atoms in α -SnO onto the $(\bar{1}11)$ plane at distance $\frac{1}{2} d_{\bar{1}11}$ from that plane.

Electron diffraction revealed that the $(\bar{1}11)$ oriented oxide grew on the (200) oriented tin substrate. Thus the $(\bar{1}11)$ oxide plane and the (200) tin plane were parallel. Obviously the $[\bar{1}11]$ oxide axis and the $[200]$ tin axis were parallel but the relationship between the two other axes of oxide and substrate could not be specified.

The most plausible relationship between the $(\bar{1}11)$ oxide plane and the (200) tin plane is that which approximates most closely to the relation between the oxygen atoms in the $(\bar{1}11)$ plane of α -SnO and the neighbouring tin atoms (as shown in Fig. 17). A possible relationship between oxide and substrate planes is shown in Fig. 18. Parallel axes are Sn [010] // SnO [112] and Sn [001] // SnO [110] .

2. Effect of water vapour on the reaction

In general, the presence of water vapour enhances the rate of metal oxidation by facilitating the removal of electrons from the metal. It was reported by Britton and Bright that the rate of oxidation of tin foil in air with 80% humidity was twice as fast as the rate of oxidation in dry air⁽⁸⁾.

When β -Sn is oxidised to α -SnO there is a 20% increase in specific volume. Under humid condition it is to be expected that there would be even greater strain in the oxide crystals due to the enhancement in oxidation rate. There was ample evidence of strain and buckling of the flakes in the numerous extinction contours visible in the oxide flakes.

There were differences in orientation between flakes separated by cracks. Under normal conditions, all oxide crystals would have the same orientation. It is feasible that the increased strain caused the oxide flakes to buckle and crack when cooled to room

temperature, leaving fragments with different relative orientations. Shadowing with platinum/carbon revealed that the flakes were indeed buckled. The appearance of the oxide flakes was reminiscent of dendrite growth. However, the perfection of alignment and regularity of the saw-toothed edge on either side of the crack would rule out the dendrite growth mechanism. The discontinuities and mis-matches in the extinction contours across the oxide flakes would indicate that one large oxide flake had ruptured in such a way that the edges of the smaller flakes were saw-toothed.

Growth steps in the flakes were not revealed by shadowing. Thus the step height in the crystal growth of α -SnO is less than 30 Å, the resolution of the platinum/carbon shadow.

3. Oxidation in electron microscope

a) Lattice relationship between α -SnO and β -Sn

In the electron microscope, perfect (200) oriented single crystals of β -Sn were oxidised to ($\bar{1}\bar{1}0$) oriented α -SnO.

Electron diffraction patterns have shown that the parallel axes were Sn [010] // SnO [$\bar{1}10$], Sn [001] // SnO [001] and parallel faces were Sn (100) // Sn ($\bar{1}\bar{1}0$).

The fit between the two crystal lattices is shown in Fig. 19. The fit between lattices is very good but there will be a certain amount of strain in the direction of the [100] tin axis. Percentage misfit along Sn [001] axis (taken over three Sn (001) spacings and two SnO (001) spacings).

$$= \frac{9.632-9.525}{9.525} \times 100$$
$$= 1.12\%$$

$$\text{Percentage misfit along Sn}[010] \text{ axis} = \frac{5.37-5.82}{5.82} \times 100$$
$$= -7.9\%$$

b) Formation of a higher oxide

It has been established⁽⁹⁾ that β -Sn is not oxidised to SnO₂ at atmospheric pressure until the reaction temperature exceeds 280°C. Tertain, Trillat and Plattard⁽¹⁰⁾ reported that when polycrystalline tin films were oxidised inside the electron diffraction camera under reduced pressure, reflections attributed to SnO₂ were not observed until the reaction temperature exceeded 600°C.

In the present work, SnO₂ was formed on single crystal tin films heated by the electron beam at oxygen pressures of 2×10^{-4} torr. The reaction was carefully monitored by electron diffraction. There was no indication at any time that localised melting of the tin film had occurred. (Molten tin is characterised by two diffuse halos). Although the oxygen pressure in the column was nominally 2×10^{-4} torr, the local oxygen pressure around the specimen would be considerably higher than this.

It was observed that as oxidation time increased, the concentration of the oriented overgrowth of α -SnO decreased and the concentration of SnO₂ increased.

It is suggested that the perfect alignment of tin atoms in the single crystal film and in the oriented overgrowth of α -SnO facilitated the adsorption of oxygen and the diffusion of oxygen ions into the substrate, thereby lowering the activation energy for the formation of SnO₂ and consequently the temperature at which the reaction proceeds.

4. Oxidation of polycrystalline tin films

In the present series of oxidation experiments, carried out at 10^{-1} torr, dendritic oxide growth was not observed. Evidently, the oxygen pressure was sufficiently high for the replacement of oxygen in the adsorbed layer to proceed at the same rate as the oxygen was incorporated into the growing oxide crystals. Thus platelets and not dendrites were formed.

If the oxide nucleus presents a face at which tin and oxygen ions can be incorporated into the lattice without undue strain or distortion, then it is to be expected that growth will occur preferentially at that face. Thus the oxide nucleus will develop into a platelet.

It is felt that the direction of growth of the platelet is not, in this case, a direct function of the orientation of the tin grains. The average tin grain size was 15,00^o Å whereas the average length of the oxide platelets was 200,00^o Å and their average width was 17,00^o Å. One would expect the orientation of the tin grain

to influence the orientation of the oxide nucleus. Preferential growth of the nucleus would proceed at that face of the growth centre which could most easily accommodate the oxide ions.

Large areas of the oxide film were in the form of interlinked islands of oxide crystals. The mean diameter of these islands was 15,000 Å which was the mean diameter of the original tin grains. Here the oxide had not developed in any particular direction.

An interesting feature of the oxidised specimens was the loops of oxide at some edges of the oxide crystals. These were not observed at the platelet edges. It would appear that instead of the oxygen ions diffusing into the tin, tin ions have migrated outwards from the bulk oxide to areas rich in oxygen, forming closed loops of tin oxide.

An analogous situation arises in the oxidation of evaporated copper films⁽⁵³⁾. When the films were oxidised at high oxygen pressures (5 torr), annular Cu_2O was formed, whereas at low oxygen pressures (10^{-5} torr) small dense crystals of Cu_2O were formed. At intermediate pressures both types of Cu_2O crystal growth were observed.

A striking feature of the oxidised films was that the oxide crystals exhibited a high degree of crystallinity and single crystals were frequently observed.

An attempt was made to correlate the morphology of the crystals with their orientation. For example, most elongated rectangular platelets had orientation $[120]$ with respect to the electron while the needle-like platelets had orientation $[3\bar{3}1]$. However, more work should be devoted to this aspect of tin oxide morphology before rigorous conclusions can be drawn.

ACKNOWLEDGEMENTS

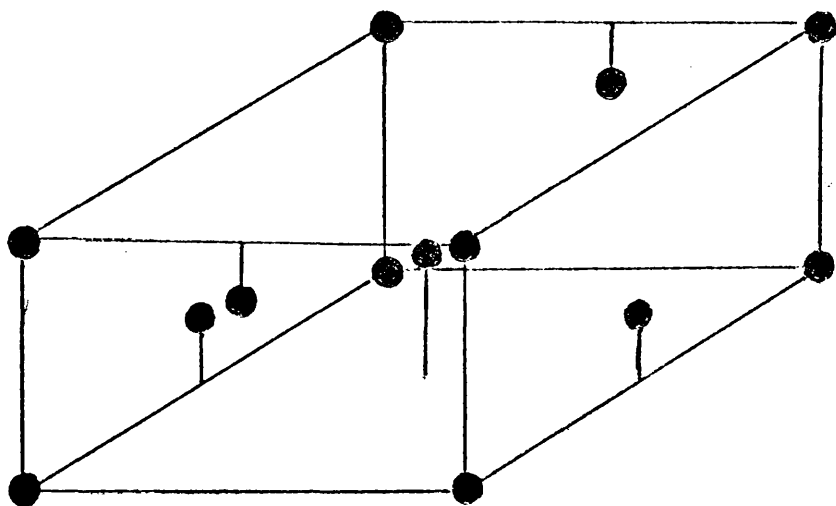
I would like to thank Mr. J. Fryer for his invaluable assistance and for reading this thesis.

REFERENCES

1. Cohen E. and von Lieshout, Z. Metallk., (1957), 48, 126.
2. Wyckoff R.W.G. Crystal Structures (Vol. 1), 2nd Ed. Interscience, New York, 1948.
3. Bragg W.L. and Derbyshire J.A. Trans. Far. Soc., 28, (1932), 522.
4. Moore W.J. and Pauling L., J. Am. Soc. 63, (1941), 1392.
5. Steinheil A., Ann. Phys. Lpz., 19, (1934), 495.
6. Jenkins R.D., Proc. Phys. Soc., 47, (1935), 109.
7. Hart R.K., Proc. Roy. Soc., 65B, (1952), 955.
8. Britton S.C. and Bright K., Metallurgia, 56, (1957), 163.
9. Shimaoka G. and Yamai I., J. Chem. Soc. Japan, 76, (1955), 965, 967.
10. Trillat J.J., Tertain L. and Plattard H.T., Compt. Rend., 240, (1955), 526.
11. Boggs W.E., Trozzo P.S. and Pellisier G.E., J. Electrochem. Soc. 108, (1961), 13.
12. Boggs W.E., Kachik R.H. and Pellisier G.E. ibid 108 (1961), 6.
13. Boggs W.E. ibid, 108 (1961), 124.
14. Spinedi P. and Verdini B., Bell. Sci. Fac. Chim. Ind. Bologna, 21, (2-3), (1963), 111.
15. Nikulin V.N. and Kochergin S.M. Zhur. Fiz. Khim. 30, (1956), 2337.
16. Nikulin V.N. and Kirov. M. ibid., 32, (1958), 1035.
17. Kubaschewski O. and Hopkins B.E. Oxidation of Metals and Alloys Butterworths, London 1962.

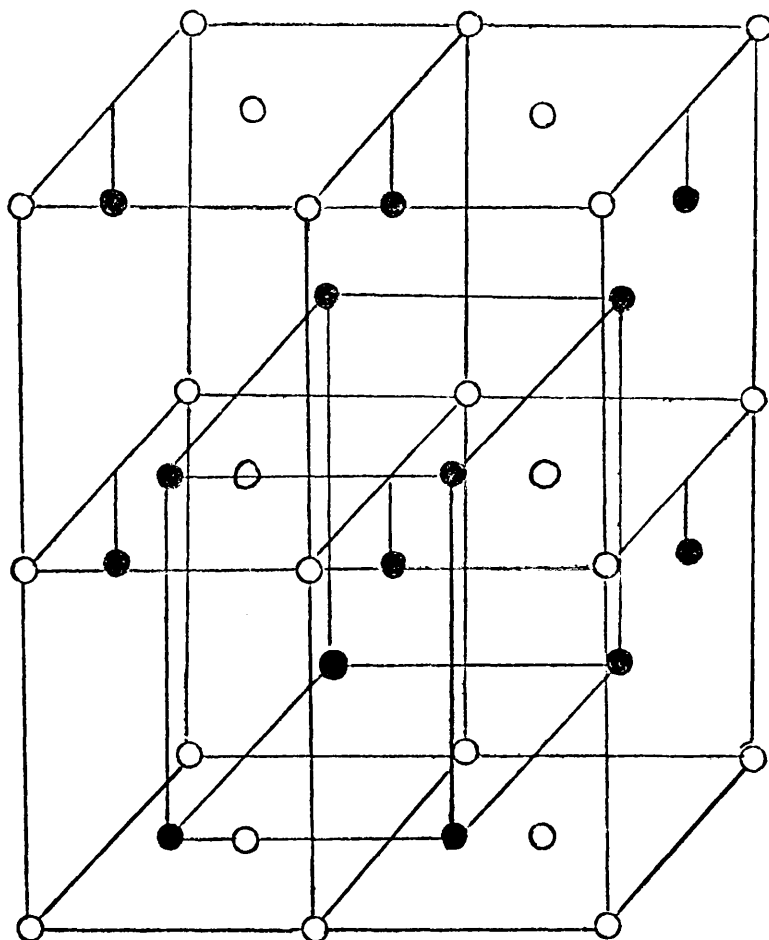
18. Hauffe K., Oxydation von Metallen und Metallegierungen, Springer, Berlin, 1957.
19. Benard J., Oxydation des Metaux, Gauthier-Villars et C^{ie}, Paris, 1962.
20. Evans U.R. The Corrosion and Oxidation of Metals, Edward Arnold Ltd., London 1960.
21. Luner C. Trans. Met. Soc. A.I.M.E. 218, (1960) 572.
22. Bilbrey J.H., Wilson D.A. and Spendlove M.J., U.S. Bureau of Mines, Rep. Invest. No. 5181 (1955).
23. Gruhl W. and Gruhl U. Metall. 6, (1952) 177.
24. Spinedi P. Gazz. chim. Ital. 86, (1956), 579, 588.
25. Evans U.R. Rev. Pure Appld. Chem. (Melbourne) (1955).
26. Royer L., Bull. Soc. franc. Mineral, 51, (1928), 7.
27. Schultz L.G., Acto. Cryst. 5, (1952), 130.
28. Finch G.I. and Quarrel A.G., Proc. Roy. Soc., 46, (1934), 148
29. Frank F.C. and van der Merwe J.H. *ibid*, A198, (1949), 205, 216; A200, 125.
30. Menzer G., Naturwissenschaften 26, (1938), 385.
31. Bruck L., Ann. Phys., 26, (1936), 233.
32. Engel O.G., J. Chem. Phys., 20, (1952), 1174.
33. Newman R.C. and Pashley D.W., Phil. Mag. 46, (1952), 917.
34. Bassett G.A., Proc. 4th Int. Conf. E. Microsc., Berlin, 1, (1958), 52.
35. Adams D., private communication.

36. Sella C. and Trillat J.J., Single Crystal Films, ed. M.H. Francombe and H. Sato, Oxford, Pergamon Press, 1964.
37. Bethge H. Phys. Stat. Sol. 2, (1962), 775.
38. Ino et al, J. Phys. Soc. Japan 17, (1962), 1024.
39. Wassermann E.F. and Hines R.L., J. Appl. Phys. 38, (1967), 197.
40. Matthews J.W. Phil. Mag. 12 (1965), 1143.
41. Rudiger O. Ann. Phys. 30, (1937), 505.
42. Vook R.W.; J. Appl. Phys., 32, (1961), 1557.
43. Curzon A.E., Cryogenics, 2(6), (1962), 334.
44. Gandais M., Rev. Opt., 40, (1961), 464.
45. Preece J.M. and Wilman H., Brit. J. Appl. Phys., Ser. 2, 2, (1969), 967.
46. Ehrhart J. and Marraud A., Rev. Opt. Theor. Instr., 43, (1964), 33.
47. Ennos A.E., Brit. J. Appl. Phys., 4, (1953), *ibid*, 5 (1954), 27.
48. Leisegang S., Proc. Int. Conf. E. Micros., London, (1954).
49. Gale B. and Hale K.F., Brit. J. Appl. Phys., 14, (1961), 218.
50. Raether H., Optik, I (1946), 296.
51. Derbyshire J.A. and Cooper E.R., Proc. Roy. Soc. A152, (1935), 104.
52. Keith H.D., Proc. Phys. Soc., London, B69, (1956), 180.
53. Bachmann L., Sawyer D.L., Siegel B.M., J. Appl. Phys., 36, (1965), 304.



$\bar{a} = b = 5.8197 \text{ \AA}$
 $c = 3.1749 \text{ \AA}$
 Atomic positions : $(4a) 000 ; 0\frac{1}{2}\frac{3}{4} ; \frac{1}{2}0\frac{3}{4} ; \frac{1}{2}\frac{1}{2}\frac{1}{2}$.

Fig. 1 Structure of β -Sn.



○ = oxygen

● = tin

Fig. 2 Structure of α -SnO

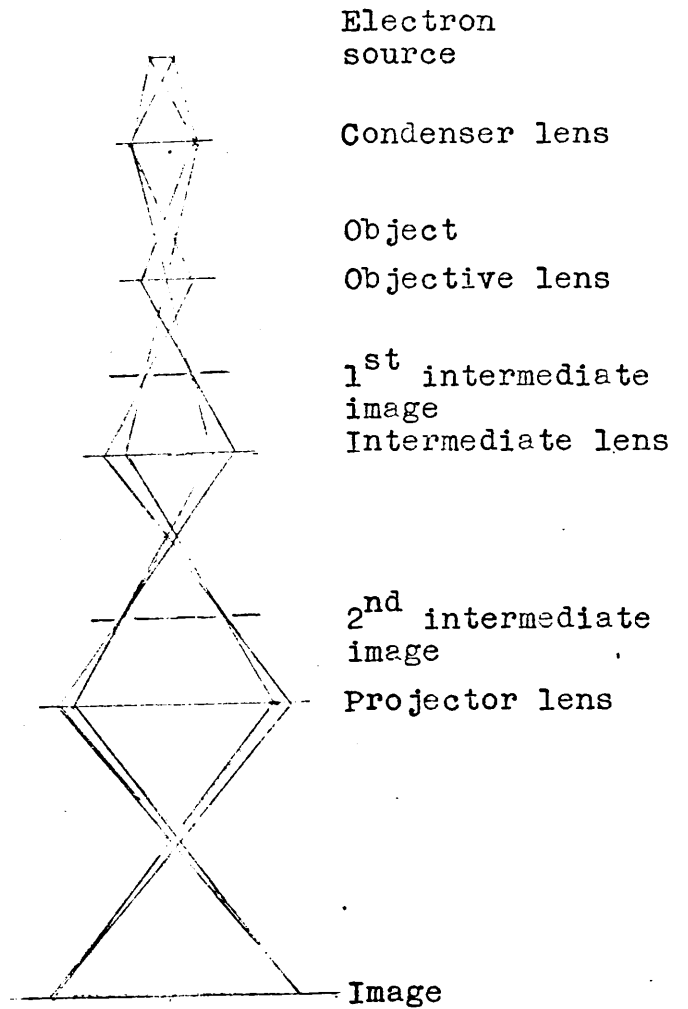


Fig. 3

Ray paths in electron microscope
(single condenser)

Fig. 4 Electron diffraction camera

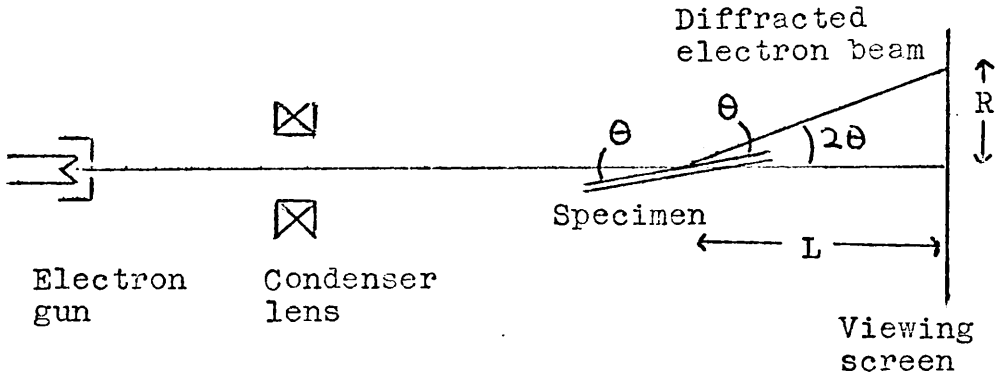
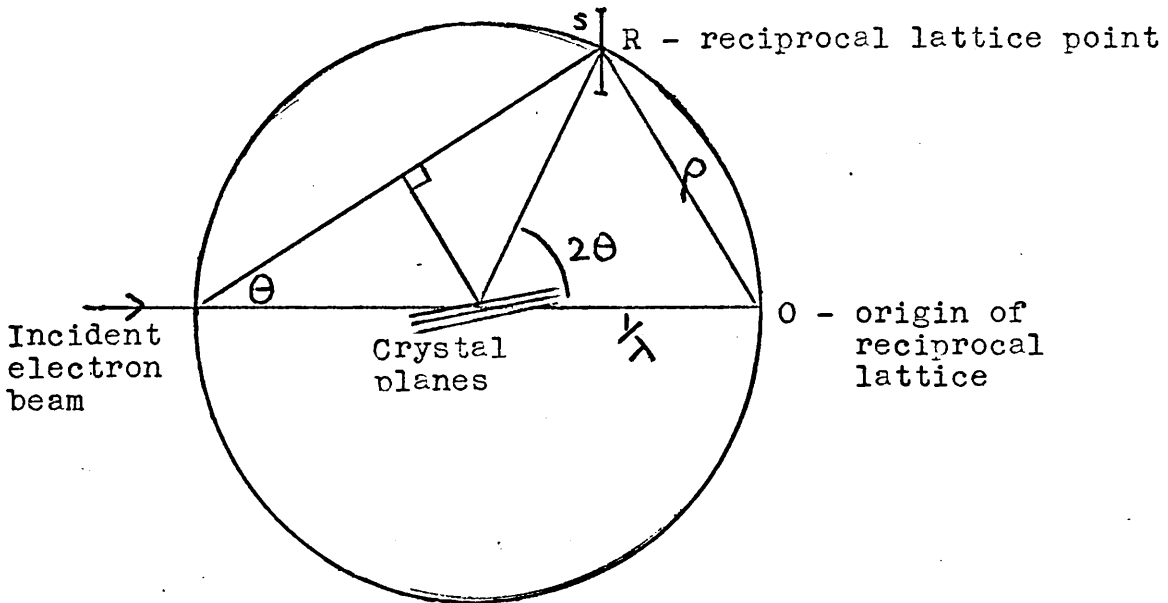


Fig. 5 Ewald sphere of reflection



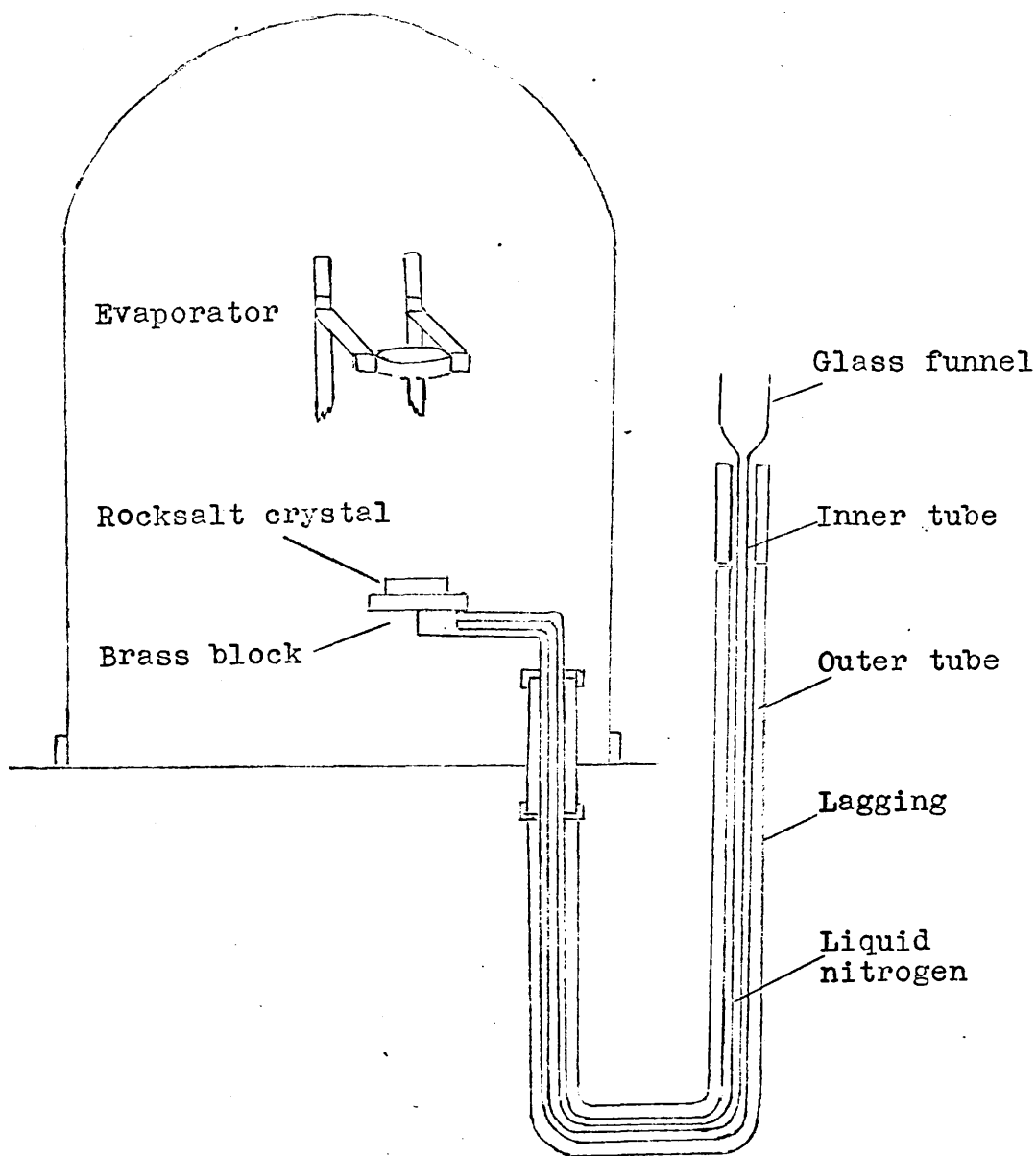
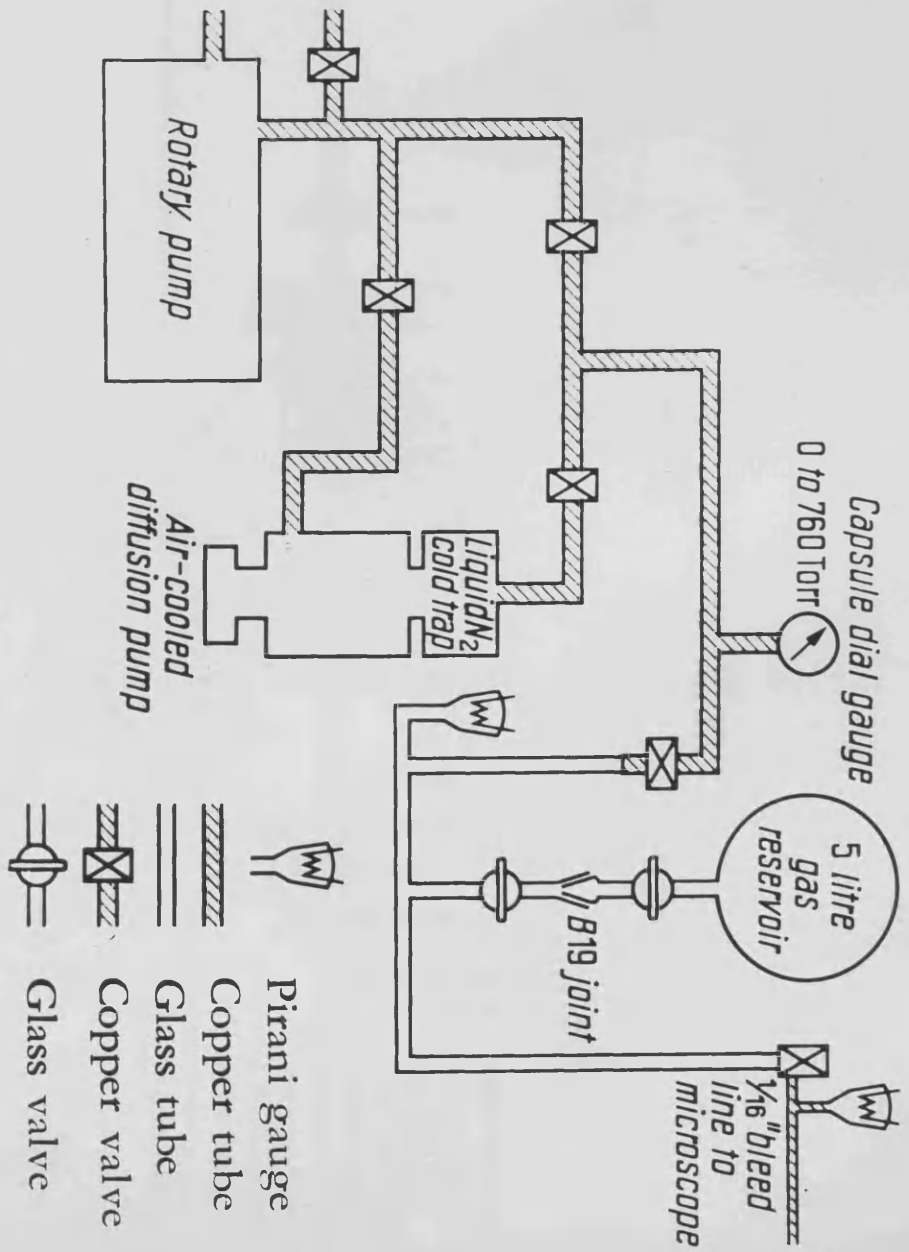


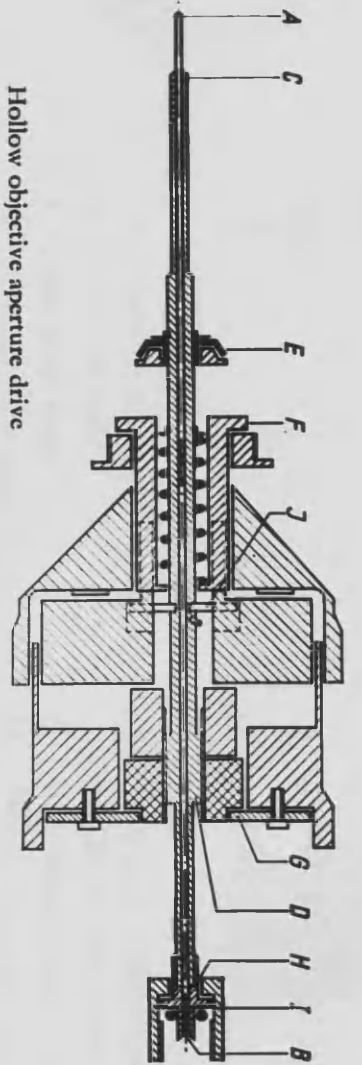
Fig. 6 Apparatus for deposition of epitaxial films

Fig. 7



Gas supply apparatus

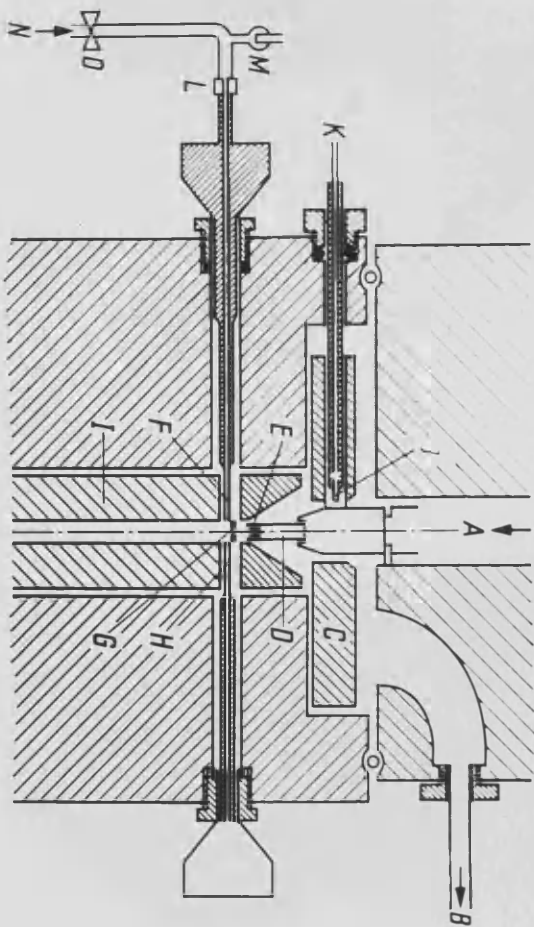
Fig. 8



- A-B 1/16" O.D. brass tubing
- C-B Larger tubing fitted outside A-B
- G-D 1/16" I.D. brass tube
- E Sealing gasket
- F-G Siemens objective aperture drive mechanism
- D-H 1/8" O.D. copper tubing
- I High vacuum union
- J Locating pins
- C, D, H Vacuum tight joints

Hollow objective aperture drive

Fig. 9



- | | | | |
|----------|-----------------------------|-------------|--------------------------------------------------|
| <i>A</i> | Electron beam | <i>J, K</i> | Electrical connections for the heating cartridge |
| <i>B</i> | Vacuum port | <i>L</i> | Standard vacuum union |
| <i>C</i> | Specimen stage | <i>M</i> | Pirani gauge for gas pressure measurement |
| <i>D</i> | Heating cartridge | <i>N</i> | Gas supply |
| <i>E</i> | Specimen | <i>O</i> | Needle valve for flow rate control |
| <i>F</i> | Hole for admission of gas | | |
| <i>G</i> | Variable objective aperture | | |
| <i>H</i> | Objective aperture holder | | |
| <i>I</i> | Objective pole piece | | |

Position of hollow objective drive in microscope column

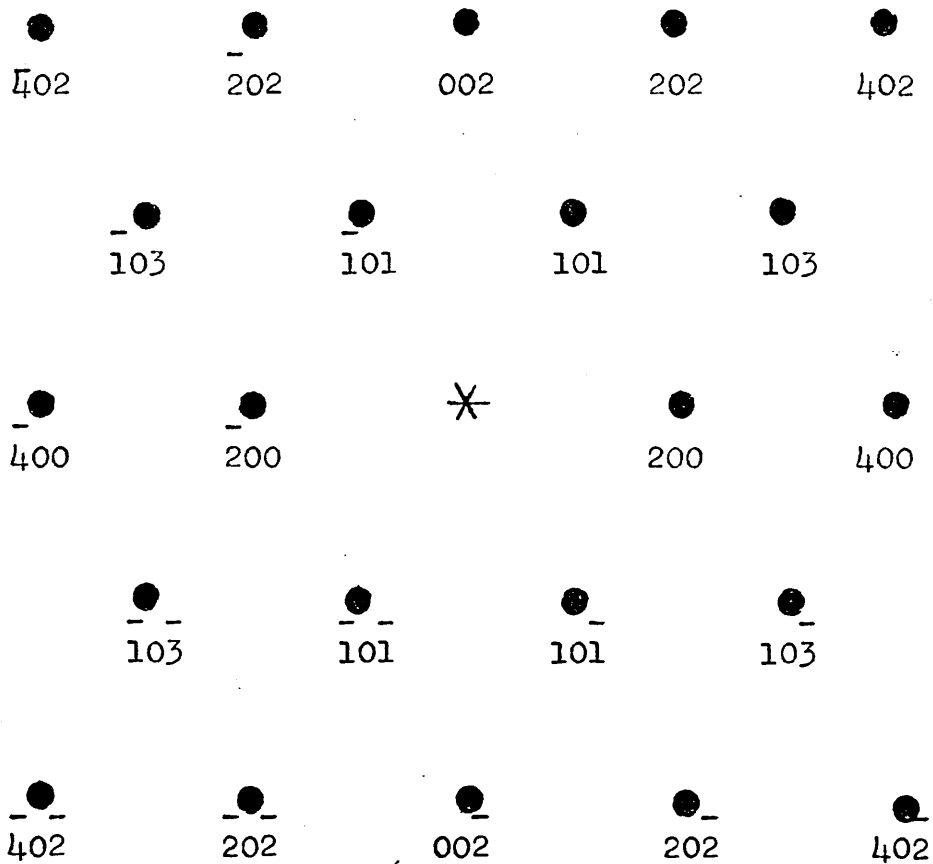


Fig. 10 $[200]$ Reciprocal lattice of β -Sn

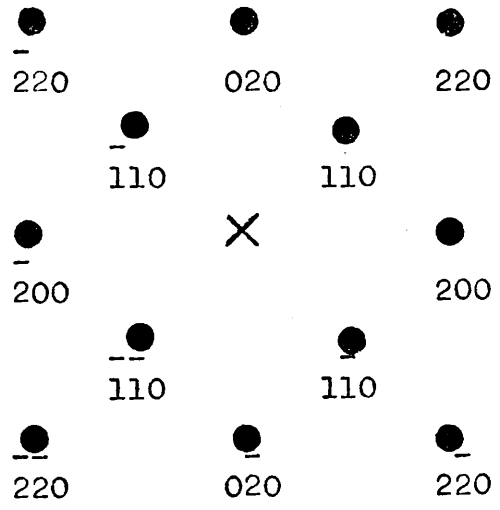


Fig. 11 [002] Reciprocal lattice of β -Sn

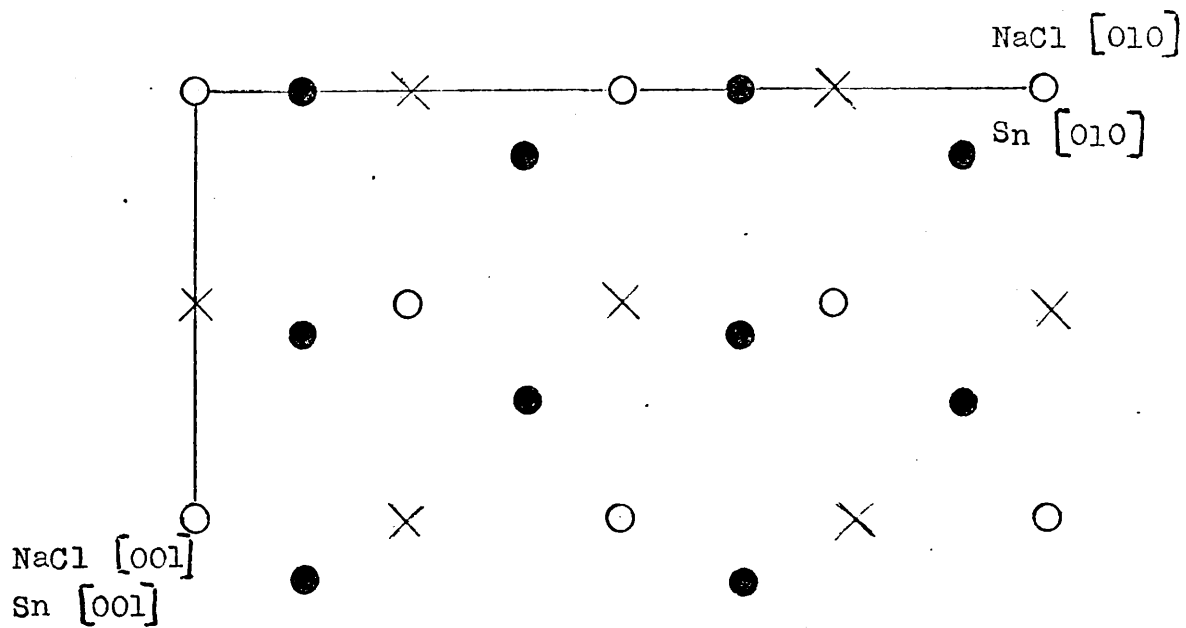


Fig. 12

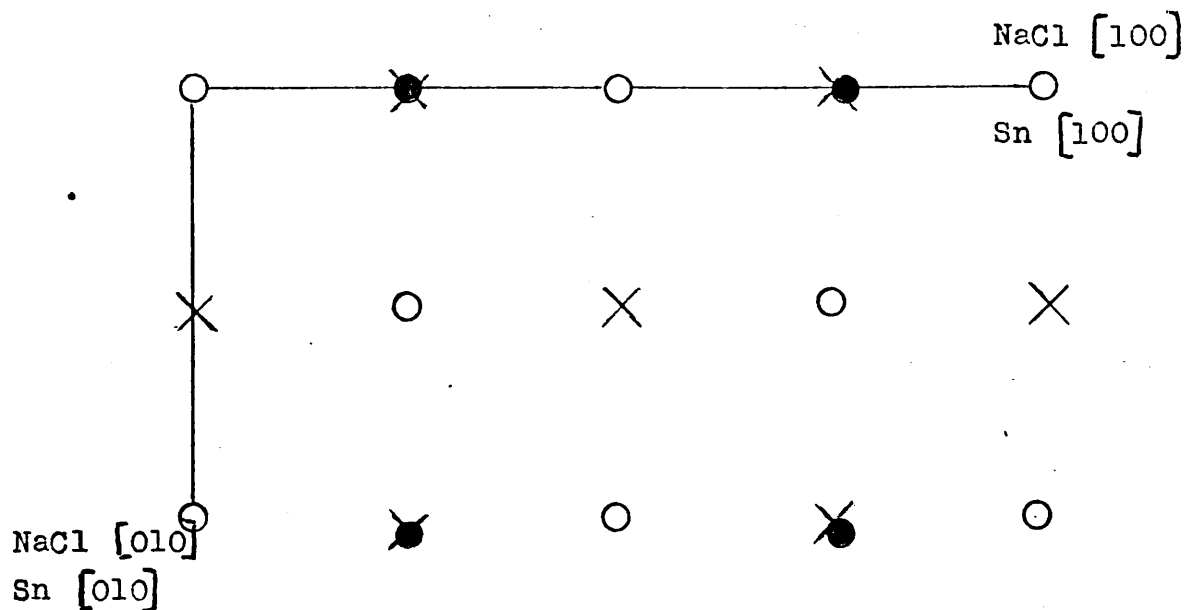


Fig. 13

- = sodium
- = tin
- ✕ = chlorine

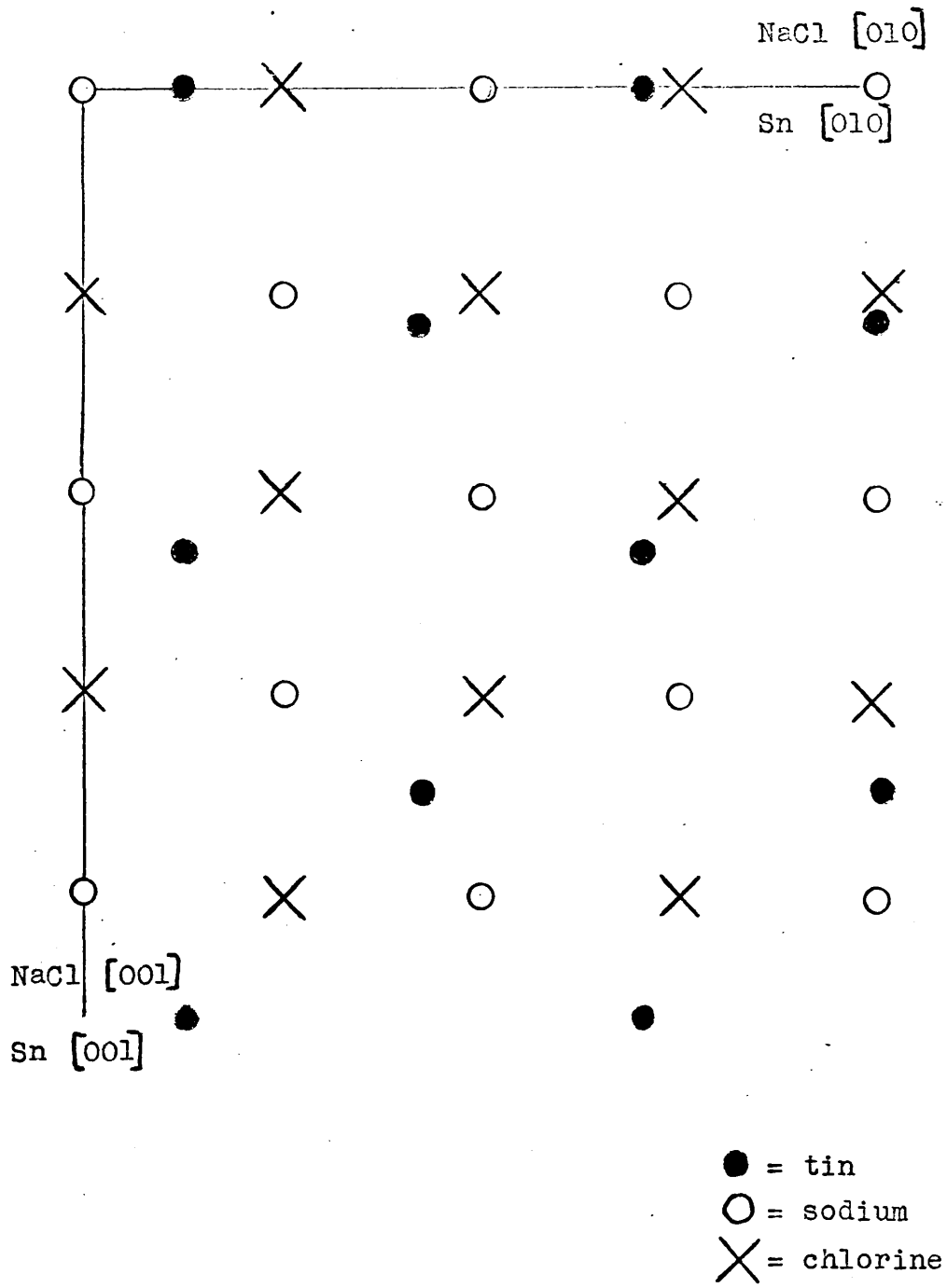
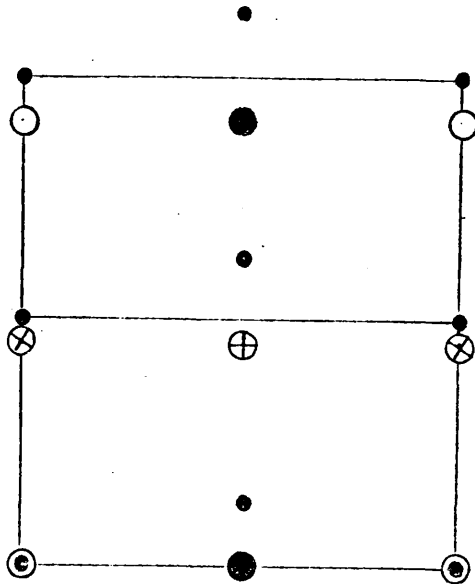


Fig. 14



● = atoms of (200) plane in a-axis orientation

⊙ = atoms of (001) plane in c-axis orientation

⊗ = atoms of plane to (001), distance $c/4$, in c-axis orientation

⊕ = atoms of plane to (001), distance $c/2$, in c-axis orientation

● = atoms of plane to (001), distance $3c/4$, in c-axis orientation

Fig. 15

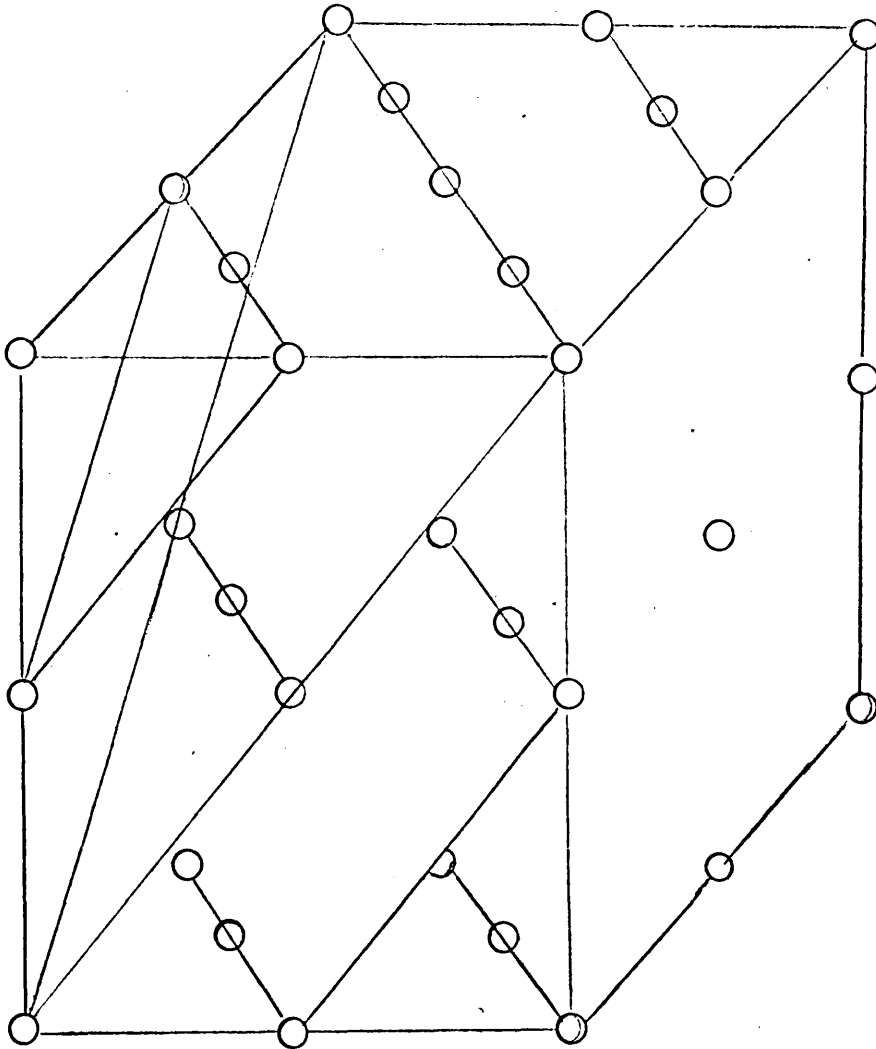


Fig. 16

All oxygen positions may be described as a series of (111) planes.

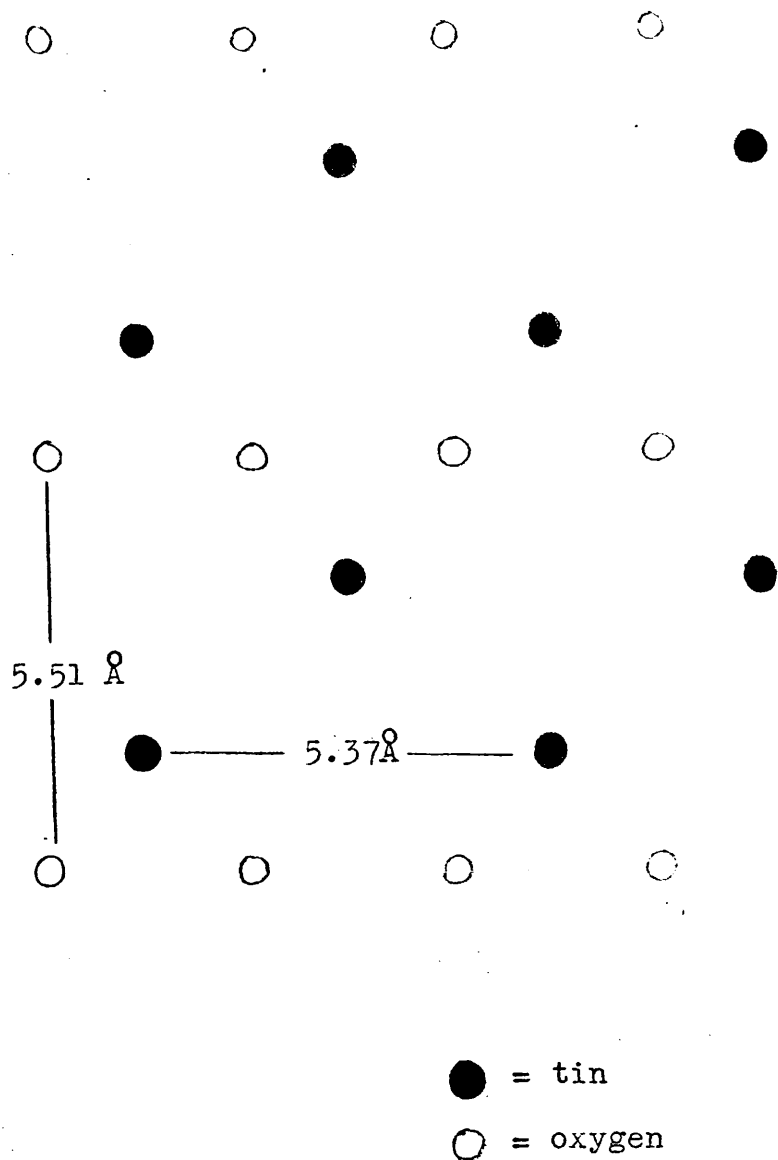


Fig. 17

Projection of tin atoms from distance $\frac{1}{2}d_{111}$ onto $(\bar{1}11)$ plane of α -SnO.

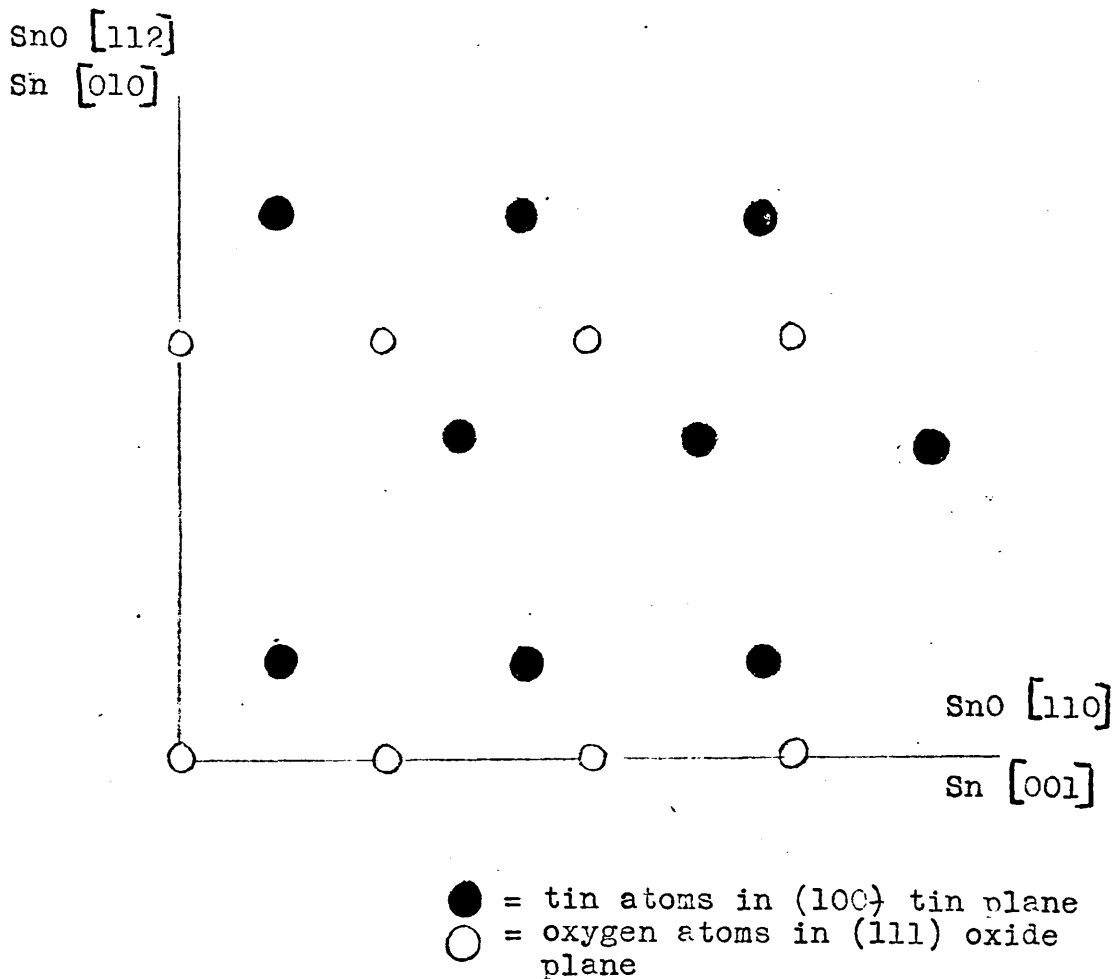


Fig.18 Lattice relationship between (111) oriented α -SnO and (100) oriented β -Sn.

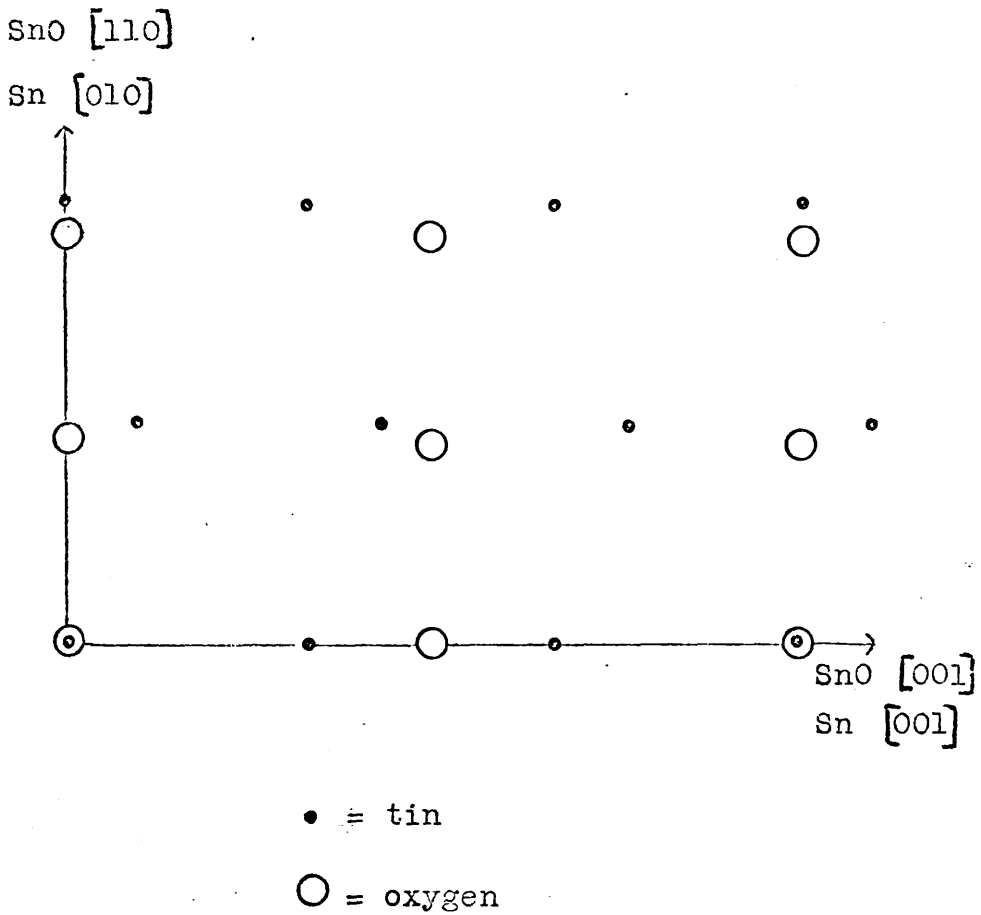
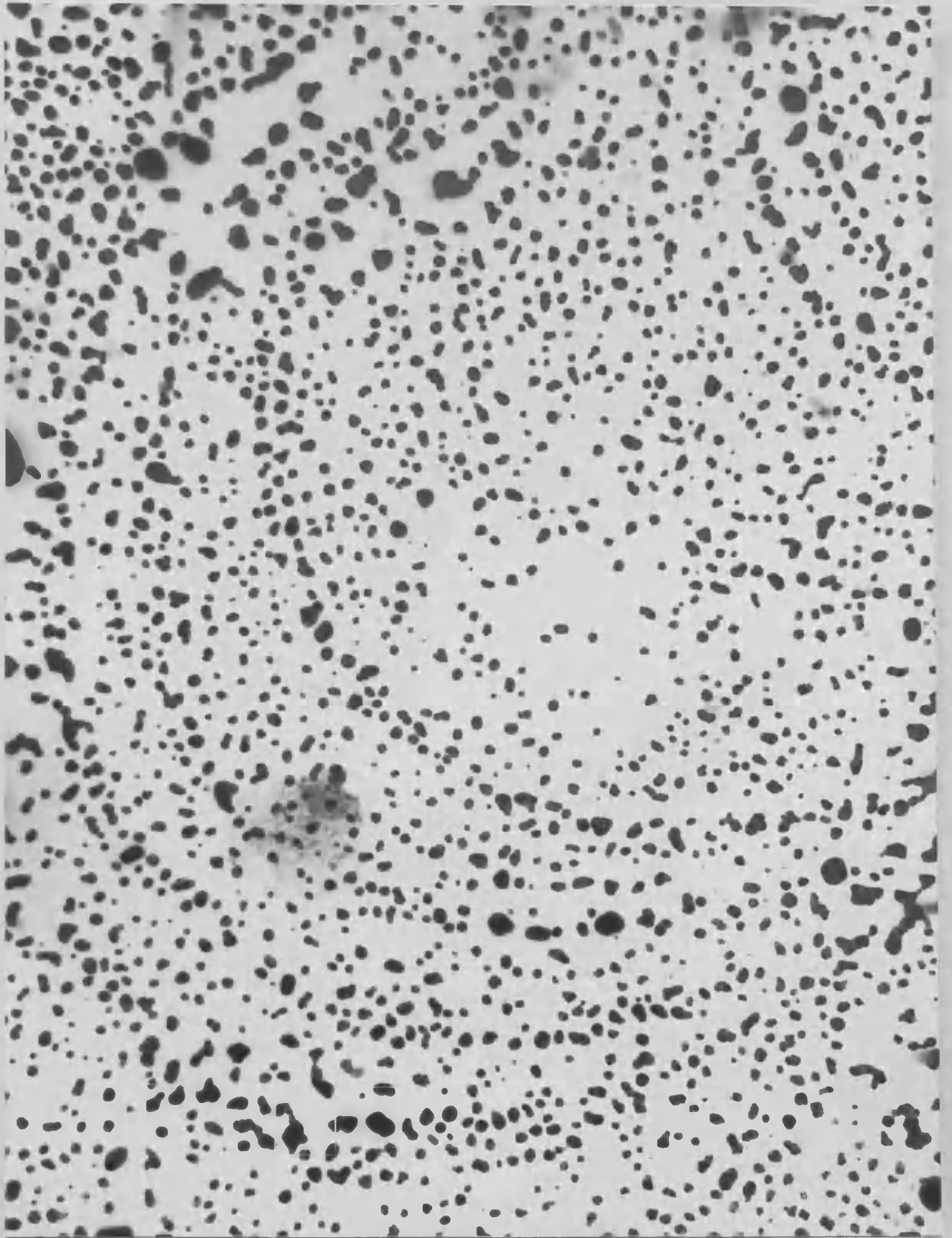


Fig. 19 Lattice relationship between $(\bar{1}\bar{1}0)$ oriented α -SnO and (200) oriented β -Sn.



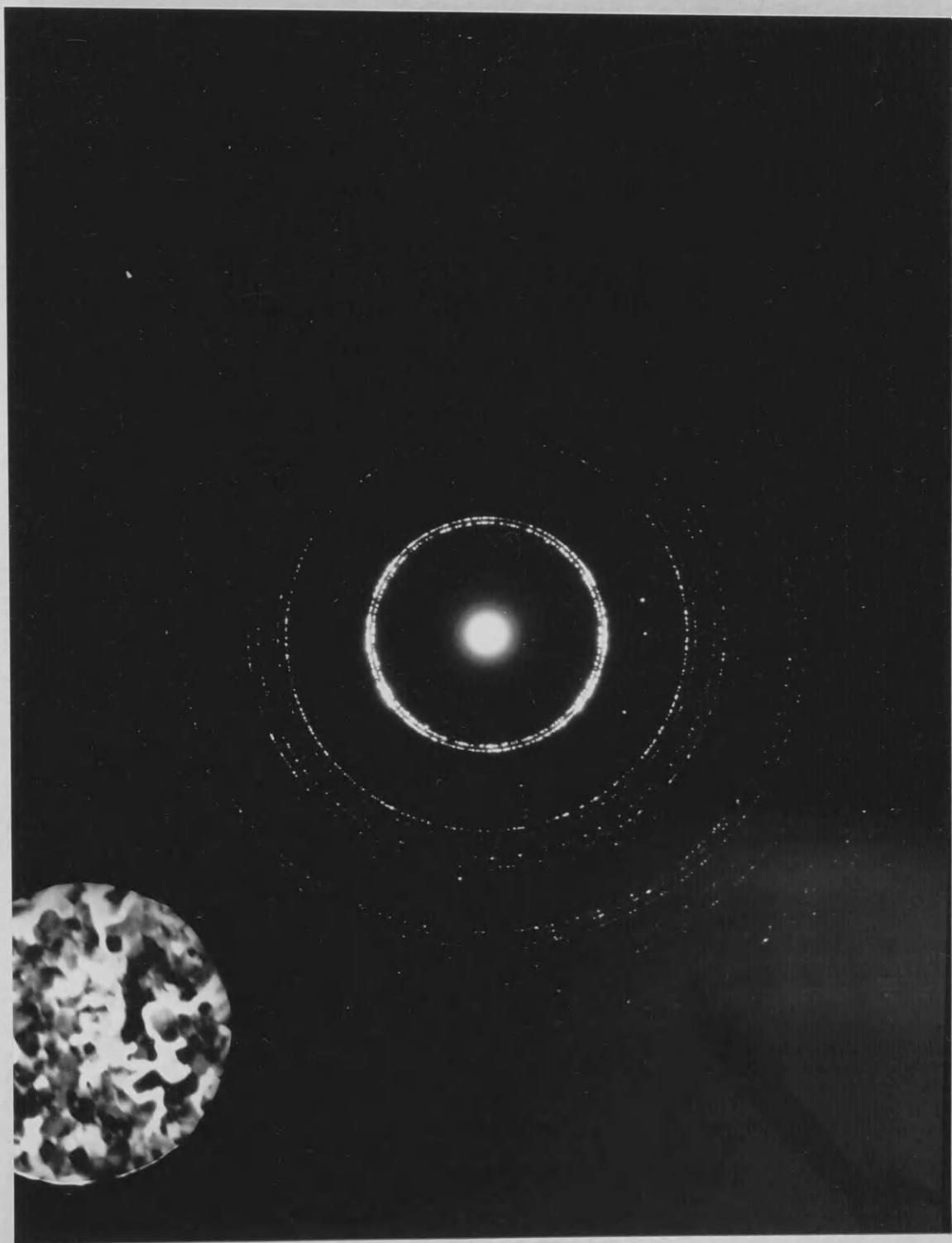




PLATE 3

X63,000

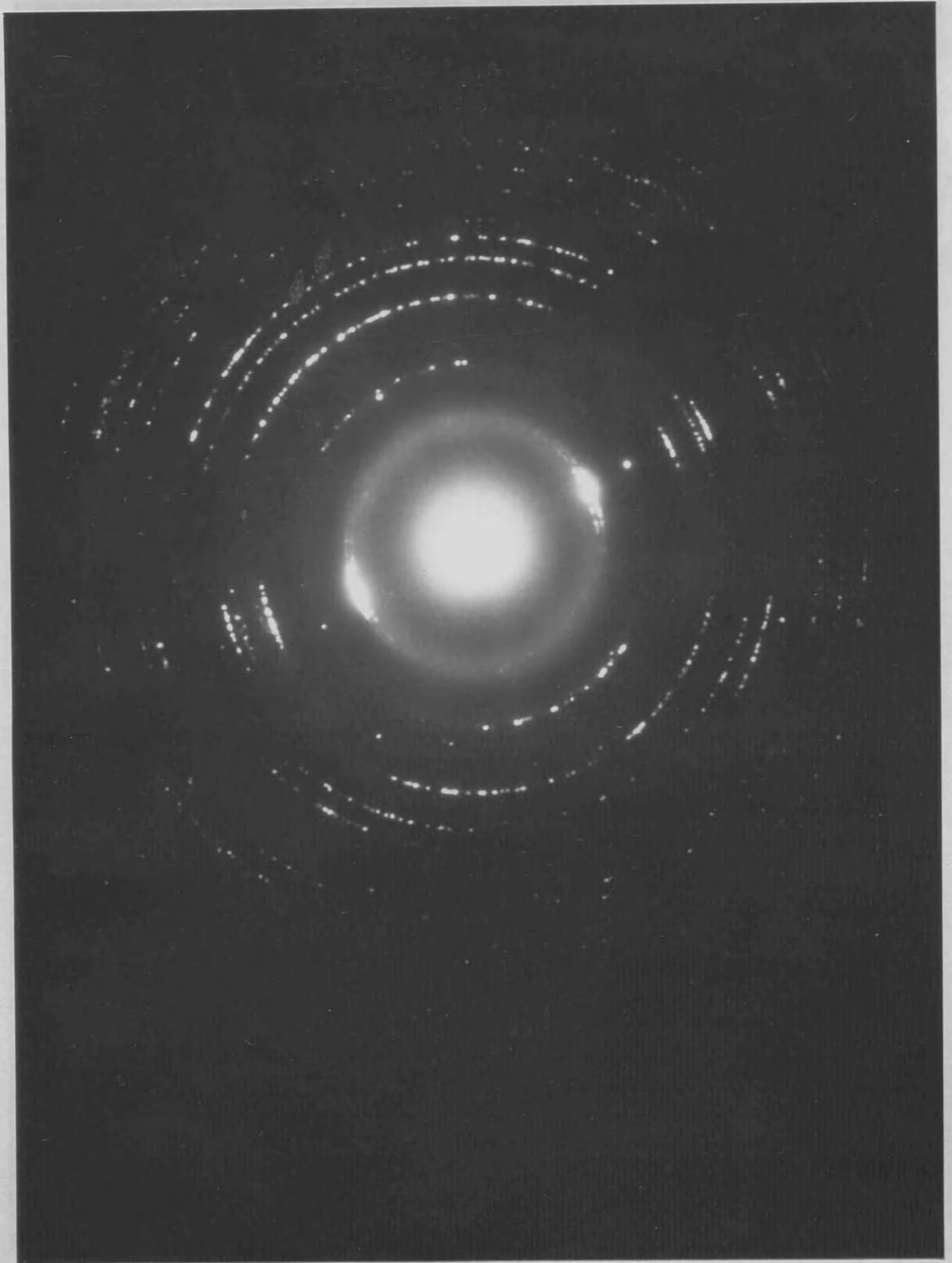
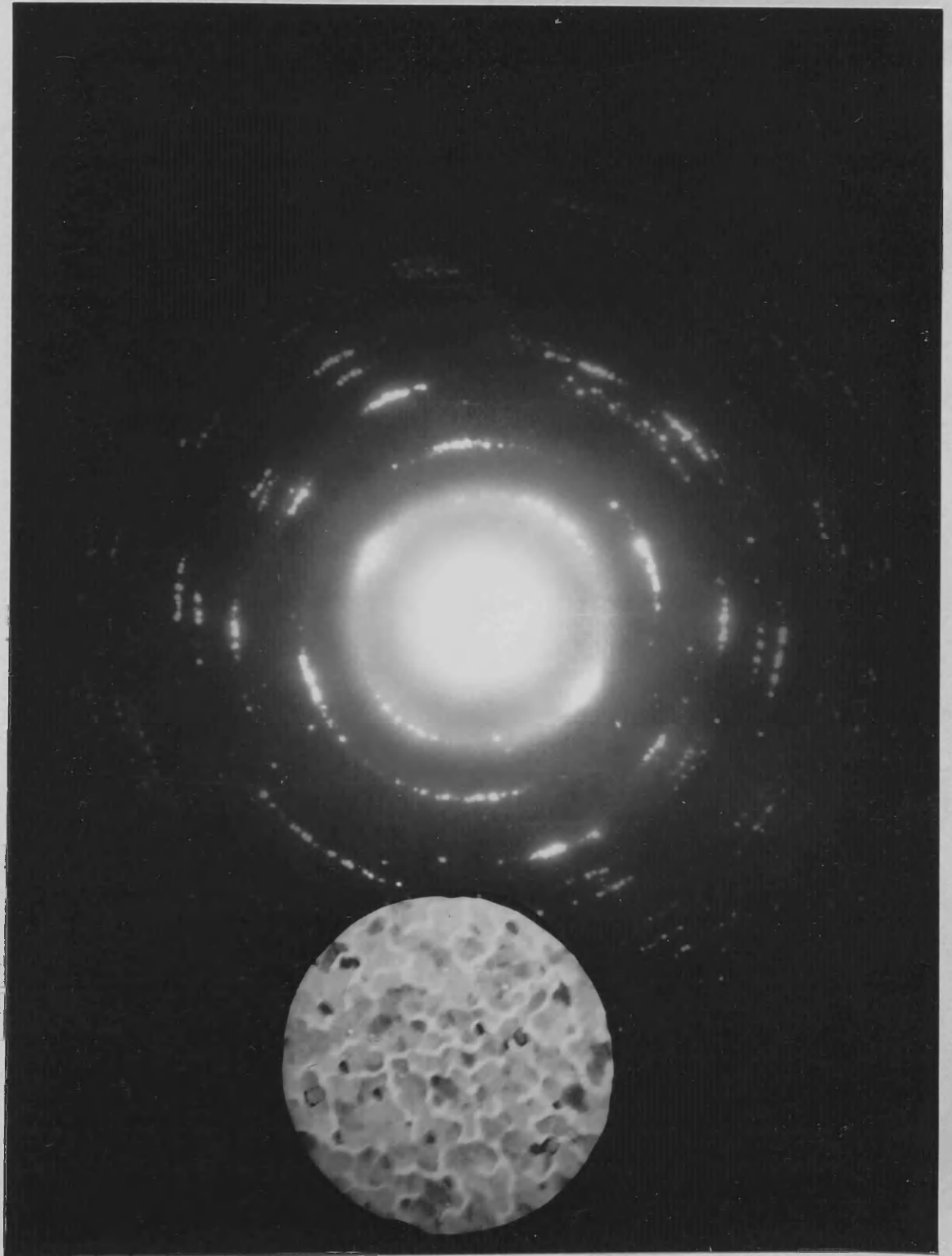


PLATE 4

X63,000



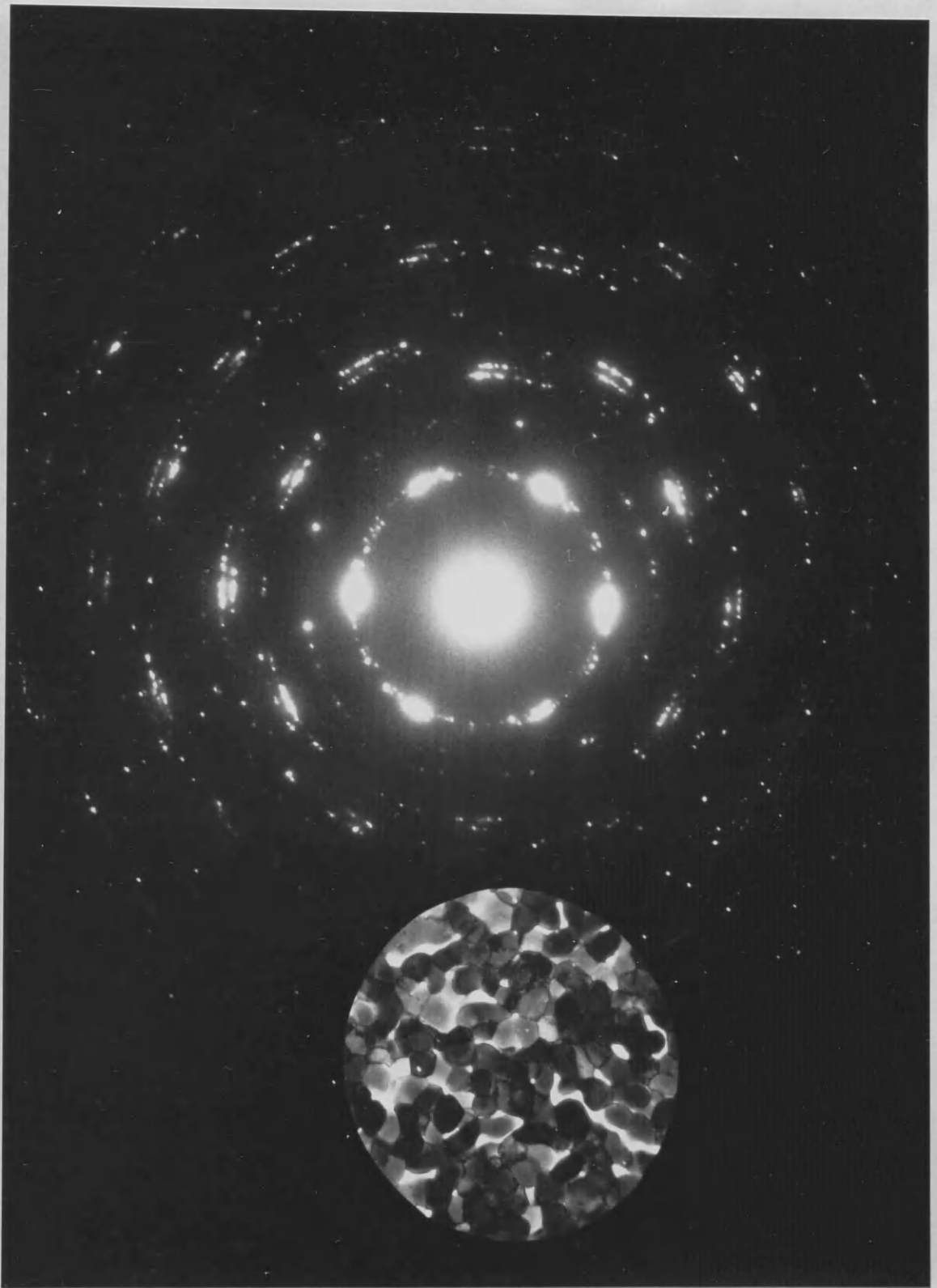


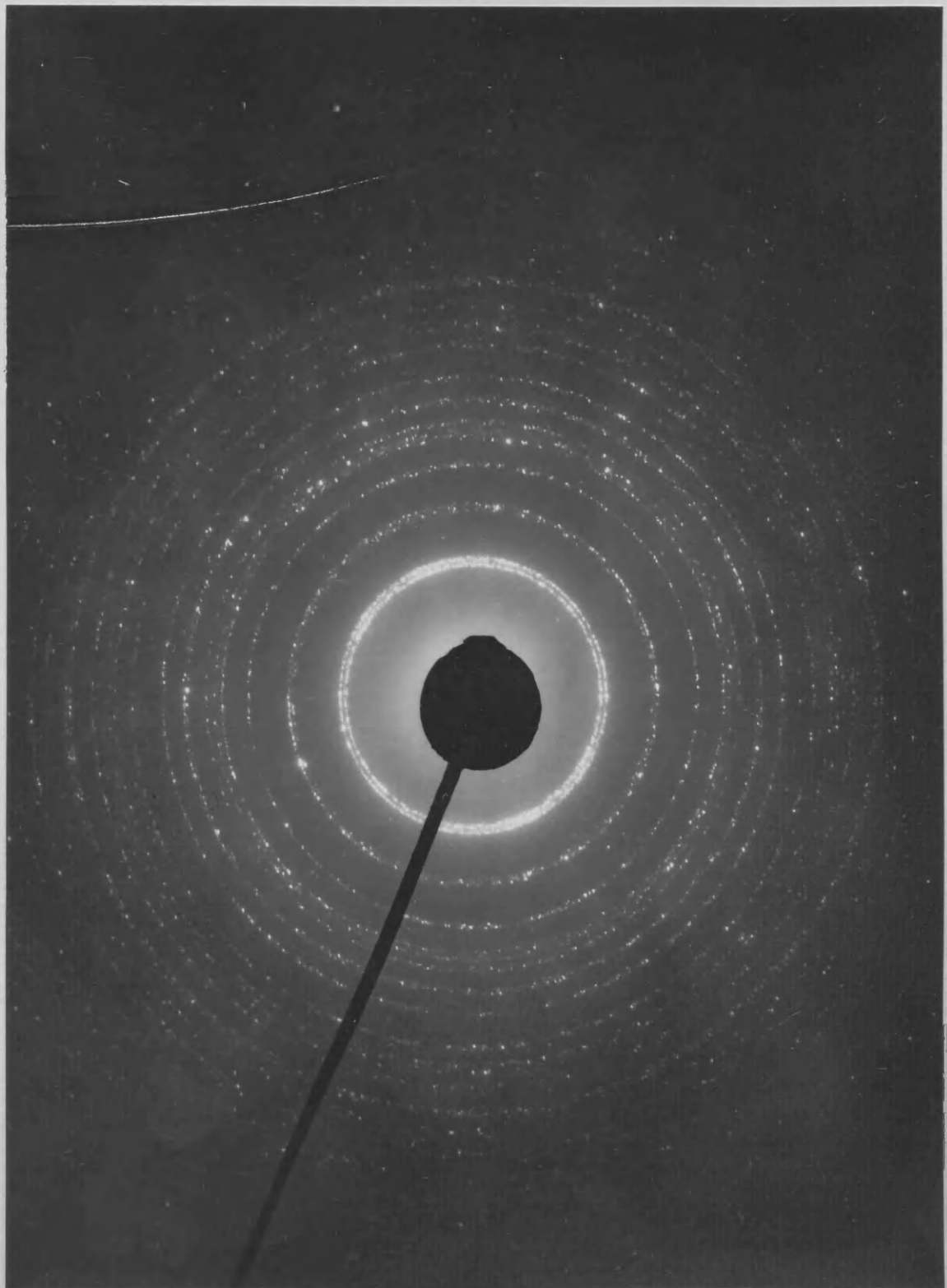
PLATE 6

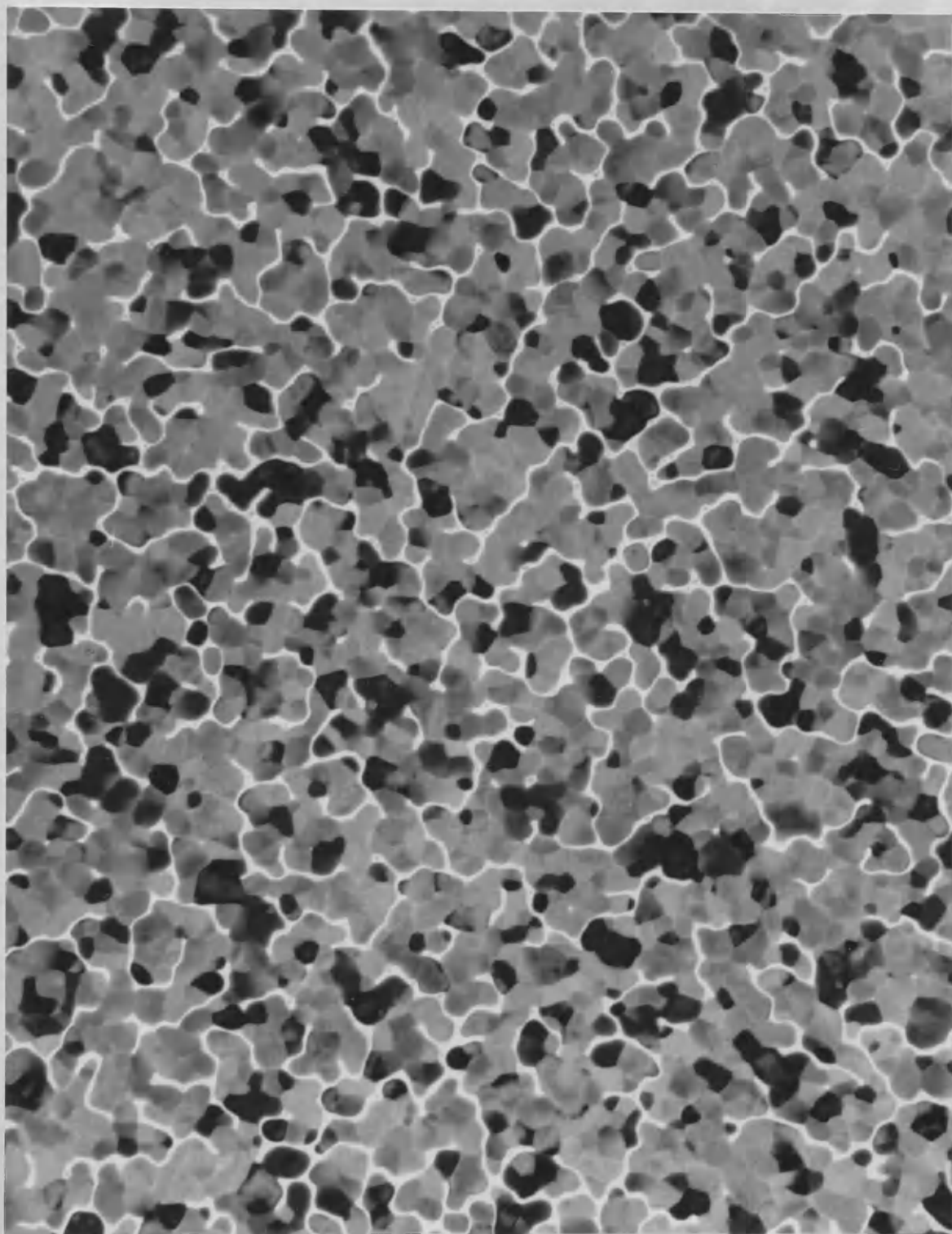
X63,000



PLATE 7

X63,000





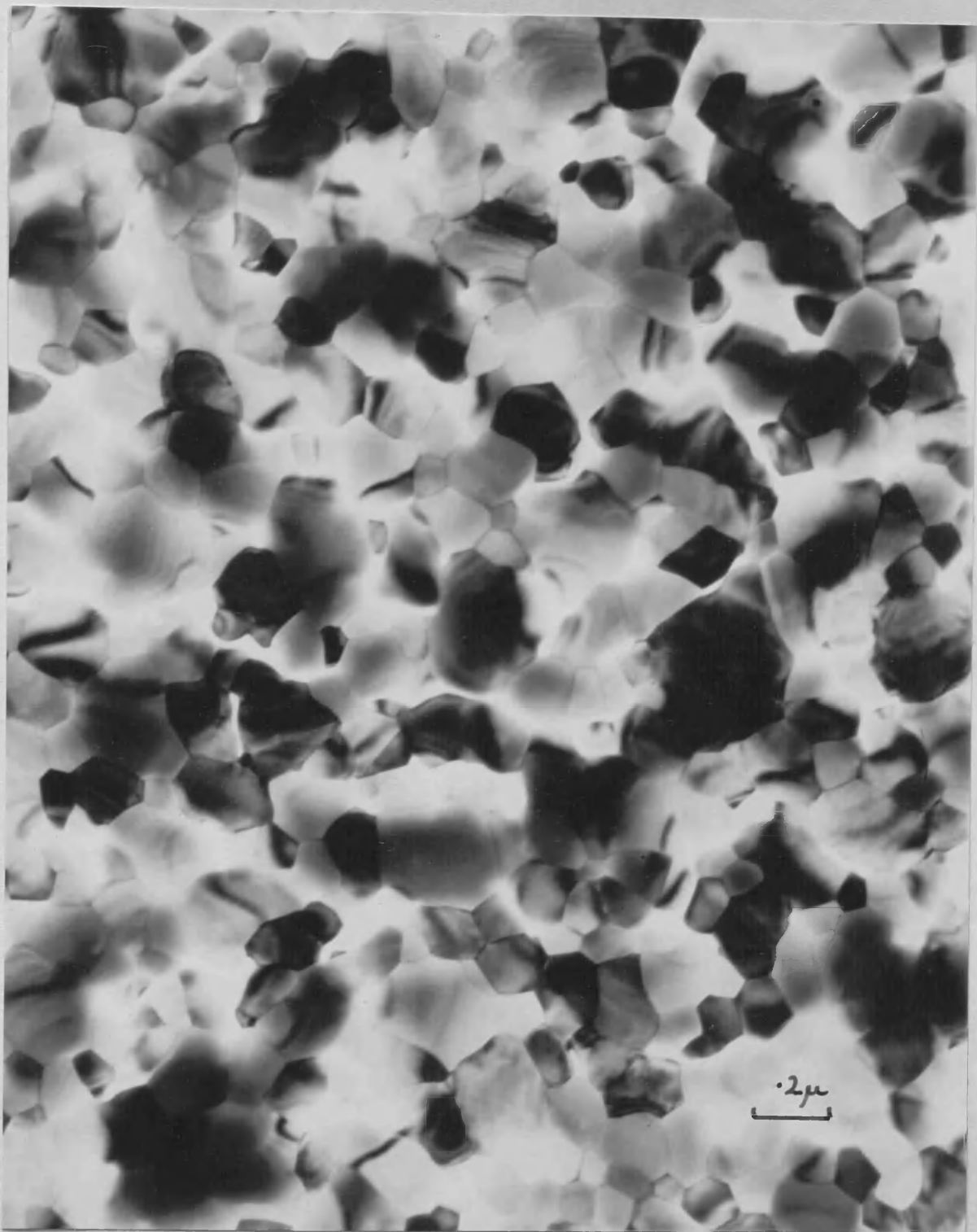


PLATE 10

X60,000

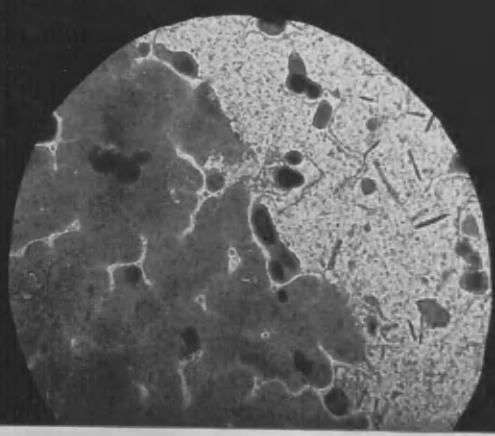
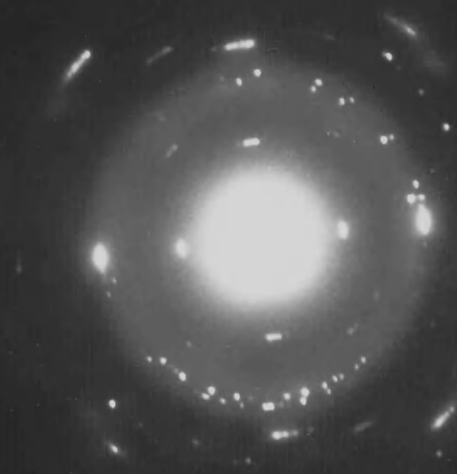
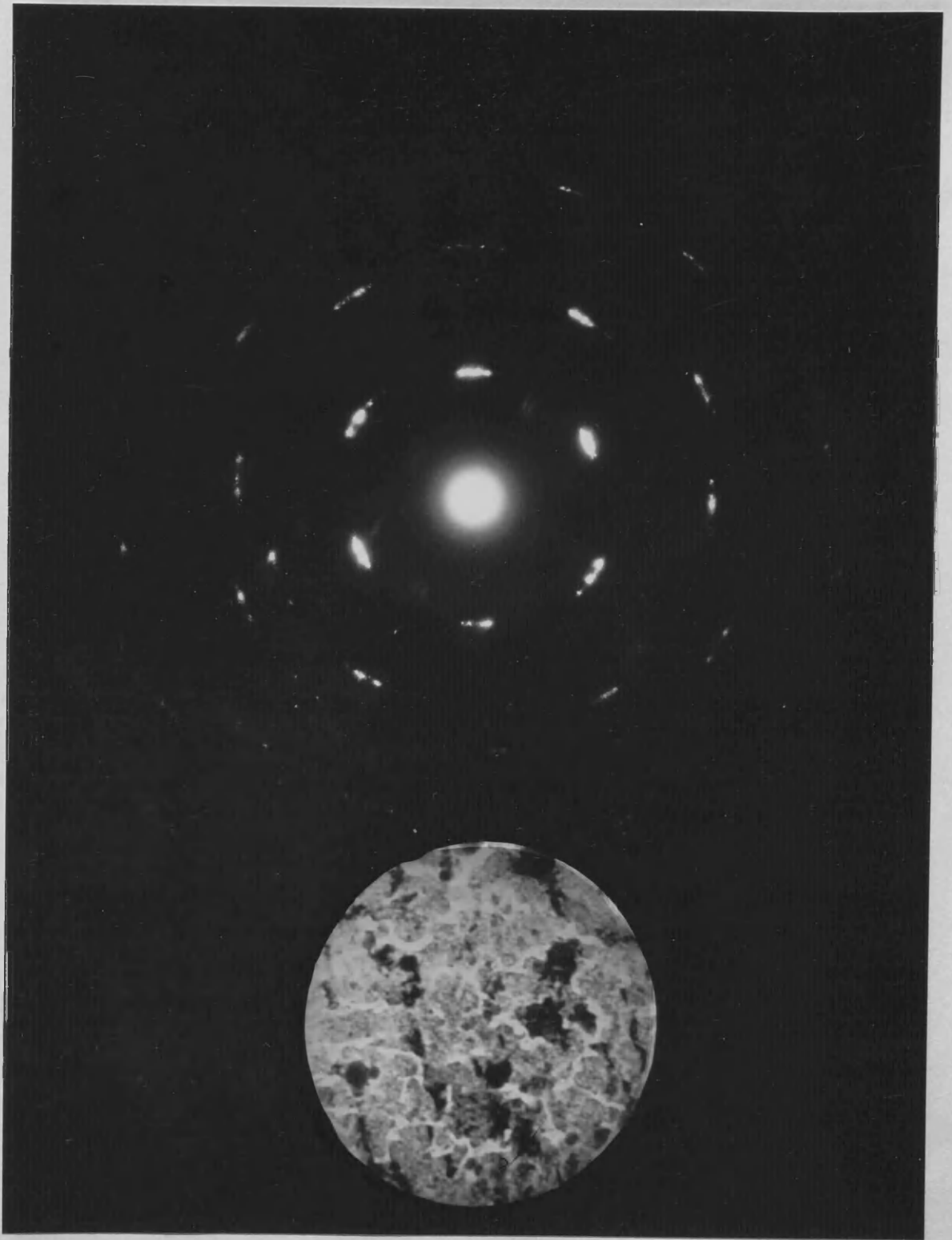


PLATE 11

X63,000



PLATE

12

X63,000



PLATE 13

X63,000

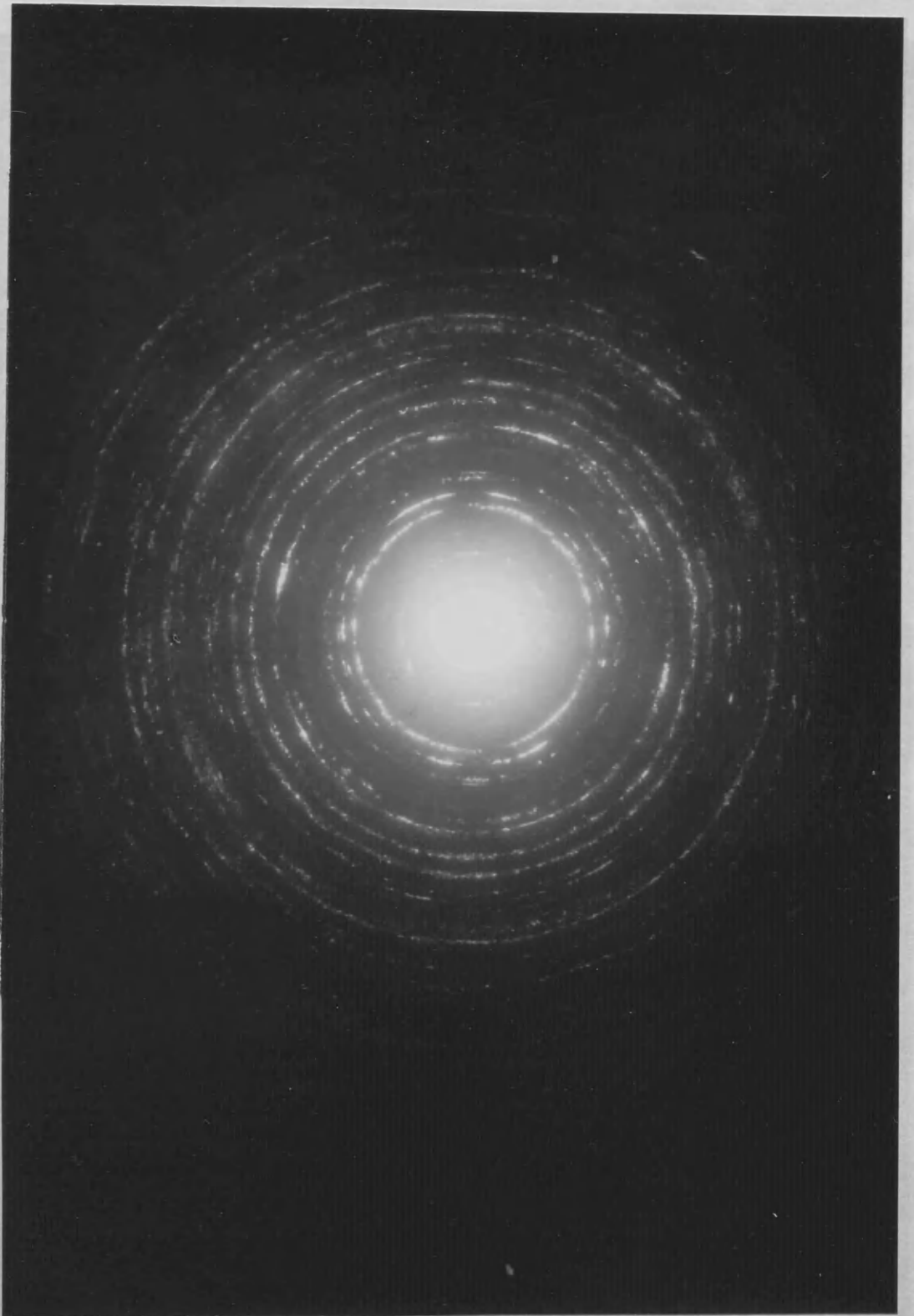


PLATE 14

X63,000

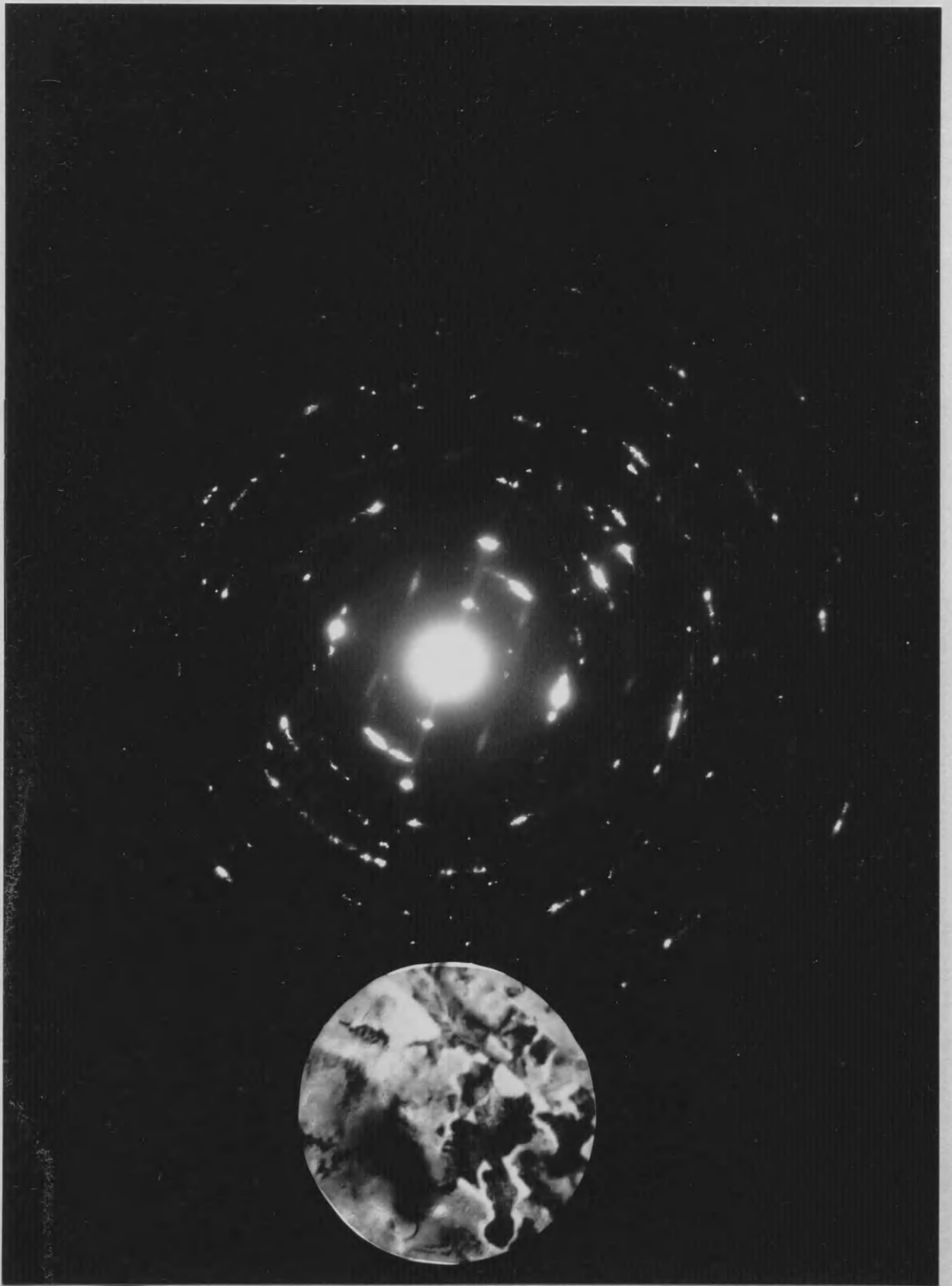


PLATE 15

X63,000



PLATE 16

X63,000

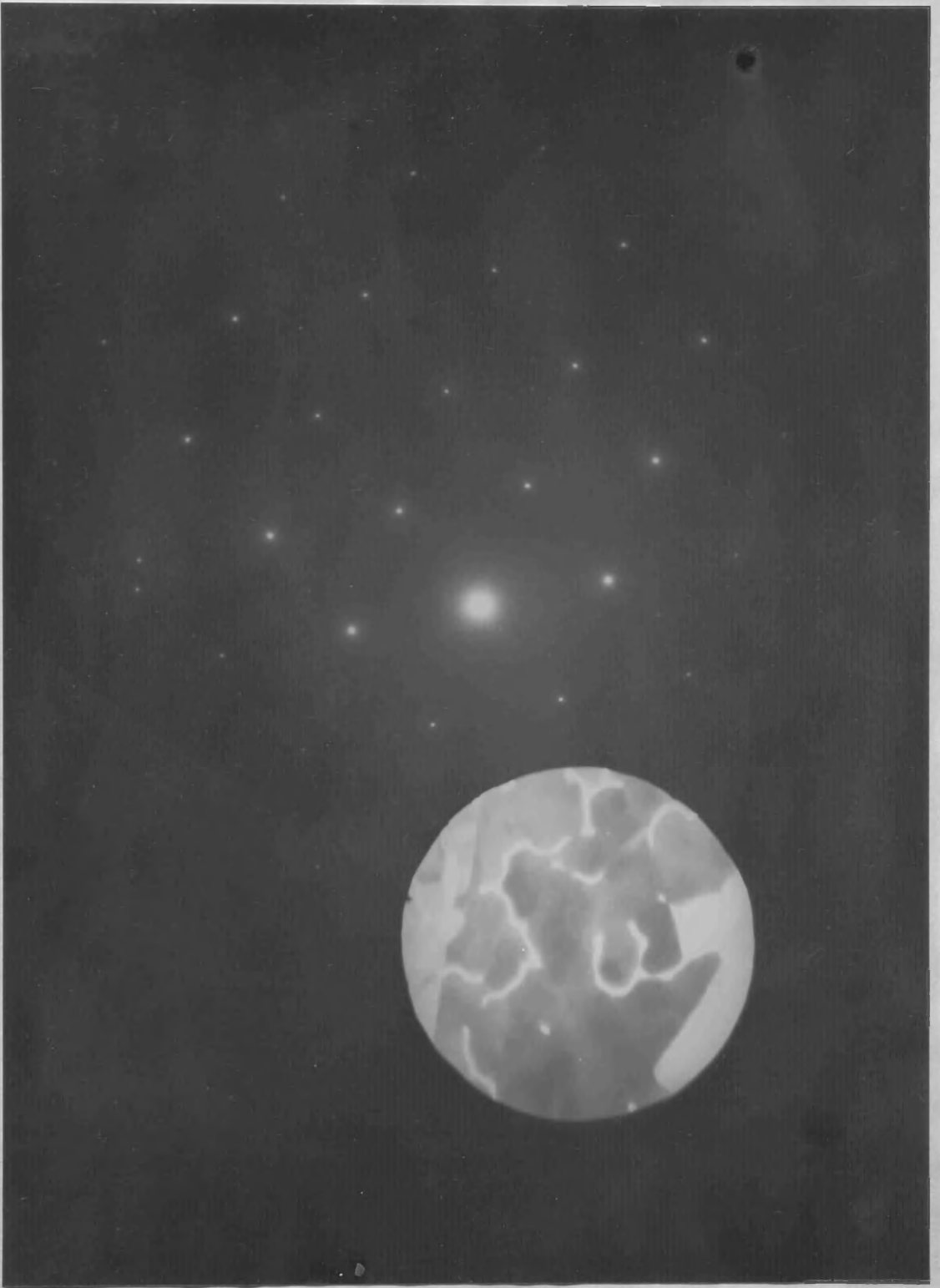


PLATE 17

X63,000



PLATE 18

X63,000

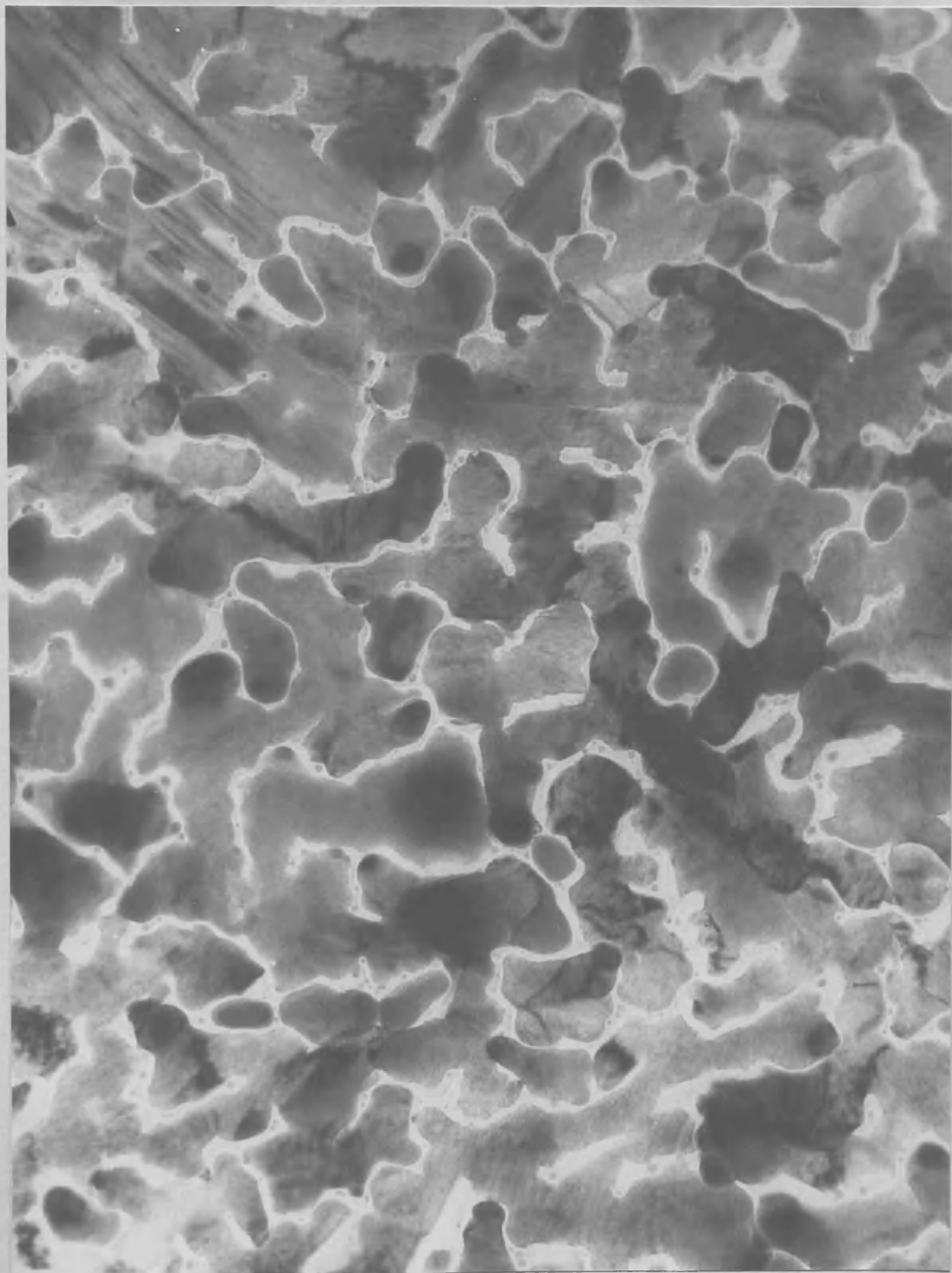


PLATE 19

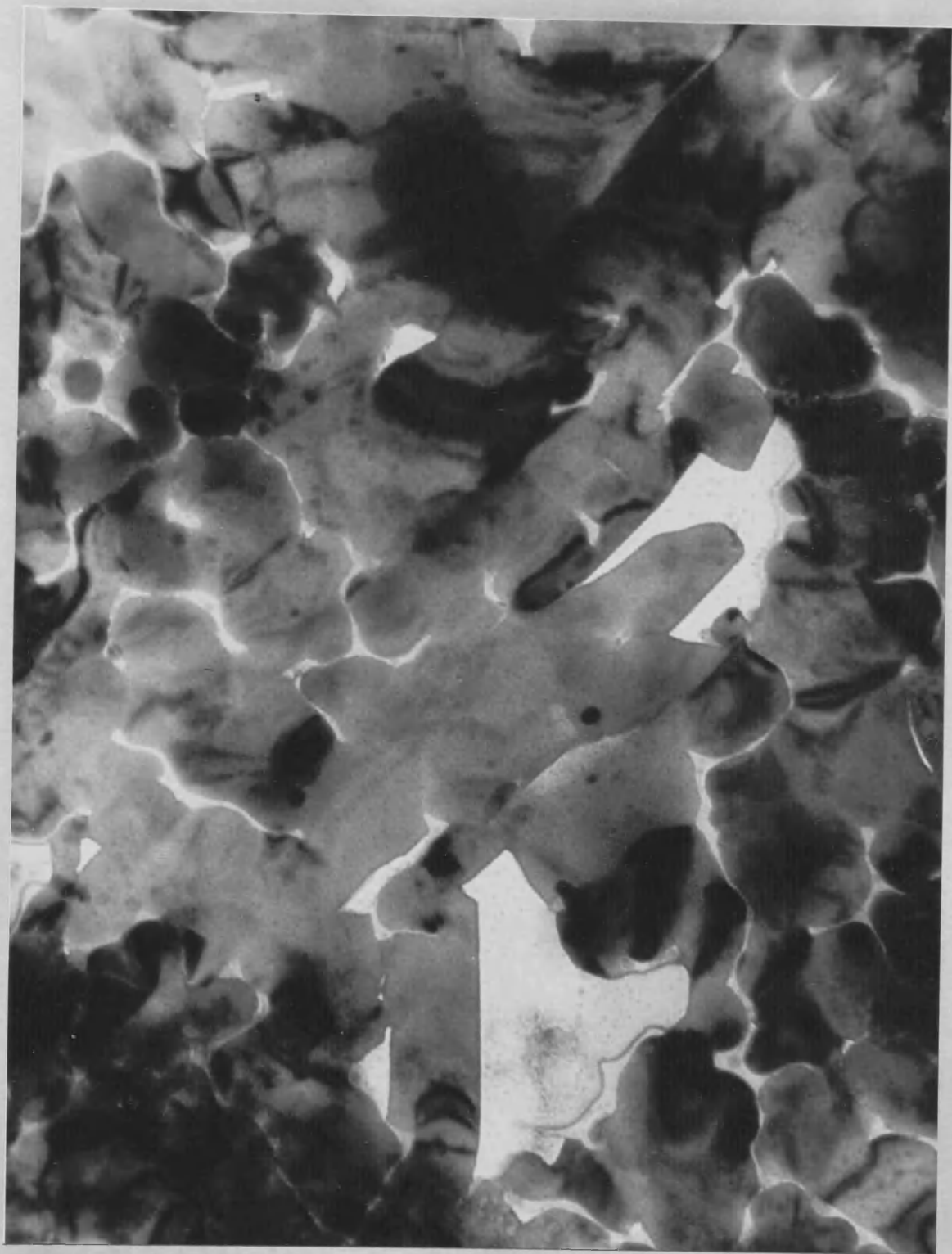
X130,000

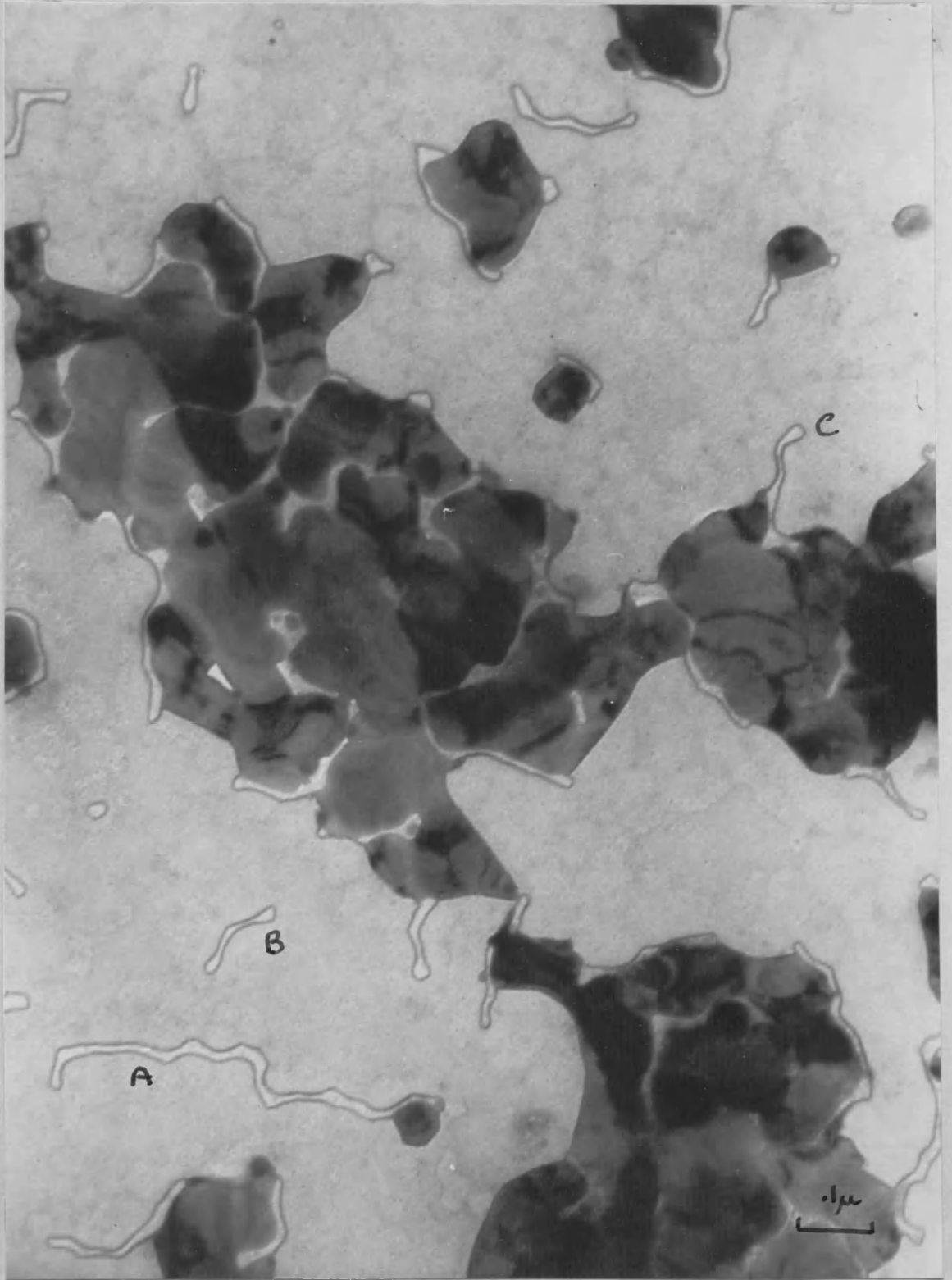


PLATE 20

X63,000





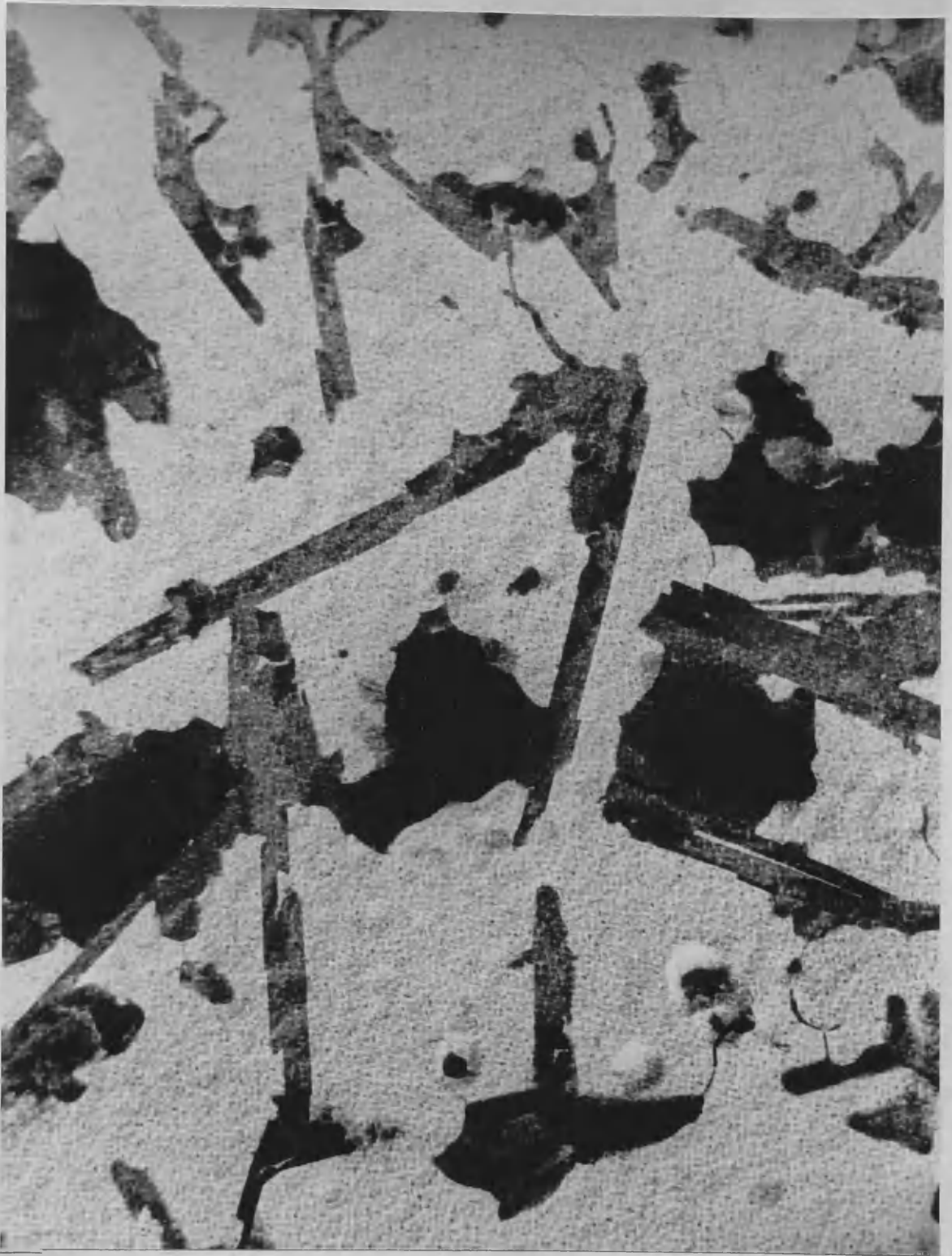




PLATE

24

X120,000



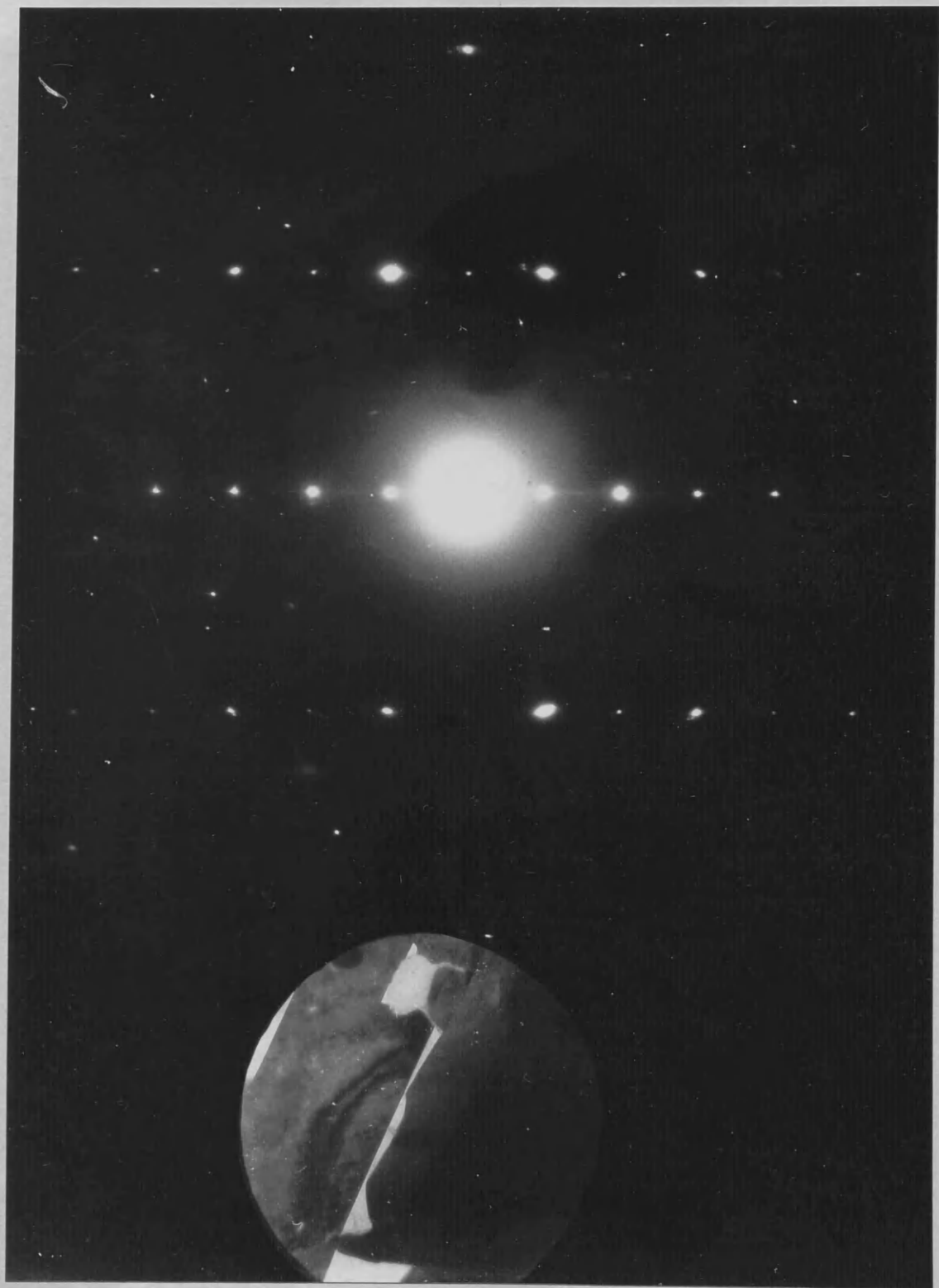
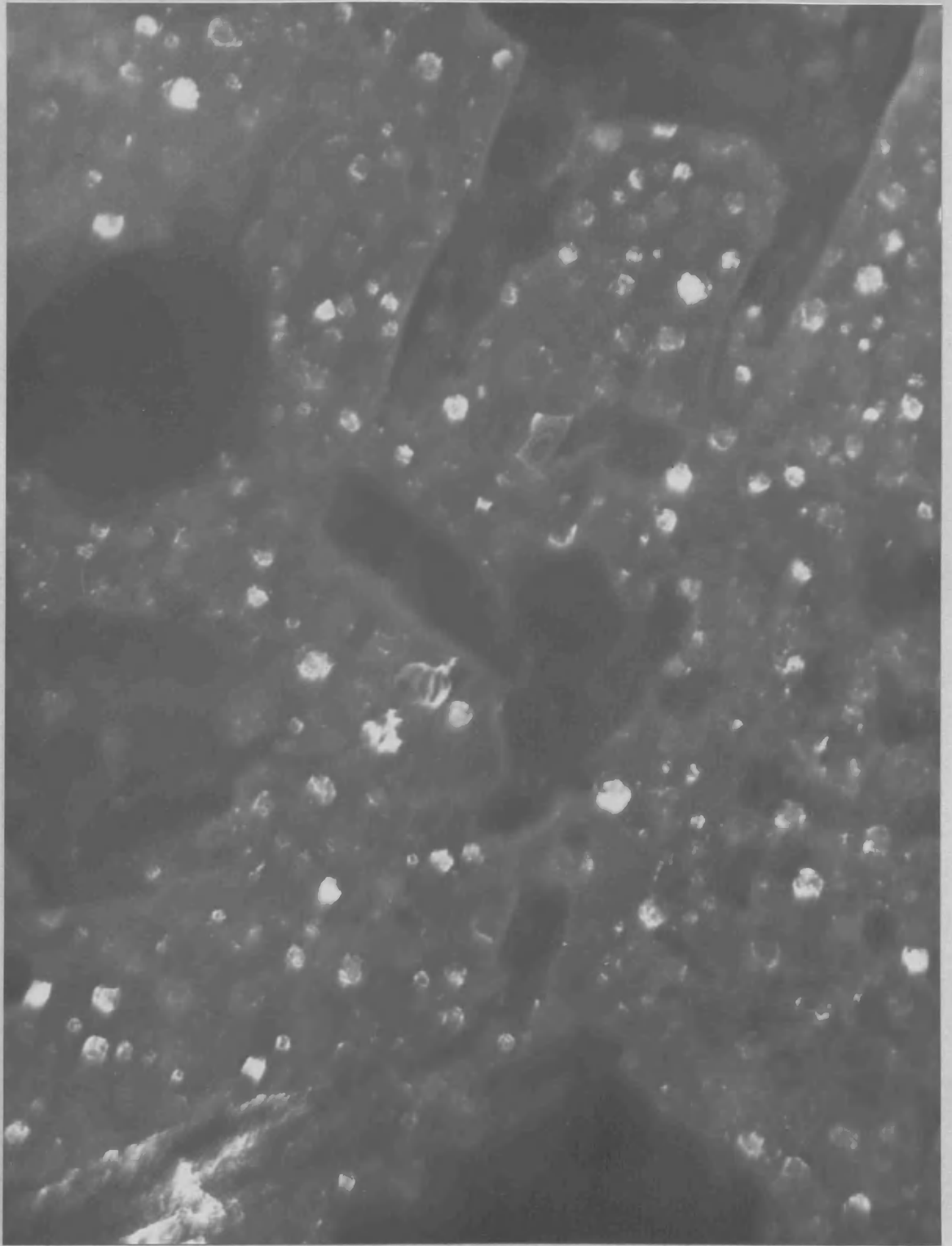
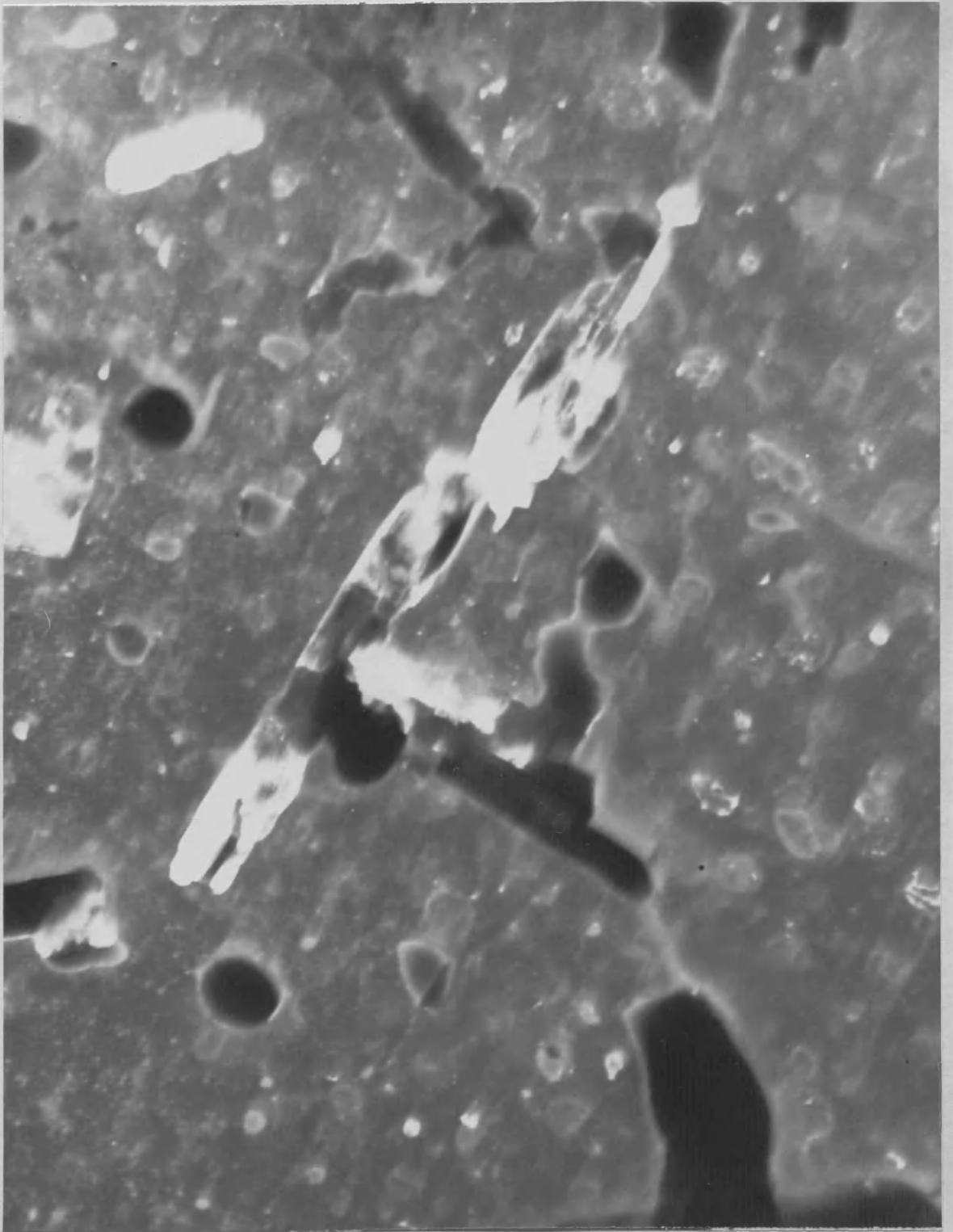


PLATE 26

X63,000





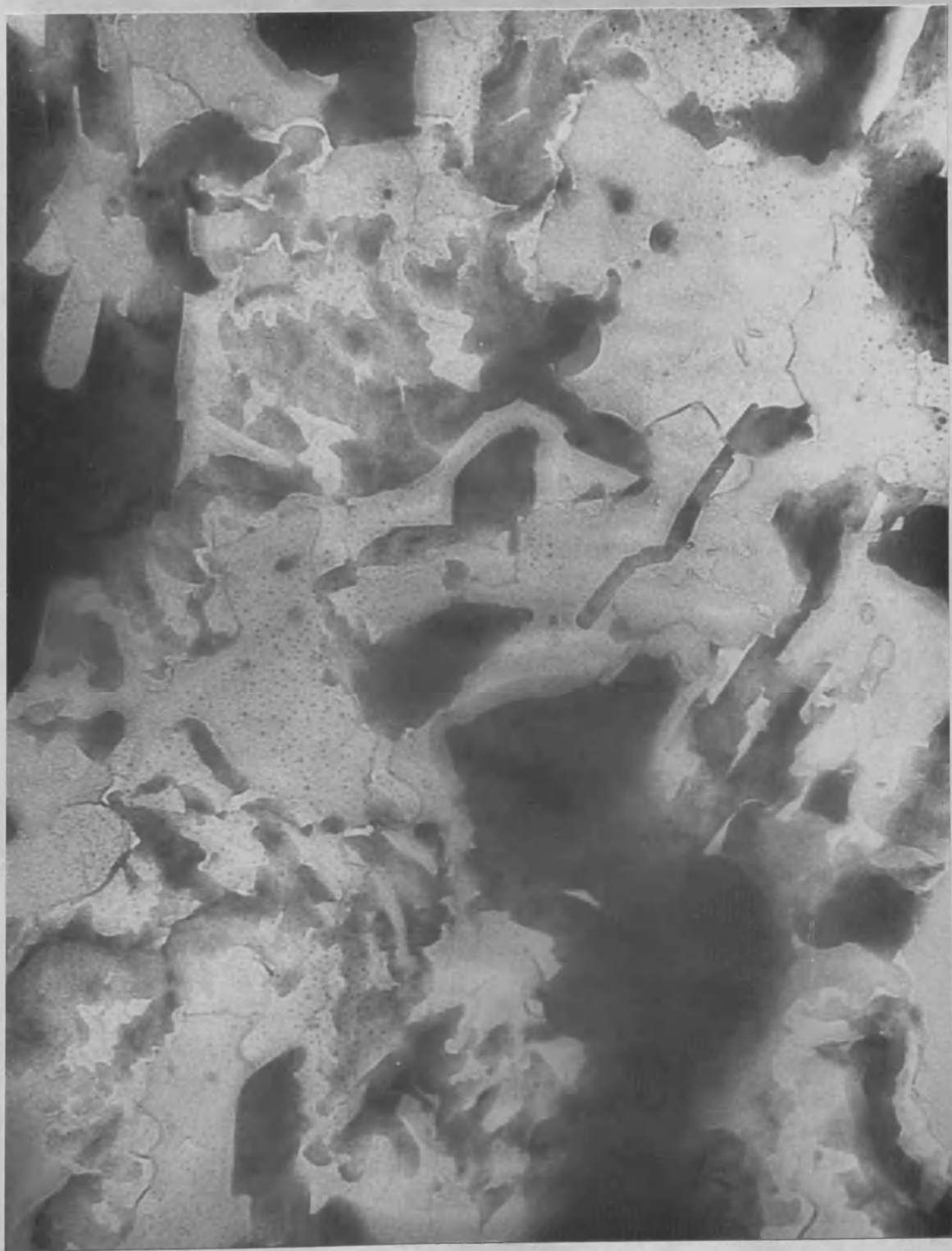


PLATE 29

X120,000



PLATE " 30

X63,000

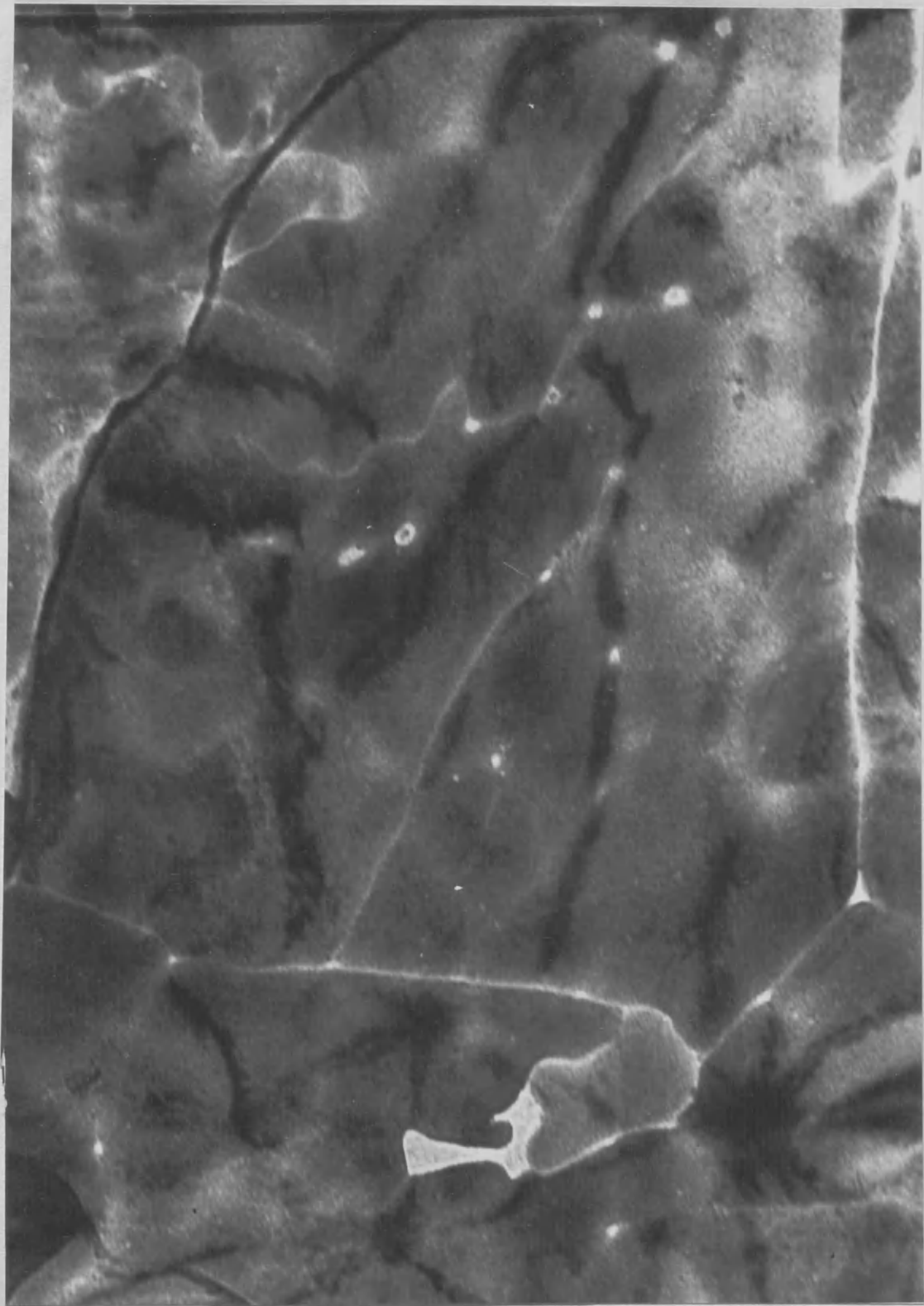


PLATE 31

X100,000